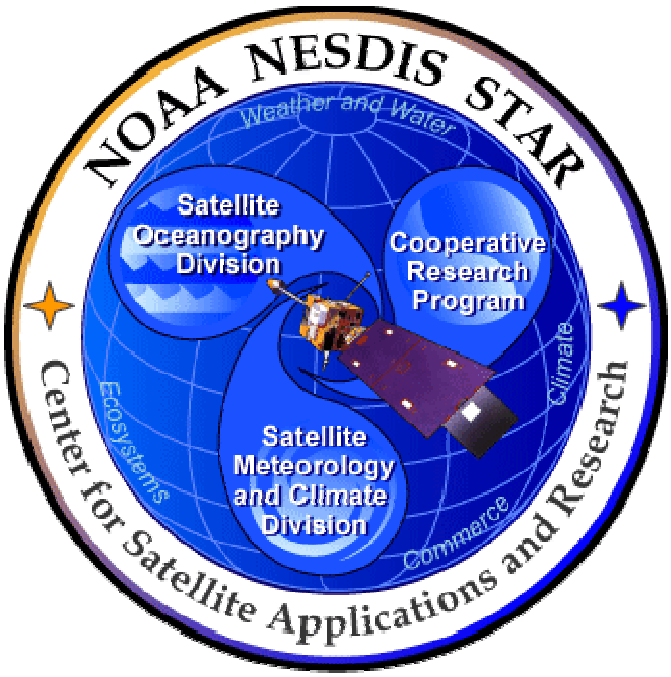

NOAA NESDIS
CENTER for SATELLITE APPLICATIONS and RESEARCH

ALGORITHM THEORETICAL BASIS DOCUMENT

ABI Cloud Mask

Andrew Heidinger, NOAA/NESDIS/STAR

Version 2.0

June 6, 2011

TABLE OF CONTENTS

LIST OF FIGURES

LIST OF TABLES

LIST OF ACRONYMS

1DVAR - one-dimensional variational
ABI - Advanced Baseline Imager
AIT - Algorithm Integration Team
ATBD - algorithm theoretical basis document
A-Train – Afternoon Train (Aqua, CALIPSO, CloudSat, etc.)
APOLLO – AVHRR Processing Scheme over Land, Clouds and Ocean
AVHRR - Advanced Very High Resolution Radiometer
AWG - Algorithm Working Group
CALIPSO - Cloud-Aerosol Lidar and Infrared Pathfinder Satellite
CASPR – Cloud and Surface Parameter Retrieval
CIMSS - Cooperative Institute for Meteorological Satellite Studies
CLAVR-x - Clouds from AVHRR Extended
CLAVR-1 Clouds from AVHRR Phase 1
CRTM - Community Radiative Transfer Model (CRTM), currently under development.
ECWMF - European Centre for Medium-Range Weather Forecasts
EOS - Earth Observing System
EUMETSAT- European Organization for the Exploitation of Meteorological Satellites
F&PS - Function and Performance Specification
GFS - Global Forecast System
GOES - Geostationary Operational Environmental Satellite
GOES-RRR – GOES-R Risk Reduction
IR – Infrared
IRW – IR Window
ISCCP – International Satellite Cloud Climatology Project
MODIS - Moderate Resolution Imaging Spectroradiometer
MSG - Meteosat Second Generation
NASA - National Aeronautics and Space Administration
NCEP – National Centers for Environmental Prediction
NESDIS - National Environmental Satellite, Data, and Information
NOAA - National Oceanic and Atmospheric Administration
NWP - Numerical Weather Prediction
PFAAST - Pressure layer Fast Algorithm for Atmospheric Transmittances
PLOD - Pressure Layer Optical Dept
POES - Polar Orbiting Environmental Satellite
RTM - radiative transfer model
SEVIRI - Spinning Enhanced Visible and Infrared Imager
SSEC – Space science and Engineering Center
SSM/I -- Special Sensor Microwave Imagers
STAR - Center for Satellite Applications and Research
UW – University of Wisconsin-Madison

ABSTRACT

This document describes the theoretical basis for the ABI cloud mask (ACM) algorithm. The function of ACM is provide the official binary clear-sky mask (clear or cloudy). In addition to this official product, the ACM also provides a 4-level cloud mask (clear, probably clear, probably cloudy and cloudy). This 4-level mask is an intermediate product and is generated for those algorithms and users who are familiar with the 4-level masks currently generated by NASA and NOAA.

The ACM uses 9 out of the 16 ABI spectral bands. Its cloud detection is based on spectral, spatial and temporal signatures. Most thresholds were derived from analysis of space-borne Lidar and current geostationary imager data. The ABI cloud tests where chosen to provide each algorithm a wide-range of cloud detection options. The ABI mask is designed to allow algorithms and users to ignore certain tests and to efficiently re-compute the cloud mask. In addition, the ACM design concept allows for easy expansion to include other tests as warranted. The current tests have their heritage in the cloud masks run operationally by NOAA, NASA and EUMETSAT.

The document first describes the satellite, ancillary and derived data used in the ACM. Then it describes the physical basis and the various tests used in the ACM as well as how the clear sky reflectance is calculated. The document concludes with the verification of the ACM's performance. Due to its fundamental sensitivity to cloud over all surface types and illumination conditions, the CALIPSO/CALIOP (a space-borne LIDAR) data collocated with data from SEVIRI, serve as the prime validation source. Comparisons to other established operational masks from NASA and EUMETSAT are also included.

1.1 Purpose of this Document

The primary purpose of this ATBD is to establish guidelines for producing the binary cloud mask from the ABI, flown on the GOES-R series of NOAA geostationary meteorological satellites. This document will describe the required inputs, the theoretical foundation of the algorithms, the sources and magnitudes of the errors involved, practical considerations for implementation, and the assumptions and limitations associated with the product, as well as provide a high level description of the physical basis for the initial estimate of the presence or absence of cloud within each ABI pixel. The cloud mask is made available to all subsequent algorithms that require knowledge of the presence of cloud.

1.2 Who Should Use this Document

The intended users of this document are those interested in understanding the physical basis of the algorithms and how to use the output of this algorithm to optimize the cloud detection for their particular application. This document also provides information useful to anyone maintaining or modifying the original algorithm.

1.3 Inside Each Section

This document is broken down into the following main sections.

- **System Overview**: provides relevant details of the ABI and provides a brief description of the products generated by the algorithm.

- **Algorithm Description**: provides a detailed description of the algorithm including its physical basis, its input and its output.

- **Assumptions and Limitations**: provides an overview of the current limitations of the approach and notes plans for overcoming these limitations with further algorithm development.

1.4 Related Documents

This document currently does not relate to any other document outside of the specifications of the GOES-R Mission Requirements Document (MRD) and to the references given throughout.

1.5 Revision History

Version 0.1 of this document was created by Dr. Andrew Heidinger of NOAA/NESDIS and its intent was to accompany the delivery of the version 0.1 algorithm to the GOES-R

AWG Algorithm Integration Team (AIT). Version 0.9 is intended to accompany the delivery of the version 3 algorithm to the GOES-R AWG AIT. Version 2.0 is intended to accompany the 100% delivery code to the GOES-R AWG AIT.

OBSERVING SYSTEM OVERVIEW
This section describes the products generated by the ABI Cloud Mask (ACM) and its associated sensor requirements.

1.6 Products Generated

The cloud mask algorithm is responsible for the initial cloud detection field for all ABI pixels. In terms of the F&PS, it is responsible directly for the Clear Sky Mask product within the Radiance Product Category. However, the cloud mask will be used by most of the ABI algorithms that require knowledge of the presence or absence of cloud within a given pixel. The current cloud mask requirement calls for a binary(yes/no) cloud mask for pixels out to a local zenith angle of 70^{o}. In concert with NASA and NOAA heritage, the ACM also generates a four-level mask whose categories are clear, probably-clear, probably-cloudy and cloudy. In addition, the cloud mask output will include all test results that were used to determine the final four-level mask to allow for modification by downstream users. The requirements for the clear sky mask from the F&PS version 2.2 are stated below.

Table 1. Requirements from F&PS version 2.2 for Clear sky Mask

Geographic coverage	Vertical Res	Horizontal Res	Measurement Range	Measurement Accuracy	Refresh Rate	Vendor allocated ground latency	Product measurement precision
CONUS	N/A	2 km	0 -1 Binary	87% Correct Detection	15 min	266 sec	N/A
MESO	N/A	2 km	0 -1 Binary	87% Correct Detection	5 min	266 sec	N/A
FD	N/A	2 km	0 -1 Binary	87% Correct Detection	15 min	806 sec	N/A

1.7 Instrument Characteristics

The cloud mask will be produced for each pixel observed by the ABI. The final channel set is still being determined as the algorithms are developed and validated. Table 2 summarizes the current channel set employed by the ACM. Note, the ACM is designed to work even when only a subset of the expected channels is provided. For example, when used with SEVIRI data, the ACM is able to account for the lack of Channel 4. The ACM also works with data from the GOES-IM and GOES-NOP imagers.

Table 2. Channel numbers and wavelengths for the ABI. (- only if channel 10 BT is not available)*

Channel Number	*Wavelength (μm)*	*Used in ACM*
1	0.47	
2	0.64	✓
3	0.86	
4	1.38	✓
5	1.61	✓
6	2.26	
7	3.9	✓
8	6.15	
9	7.0	✓*
10	7.4	✓
11	8.5	✓
12	9.7	
13	10.35	
14	11.2	✓
15	12.3	✓
16	13.3	

The algorithm relies on spectral, spatial and temporal tests. The performance of the cloud mask is therefore sensitive to any imagery artifacts or instrument noise. Calibrated observations are also critical because the cloud mask compares the observed values to those from a forward radiative transfer model. The channel specifications are given in the GOES-R MRD, version 3.7, section 3.4.2.1.4.0. We are assuming the performance outlined in this section during our development efforts.

ALGORITHM DESCRIPTION
This section provides a complete description of the algorithm at the current level of maturity (which will improve with each revision).

1.8 Algorithm Overview

The cloud mask serves a critical role in the GOES-R ABI processing system. It is a fundamental cloud property in itself but also serves to determine which pixels can be used for clear-sky applications (SST, NDVI, etc.). The following heritage cloud mask algorithms have influenced the ACM:

- CLAVR-x cloud mask from NESDIS
- The MOD/MYD35 MODIS cloud mask from UW CIMSS
- The Clouds and the Earth's Radiant Energy System (CERES) MODIS cloud mask from NASA Langley Research Center
- CASPR cloud mask used in the AVHRR Polar Pathfinder Extended (APP-x)

As with the above masks, the ACM combines spectral and spatial tests to produce a 4-level classification of cloudiness. The 4-levels of the ACM cloud mask are:

- Clear,
- Probably Clear,
- Probably Cloudy, and
- Cloudy.

These categories are the same as those employed in the CLAVR-x and MYD35 masks. In general, the cloud mask is designed so that the clear and cloudy pixels are suitable for clear and cloudy product generation.

In addition to the 4-levels of cloudiness, the ACM also provides the results of every test used to compute the 4-level mask. This information is provided to allow other applications to modify the cloud mask to suit their specific needs.

1.9 Processing Outline

The processing outline of the ACM is summarized in Figure 1 below. The current ACM is implemented within the GOES-R AWG AIT Framework. The Framework provides all of the observations and ancillary data, such as the data from the NWP and RTM. The ACM is designed to run on segments of data where a segment is comprised of multiple scan lines.

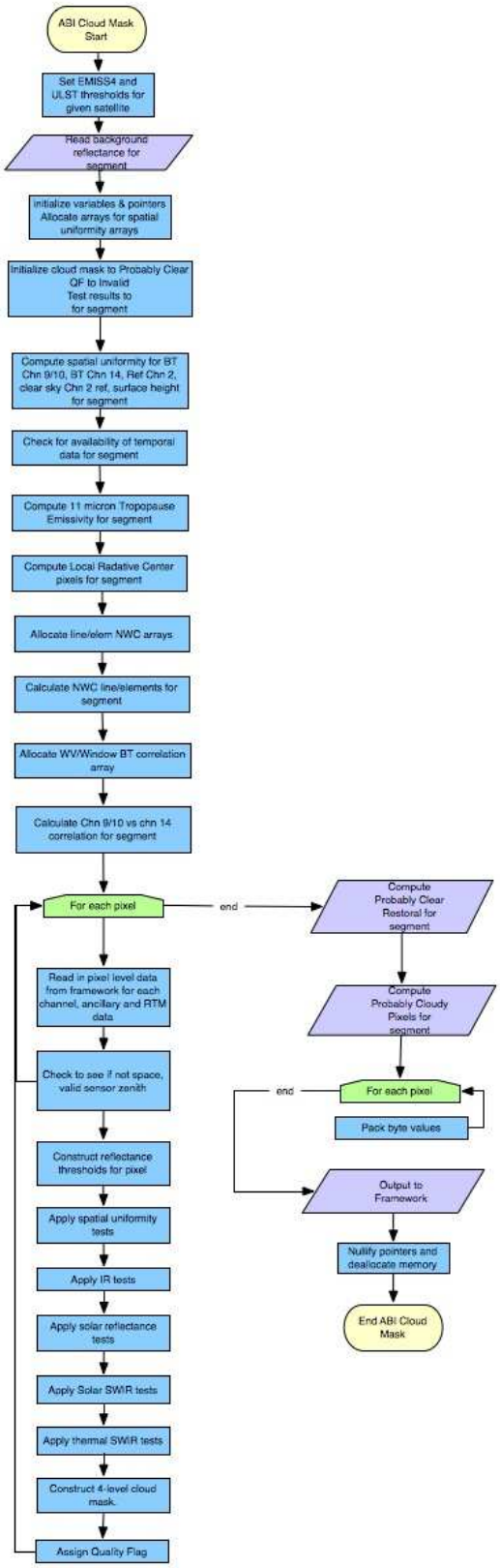

Figure 1 High Level Flowchart of the ACM illustrating the main processing sections.

1.10 Algorithm Input

This section describes the input needed to process the ACM. While the ACM is derived for each pixel, it does require knowledge of the surrounding pixels. Currently, the ACM is run on segments that contain 200 scan-lines. While the final size of the segments is to be determined, the ACM should not be run with information from only one line.

1.10.1 Primary Sensor Data

The list below contains the primary sensor data used by the ACM. By primary sensor data, we mean information that is derived solely from the ABI observations and geolocation information. It should be noted that the 0.65 μm channel will be sub-sampled to the resolution of the IR channels, which is currently 2km.

- Calibrated solar reflectance percents (0-100%) for channels 2, 4, 5 and 7
  NOTE – Reflectances are normalized in the algorithm in the terminator region. This process is described in section 3.4.3 of this ATBD.

- Calibrated radiances for channels 7, and 14
- Calibrated brightness temperatures for channels 7, 9, 10, 11, 14, 15 and 16
- Calibrated brightness temperatures for channel 14 and 15 at neighboring warm center (NWC) for each pixel. Process to calculate NWC in Section 3.3.3
- Bad pixel mask for each channel
- Space mask
- Derived channel 7 emissivity, which is described in section 3.4.1.3.1
- Channel 7 solar energy (mW/m^2/cm^-1)
- Local zenith angle.
  NOTE: The requirement is to produce the clear sky mask out to a local zenith angle of 70^{o}

- Solar zenith angle
- Relative azimuth angle
- Glint zenith angle
- Scattering angle
- Cosine of sensor, scattering and solar zenith angles
- Number of lines and elements for the given segment
- Satellite name
- Channel 14 brightness temperatures from the image 15 minutes prior
- Channel 11, 14 and 15 brightness temperatures from the image one hour prior

1.10.2 Ancillary Data

The following data lists the ancillary data required to run the ACM. By ancillary data, we mean data that requires information not included in the ABI observations or

geolocation data. A more detailed description is provided in the GOES-R Algorithm Interface and Ancillary Data Description Document (AIADD). The NWP and RTM data, which are at NWP resolution, are interpolated to pixel level as described in the AIADD.

- **Sun earth distance**

- **Surface elevation**
  Both the surface height and maximum surface elevation in a 3x3 box are used in the ACM

- **Land mask**
  Using the land mask, each pixel is flagged internally as land or water.

- **Coast mask**
  Using the coast mask, each pixel is flagged internally as coast or not coast.

- **Desert mask**
  Using the desert mask, each pixel is flagged internally as desert or clear

- **Snow mask**
  Using the snow mask, each pixel is flagged internally as snow or clear. In addition, if a pixel has a 11 μm brightness temperature of greater than 277K, the snow mask is turned off.

- **Surface emissivity of channel 7 from SEEBOR**
  Surface emissivity for each pixel and neighboring warm center (NWC) for each pixel are required. NWC described in Section 3.3.3.

- **NWP level associated with the surface**

- **NWP level associated with the tropopause**

- **Local Zenith Angle bin**

- **NWP Line and element indices**

- **Surface temperature from NWP**

- **Surface temperature uniformity from NWP**

- **Total precipitable water from NWP**

- **Total column ozone from NWP**

- **Clear-sky Infrared RTM Calculations**

- Clear-sky top-of-atmosphere (TOA) radiances for channel 7
- Clear-sky top-of-atmosphere (TOA) brightness temperatures computed for channels 14 and 15.
- Clear-sky transmission profiles for channel 7
- Equivalent blackbody radiance of a cloud emitting at the temperature of the Tropopause for channel 14.
- Clear-sky TOA channel-14 brightness temperature from the image 15 minutes prior.

- **Clear-sky Reflectance**
  - The clear sky reflectance is first corrected for atmospheric scattering by adding in the Rayleigh single scattering reflectance and transmission
  - In the terminator region, the clear sky reflectance is renormalized
  - Both the clear sky reflectance for each pixel as well as the standard deviation of the clear sky channel 2 reflectance over a 3x3 pixel array are both used.

1.10.3 Derived Data

The following lists and briefly describes the data that are required by the ACM that are provided by other algorithms.

- **Valid pixel mask**
  A pixel is determined to be valid if it is not a space pixel, has a local zenith angle of less than 40^o, and has a valid measured and clear sky 11μm brightness temperature.

- **Cloud Mask**
  For the Terminator Thermal Stability Test (TERM_THERM_STAB), the cloud mask from one hour prior is required.

- **Local Radiative Centers**
  Given a derived channel 14 top of troposphere emissivity, $\varepsilon_{stropo}(11\mu m)$, the local radiative center (LRC) is defined as the pixel location, in the direction of the gradient vector, upon which the gradient reverses or when an emissivity value ($\varepsilon_{stropo}(11\mu m)$) greater than or equal to 0.75 is found, whichever occurs first. The gradient filter routine is provided by the framework and is required as an input to the ACM. The required inputs to the gradient filter are:
  - $\varepsilon_{stropo}(11\mu m)$,
  - The line and element size of the segment being processed,
  - A binary mask for the segment of pixels that have non-missing $\varepsilon_{stropo}(11\mu m)$ for the segment,
  - The minimum and maximum valid emissivity values (0.0 and 1.0 respectively), and
  - The maximum $\varepsilon_{stropo}(11\mu m)$ value to be considered (0.75).

The outputs from the gradient filter are the line and element of the LRC. A further description of how the LRC is calculated using the gradient filter is described in Pavolonis (2009) and in the AIADD.

- **Neighboring Warmest Center**
  The ACM employs a check for the line and element location of the warmest (largest 11 μm brightness temperature) pixel limited to a 10x10 region The 10x10 region is one that surrounds each pixel. and classifies those as Neighboring Warmest Center (NWC). The assumption here is that the NWC points represent the optically thinnest pixel in the local area.

- **Correlation of channel 9/10 brightness temperature to channel 14 brightness temperature**
  The ACM computes the Pearson Correlation Coefficient between the channel 10 and channel 14 brightness temperatures for each pixel. If channel 10 is not available, then the channel 9 brightness temperature can be used.

- **Derived channel 14 top of the Tropopause emissivity**
  The ACM derives the channel 14 top of troposphere emissivity using the measured channel 14 radiance, clear sky channel 14 radiance, space mask, latitude/longitude cell index from the NWP, Tropopause index from the NWP, local zenith angle bin index, and channel 14 micron blackbody radiance. Both the channel 14 top of Troposphere emissivity for each pixel as well as the LRC channel 14 top of Troposphere emissivity for each pixel are required.

- **Minimum channel 2 reflectance over a 3x3 pixel array**
- **Mean channel 2 reflectance over a 3x3 pixel array**
- **Standard deviation channel 2 reflectance over a 3x3 pixel array**
- **Maximum channel 14 brightness temperature over a 3x3 array**
- **Standard deviation of the channel 14 brightness temperature over a 3x3 pixel array**
- **The standard deviation of either the channel 9 or channel 10 brightness temperature. NOTE:** Channel 9 is only used if channel 10 is not available.

- **Cold surface pixel**
  If a pixel has a surface temperature of less than 265K, it is defined as a cold surface.

- **Glint mask**
  A glint mask is initially defined based upon the glint zenith angle. Any pixels that have a glint zenith of less than 40^{o} are classified as "glint." However, those pixels that have been marked as glint and have an 11μm brightness temperature of less than freezing (273K), or the 11μm brightness temperature is less than the clear sky 11μm brightness temperature minus 5, have the glint flag turned off. Turning the glint mask off is an attempt to restore cold pixels in the glint zone. Further

checks to look at pixels that have a uniform 0.64μm reflectance are performed. A check is done by checking to see if a glint pixel has a standard deviation channel 2 reflectance over a 3x3 pixel array less than 0.10 * the mean channel 2 reflectance over a 3x3 pixel array. If it does, the pixel is restored to non-glint.

- **Day/Night mask**
  A day/night mask is defined based upon the solar zenith angle. Any pixels that have a solar zenith of less than 87^o are classified as "day" and those greater than 87^o are classified as night.

- **Terminator mask**
  We classify those pixels that are between 87^o and 93^o as pixels that are in the terminator region.

1.11 Theoretical Description

Cloud detection is the process of separating cloudy from clear pixels. It always involves assumptions of the radiometric characteristics of the clear and/or cloudy state and looking for departures from them. In the ACM, spectral, spatial and temporal tests are used to look for clouds by identifying pixels that do not exhibit the expected behavior of the clear-sky state. Each test described is applied to each pixel, resulting in a cloud/no cloud score, which is then used to decide whether a pixel is cloudy or clear.

1.11.1 Physics of the Problem

The challenge for any cloud mask is to exploit spectral, spatial and temporal signatures that maximize the sensitivity to the presence of cloud while simultaneously minimizing the false detection of cloud. The ACM algorithm makes extensive use of information from NWP fields, coupled with a Radiative Transfer Model (RTM), to generate the expected clear-sky state for the spectral and temporal tests. This approach has also been adopted by EUMETSAT (Dybrroe et al., 2005) however EUMETSAT uses lookup tables that pr-computed using results from an RTM. The ACM uses RTM results specific to the scene being processed. While the current NWP fields often have errors in some critical fields, such as the surface temperature over land, they provide needed and useful information. Over the coming years before the launch of GOES-R, the NWP fields are expected to improve in both accuracy and spatial resolution. For the spatial thresholds, we have no reliable information from the NWP fields and must rely on other sources. For example, the thresholds for the spatial uniformity tests rely on information from pre-computed high resolution maps of surface elevation and surface reflectance (see 3.4.2.2).

In addition, the spectral tests are broken into those that use infrared channels, shortwave-infrared, and solar-reflectance channels. All applicable tests are used to construct the ACM. However, users that wish to have a cloud mask with consistent day-night performance are encouraged to use the cloud mask generated *without* the solar reflectance tests considered.

The other major type of test in the ACM is the restoral test. The restoral tests are separated into tests that "restore" probably cloudy pixels to clear pixels and tests that

"restore" cloudy pixels to probably cloudy pixels. As defined, the effect of these restoral corrections is to provide a conservative estimate on cloudiness (i.e., minimize false alarms in the ACM). Note many of the cloud detection names arise from the Clouds from AVHRR (CLAVR) cloud mask developed by Stowe et al. (1999).

1.11.1.1 Use of CALIPSO Data in Determining Cloud Mask Thresholds

An important part in the development of ACM is the use of CALIPSO observations to help define the thresholds. Because CALIPSO provides one of the most unambiguous and direct measures of the presence of the highest cloud layers (i.e., those also observed by the ABI), it has been used to help understand the behavior of each cloud mask test for clear and cloudy pixels. The actual determination of cloud mask thresholds is described later in the Mathematical Description Section. While many cloud masks have used RTM simulations to set cloud detection thresholds (i.e., CASPR), the goal of the ACM is to use the availability of pixel-level clear-sky information to derive new cloud mask metrics that maximize the separation of cloudy and clear pixels. The main advantage of using an observationally based approach (collocation of CALIPSO and geostationary test data) to threshold definition is that simulations may not capture the true variability present in real scenes. The ACM allows for threshold modification when warranted.

In this analysis, the 1 km cloud layer product from the standard CALIPSO processing (Vaughan et al., 2005) was used together with data from the SEVIRI instrument. The CALIPSO product, developed by NASA Langley, provides top, base and number of cloud layers for up to 10 layers in a 1 km footprint, and attempts to distinguish cloud from aerosol, smoke and dust. The data used for these analyses are Version 3. For the purposes of this study, a cloud mask from CALIPSO was determined noting the number of cloud layers in each 1 km pixel (column). Any CALIPSO column with more than zero cloud layers was assigned to the cloudy category. In addition, a cloud fraction from CALIPSO was computed using results from all lidar fields of view that fell within each SEVIRI pixel. Using the method described in Heidinger and Pavolonis (2009), the temperature of the highest cloud layer is used in conjunction with the 11 μm clear radiance calculation and 11 μm SEVIRI observations to compute an 11 μm cloud emissivity. This value represents the emissivity that a cloud must have if it existed at the level measured by CALIPSO with the observations measured by the geostationary sensor (i.e., ABI). This is hereafter referred to as the CALIPSO emissivity.

As a lidar with an inherent vertical resolution of 30 m, CALIPSO can detect clouds with opacities and spatial scales far exceeding the capabilities of passive visible/infrared sensors such as SEVIRI or the ABI. In order to use CALIPSO to determine meaningful thresholds for passive detection of clear and cloudy conditions, filtering is required to attempt to make the CALIPSO detection comparable to the performance expected from the passive observing system. In this analysis, we ignored all CALIPSO results which had cloud fractions between 0.1 and 0.9. The purpose of this filter is to restrict the analysis to CALIPSO data that is uniform over the spatial scales of the coarser SEVIRI (or ABI) pixels. In addition, a threshold of 0.1 was applied to the CALIPSO emissivity

in an attempt to remove from consideration any pixels with very low optical depths that would fall below the detection capabilities of the channels on the ABI sensor.

In the remaining part of this section, CALIPSO data matched in space and time with SEVIRI observations are used to demonstrate the skill of the cloud mask tests in the ACM. The collocations occurred during an eight-week period comprised of two weeks in four seasons from 2006 and 2007. Unless stated otherwise, all references to CALIPSO results refer to data from the SEVIRI/CALIPSO collocations for this eight-week dataset. The collocation tool used here was provided by Michael Pavolonis of NOAA.

1.11.1.2 Infrared Cloud Detection Tests

1.11.1.2.1 ETROP – Channel 14 Emissivity Referenced to the Tropopause

The ETROP test assumes that clouds produce colder 11 μm brightness temperatures than what would have been observed under clear-sky conditions. This is limited to 11 micron brightness temperatures between 170K and 310K as well as clear sky 11 micron brightness temperatures of above 24K. Traditionally, infrared window (IRW) brightness temperatures are used in gross contrast tests to identify cold pixels. The ETROP, however, operates on the 11μm emissivity, computed assuming the cloud top resides at the Tropopause. This Tropopause-relative emissivity is computed as follows:

$$\varepsilon = (I - I\_clear) / (I\_bb - I\_clear)$$

where ***I*** is the observed radiance**,** ***I_clear*** is the computed clear-sky radiance (from the RTM) and ***I_bb*** is the equivalent blackbody radiance of a cloud emitting at the temperature of the Tropopause. As noted in the ancillary data section, ***I_bb*** is provided to the ACM as an input and described in the AIADD.

The benefits of the ETROP are that a threshold based on ε has a more direct physical meaning than one based on a brightness temperature. By including the clear-sky radiative transfer through the computation of ε, the ETROP test should be independent of surface temperature and atmospheric profiles. Because ε is referenced to the Tropopause (recalling again that the cloud top temperature here is assumed to be that of the Tropopause), opaque clouds that are positioned at lower and warmer levels will generate ε values less than one. The Tropopause-relative emissivity approximates the true emissivity only for clouds in the upper Tropopause. In clear conditions, the Tropopause-relative emissivity should approach zero. Negative values are possible when the computed clear-sky radiance is greater than the observed clear sky radiance.

Figure 2 and Figure 3 show the probability density functions (pdfs) of the values of ε measured for the collocated SEVIRI/CALIPSO observations. The CALIPSO cloud mask, described above, was used to compute the separate clear and cloudy pdfs. The pdfs show a significant separation between the clear and cloudy regions. The clear-sky pdf has a peak near zero and the cloudy pdf peaks off zero. The separation is less for

land pixels but still offers skill at unambiguous cloud detection for a significant range of ε.

In addition to using the pixel's own values of ε, the ETROP also compares against the values of ε for the 'local radiative center' (LRC) where defined. As described above, the LRC represents the closest local opaque center determined by applying a gradient filter applied to ε. LRC pixels therefore always have an equal or higher value of ε than the non-LRC pixel with which they are associated. The goal here is to extend the detection of the cloud to the cloud edges. Figures 4 and 5 show the same pdfs as Figure 2 and Figure 3 except computed for the ε values for the LRC.

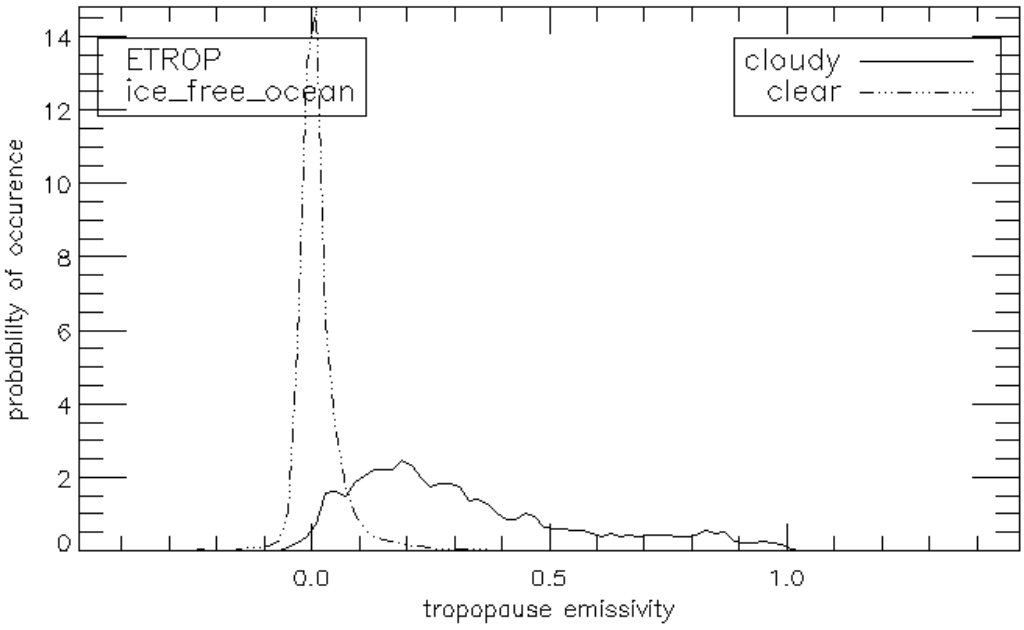

Figure 2 PDF of the channel 14 emissivity referenced to the tropopause for clear and cloudy pixels as determined by CALIPSO for ice-free ocean regions.

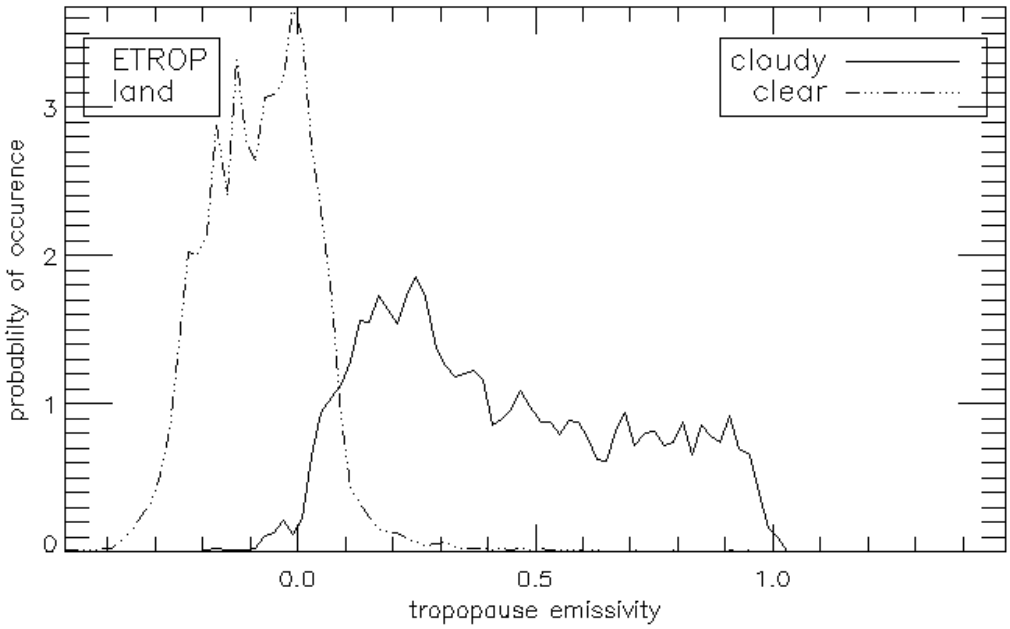

Figure 3 Same as Figure 2 for ice-free land regions.

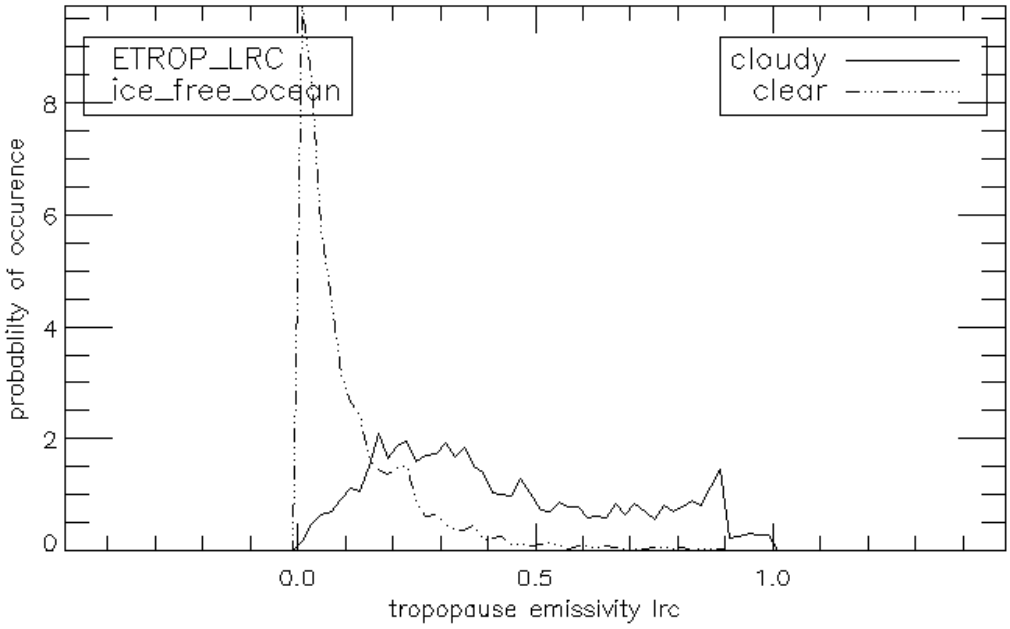

Figure 4 PDF of the 11 μm (channel 14) emissivity referenced to the tropopause computed for local radiative centers (LRC) for clear and cloudy pixels as determined by CALIPSO for ice-free ocean regions.

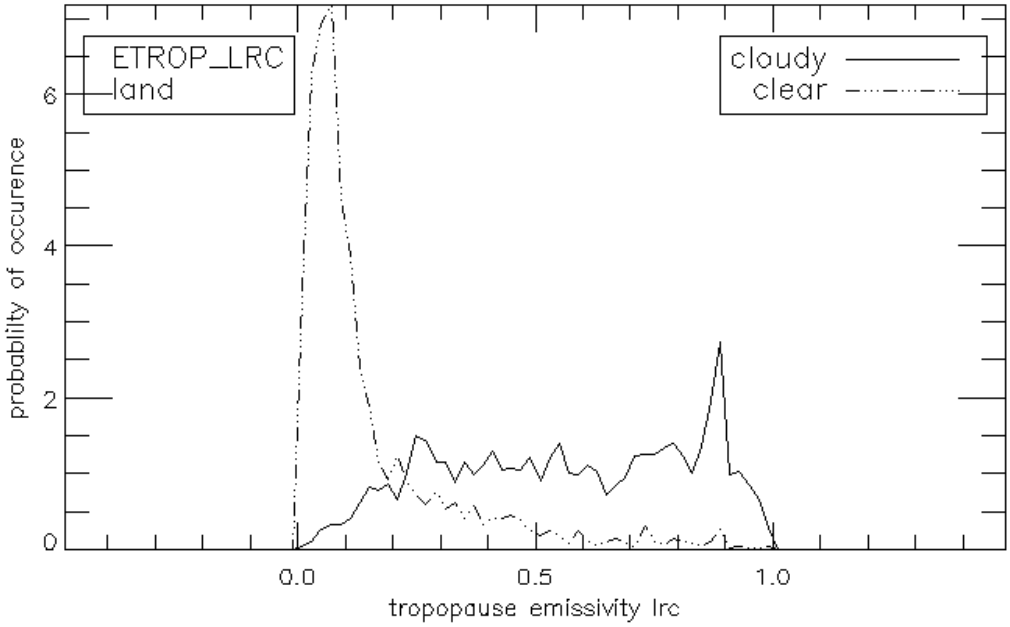

Figure 5 Same as Figure 4 for ice-free land regions.

If either the emissivity or the emissivity at the Local radiative center surpasses the threshold, this gives a positive result for this test.

1.11.1.2.2 Relative Thermal Contrast Test (RTCT)

While the ETROP tests works on the absolute deviation of the 11 μm observation from the clear-sky estimate, the Relative Thermal Contrast Test (RTCT) works on the relative spatial variation of the local 11 μm observations. The underlying assumption applied in the RTCT is that pixels significantly colder than their warmest neighbors are likely to be cloudy. In the RTCT, the metric is the difference between the maximum 11 μm brightness temperature in a 3x3 box and the measured pixel's 11 μm brightness temperature. The targeted cloud features in this test are small scale clouds and cloud edges. This test is not performed on pixels where the minimum 11 μm brightness temperature in a 3x3 box is warmer than 300K, pixels that are coastlines, cold surfaces or snow. The threshold for the test is determined by taking the specific threshold for ocean and land pixels and modifying it by 3 + 7 * (standard deviation of the surface height in a 3x3 box in km).

Figure 6 and Figure 7 show the distribution of the RTCT metric derived from the CALIPSO cloud mask collocated with SEVIRI observations. Due to the smaller surface temperature variations of the ocean surface compared to land surfaces, the clear-sky peak in the RTCT metric is narrower for ocean surfaces compared to that seen for land surfaces. However, there is a range of the RTCT metric for both surfaces where cloudy values dominate the distribution. One of the main benefits of this test is that it is entirely independent of the RTM+NWP calculations that play a large role in many of the other tests.

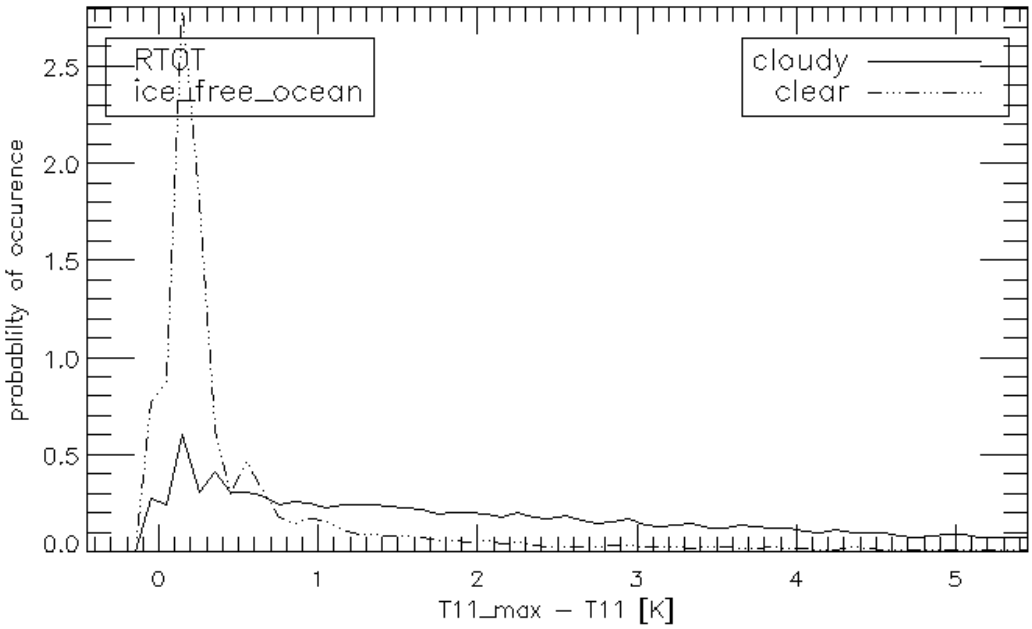

Figure 6 PDF of the difference in the maximum 11 μm brightness temperature over a 5x5 array and 11 μm brightness temperature pixel observation for clear and cloudy pixels as determined by CALIPSO for ice-free ocean regions.

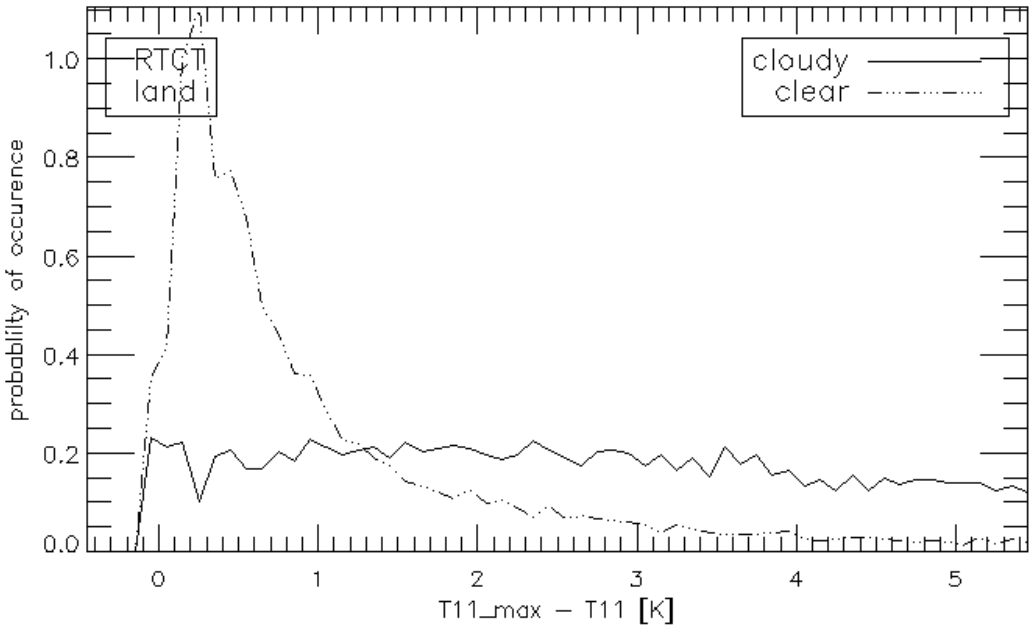

Figure 7 Same as Figure 6 for ice-free land regions.

1.11.1.2.3 Temporal Infrared Test (TEMPIR)

One of the benefits of the GOES-R ABI sensor over the GOES-NOP series imagers is the availability of remapped data taken with a high temporal resolution. The remapping of the ABI data ensures that pixel position is maintained from image to image. The Temporal Infrared Test (TEMPIR) takes advantage of this capability to detect cloud. The assumption is that as clouds move and previously clear pixels in one image become cloudy in the next, the presence of cloud can be detected by rapid cooling of the observed 11 μm brightness temperature of any one pixel. This type of information has been used successfully in the GOES era as demonstrated by Wu et al. (1999).

The metric chosen for the TEMPIR is the difference between the 11 μm brightness temperature collected from the image 15 minutes prior and the current value:

$$TEMPIR = BT11(T\text{-}15min) - BT11(T)$$

A 15-minute temporal window was chosen because that is the current nominal temporal spacing of the SEVIRI data that comprises our test data set. The only restriction of this test is a maximum clear sky or measured 11 micron brightness temperature of 330K from the previous time step. Future studies will include analysis of 5-minute data and will attempt to determine the optimal temporal window for this test. Figure 8 and Figure 9 show the distributions of the TEMPIR metric for clear and cloudy pixels as determined by CALIPSO. What we are looking at in Figure 8 and 9 is the BTD of the previous image minus that of the current image. The presence of cloud is determined only for the current image whose time is close to that of the CALIPSO overpass.

As expected, the clear peaks in both the land and ocean surface are primarily centered on zero and the cloudy distributions show a much broader distribution. The intent of the TEMPIR is to use the positive values of the metric for detecting cloud. The negative values of metric are not currently used by the TEMPIR but may offer skill in adjusting the cloud detection results for the previous image.

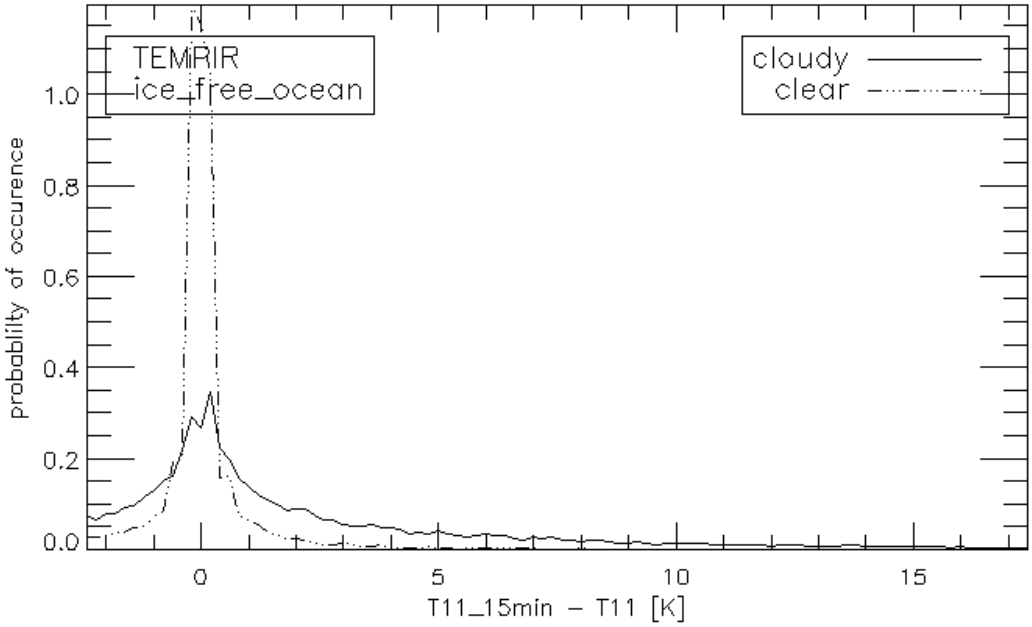

Figure 8 PDFs of the difference in the 11 μm brightness temperature observation from an image taken 15 minutes prior minus the 11 μm brightness temperature pixel observation for clear and cloudy pixels as determined by CALIPSO for ice-free ocean pixels.

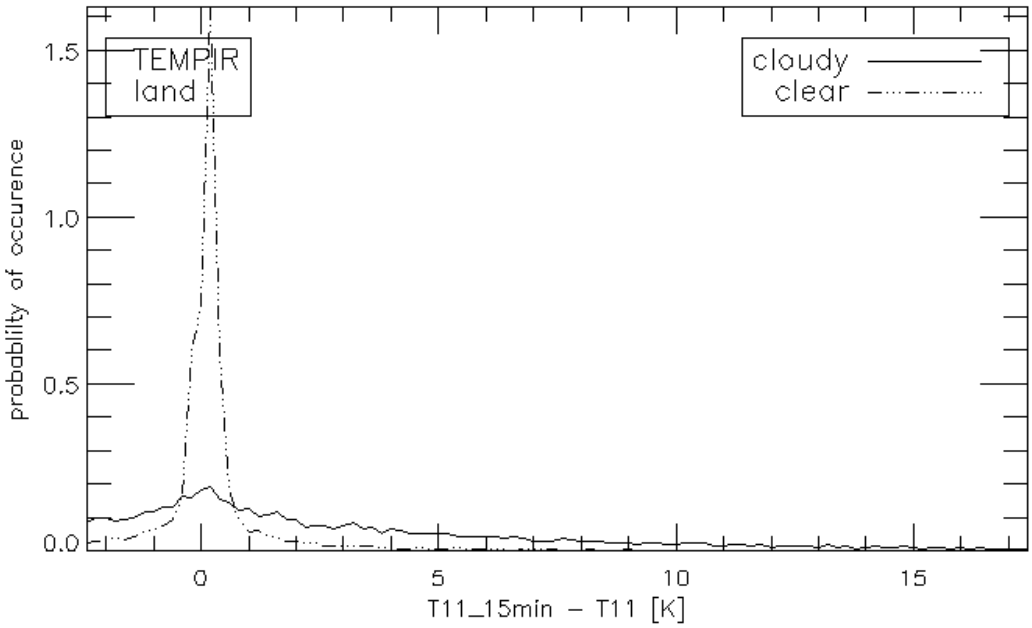

Figure 9 Same as Figure 8 for ice-free land regions.

1.11.1.2.4 Positive Four Minus Five Test (PFMFT)

Cloud detection tests that use split-window (11 and 12 μm) observations are common in many cloud mask algorithms. For example, they are employed in the MYD35, CASPR, APOLLO and CLAVR-1 schemes. Due to the spectral variation in cloud transmission, the presence of semi-transparent cloud leads to a positive value of the 11-12 μm brightness temperature difference (BTD[11-12]). Unfortunately, the physics of water vapor continuum absorption also generate positive values for clear-sky conditions especially for warm and moist atmospheres. More detailed discussions of the use of this information for cirrus cloud detection are given by Inoue (1985) and Prabhakara et al. (1988). Figure 10 shows the variation of BTD[11-12] with BT11 for clear-sky conditions computed using the LOWTRAN radiative transfer model coupled with a raob database. The axes in Figure 10 are labeled using the AVHRR nomenclature where channels 4 and 5 provide the split-window measurements (*FMFT – Four Minus Five Test*). The general increase in BTD[11-12] with BT11 is due to the natural correlation of total precipitable water with surface temperature. The black line in Figure 10 represents the threshold chosen for the CLAVR-1 algorithm. Cloudy pixels would be those that fell above the threshold.

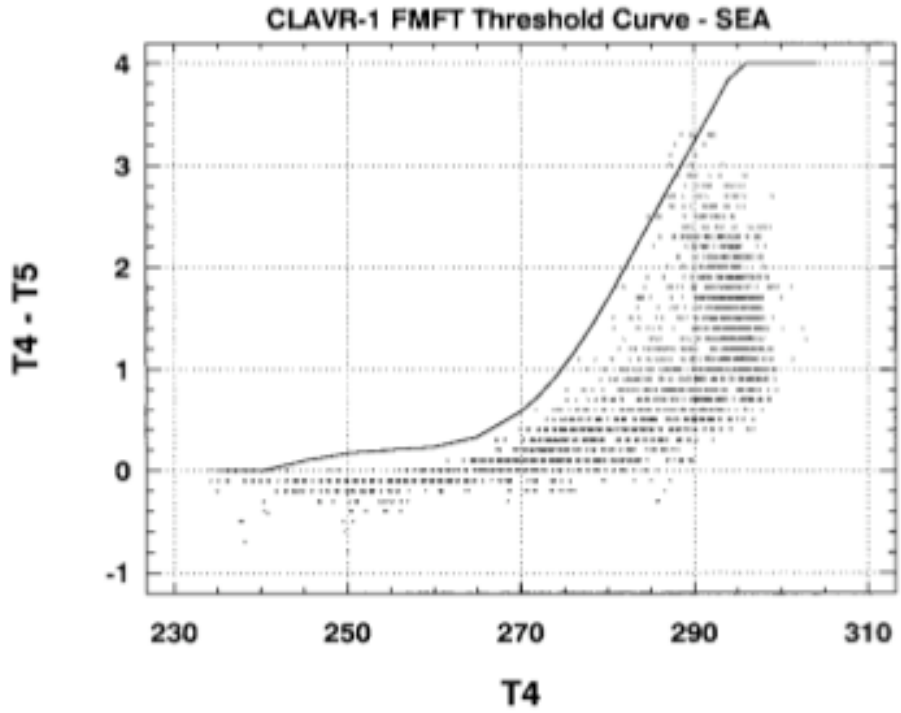

Figure **10** Variation of the 11 – 12 μm brightness temperature difference (T4 -T5) versus the 11 μm brightness temperature (T4) computed using the LOWTRAN radiative transfer model coupled with a raob database for oceanic conditions. Solid line represents CLAVR-1 threshold. (Figure taken from Stowe et al., 1999)

In the ACM, the PFMFT serves the same purpose as the FMFT in CLAVR-1 in that positive values of the BTD[11-12] are used to detect the presence of semi-transparent

cloud. Because the ACM has a clear-sky calculation of BTD[11-12] and BT11 for each pixel, it attempts to generate the test thresholds for each pixel dynamically. To do this, it assumes that the clear-sky BTD[11-12] approaches 0 K when BT11 approaches 260 K. This assumption is consistent with Figure 10. This assumption coupled with the clear-sky calculations can be used to estimate a threshold when BT11 is warmer than 260 K.

Mathematically, the estimate of the threshold, χ, is computed using the following relation

$$\chi = BTD_{11,12}^{clear}\left(BT_{11} - 260.0 \Big/ BT_{11}^{clear} - 260.0 \right)$$

where $BTD_{11,12}^{clear}$ and BT_{11}^{clear} are the computed values of BTD[11-12] and BT11 for clear-sky conditions. For pixels with values of BT11 < 260 K, χ is set to zero. The actual metric used in the ACM's PFMFT is BTD[11-12] – χ which physically represents the difference between the observed BTD[11-12] and what a clear-sky pixel should produce to be consistent with the observed BT11. The PFMFT test, though, cannot be performed on pixels with large variability (where the 3x3 11 micron BT standard deviation is larger than 0.3), warm surfaces (11 μm brightness temperatures greater than 310 K) or where the clear sky 12 μm channel BT is larger than the clear sky 11 μm BT.

Figure 11 shows the variation of the PFMFT metric for clear and cloudy conditions as determined by CALIPSO for oceanic pixels. Figure 12 shows the same computation for land pixels. As expected, this metric exhibits a significant separation for clear and cloudy pixels. While clear values hover near zero, many cloudy pixels show significant positive values that are greater than those seen for clear pixels. Figure 12 illustrates that the peak in the clear-sky distribution for land pixels is broader than that observed for clear-sky ocean pixels. This result may be a due to the larger uncertainties associated with clear radiative transfer over land than over water.

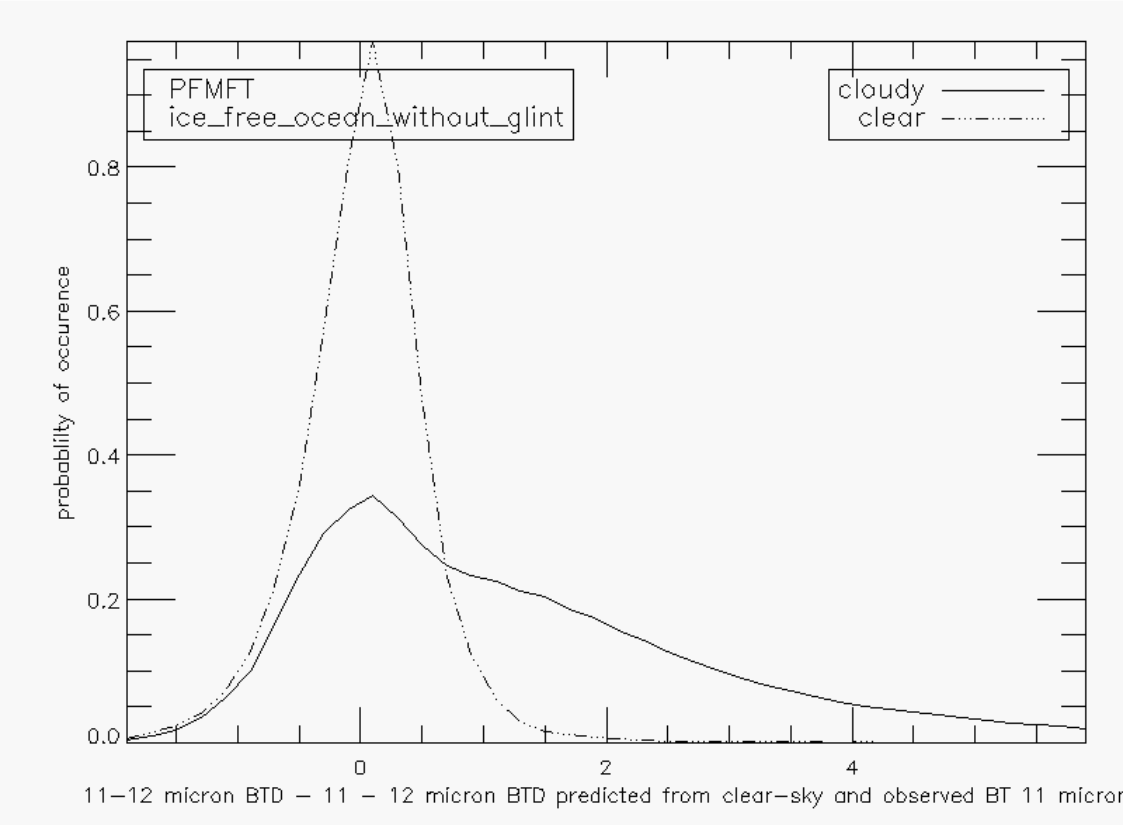

Figure 11 Variation of the PFMFT metric for clear and cloudy pixels over ocean surfaces. PFMFT metric is the observed 11-12 μm brightness temperature difference minus an estimate of the clear-sky 11-12 μm brightness temperature difference based on the clear-sky RTM and observed 11 μm brightness temperatures.

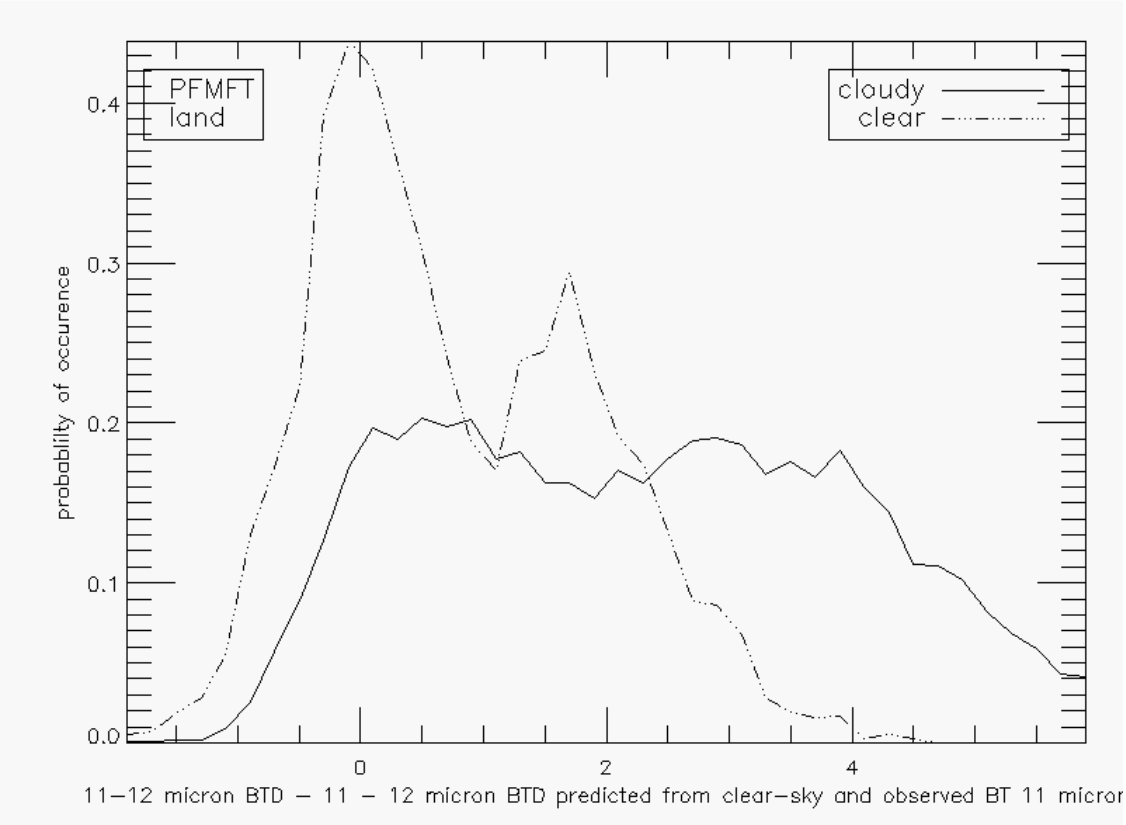

Figure 12 Same as Figure 11 for ice-free land pixels.

1.11.1.2.5 Negative Four Minus Five Test (NFMFT)

The PFMFT, described above, looks for the positive BTD[11-12] values generated by semitransparent cloud. Opaque clouds can also generate BTD[11-12] values that are less than the clear-sky estimates because opaque clouds (which typically produce a small BTD[11-12]) reside above the bulk of the water vapor that is responsible for elevated clear-sky BTD[11-12] (which arise from spectral variation of the water vapor continuum absorption). Scattering of infrared radiation may also contribute to negative BTD[11-12]. In polar regions, this test is also effective due to the positive BTD[11-12] characteristic of many snow-covered surfaces (see CASPR documentation). To exploit these characteristics, the Negative FMFT (NFMFT) test is used in the ACM.

The metric used in NFMFT is

$$\chi = BTD_{11,12}^{clear} - BTD_{11,12}$$

As defined, the presence of cloud should be represented by positive values of this metric.

Figure 13 and Figure 14 show the derived clear and cloudy distributions of the NFMFT metric for ocean and land surfaces. These distributions confirm the hypothesis that the

NFMFT metric applied under conservative thresholding can be used to detect clouds. While the amounts of cloud detected unambiguously by this test are not large, the NFMFT test provides additional information that complements information from other tests.

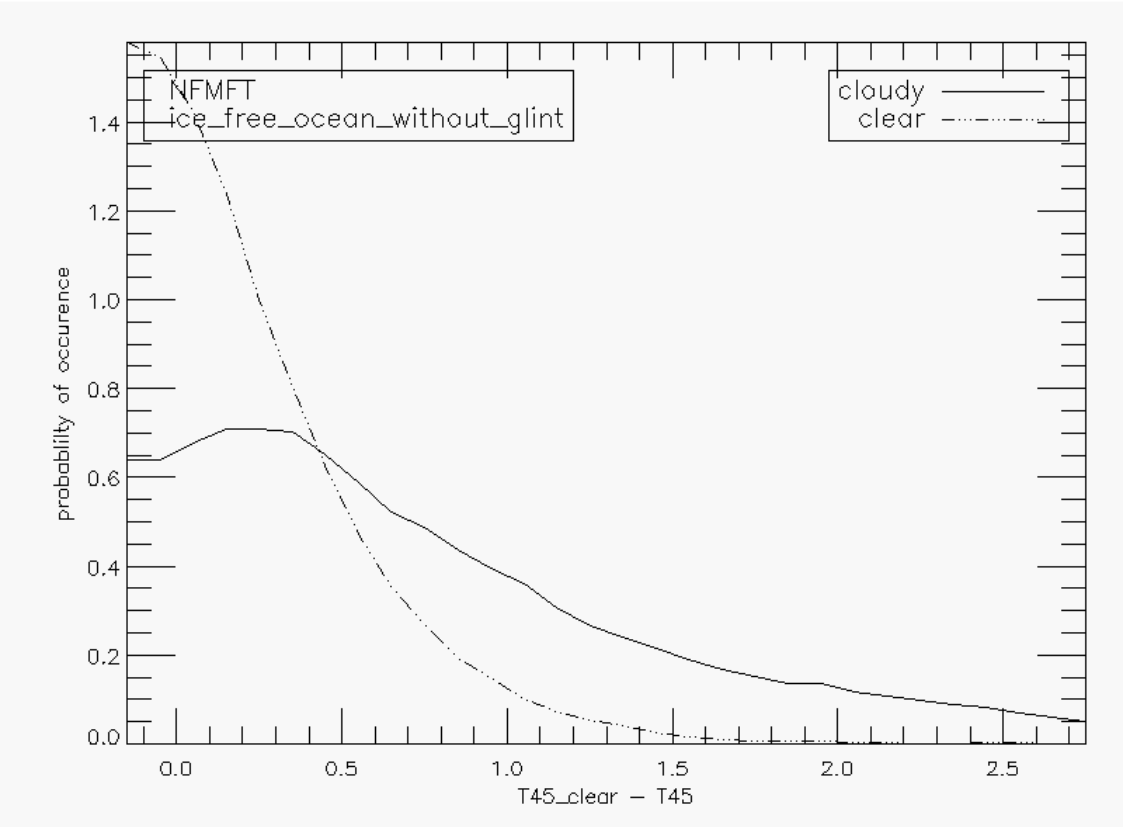

Figure 13 Variation of the NFMFT metric for clear and cloudy pixels over ocean surfaces. NFMFT metric is the computed clear-sky 11-12 μm brightness temperature difference minus the observed 11-12 μm brightness temperature.

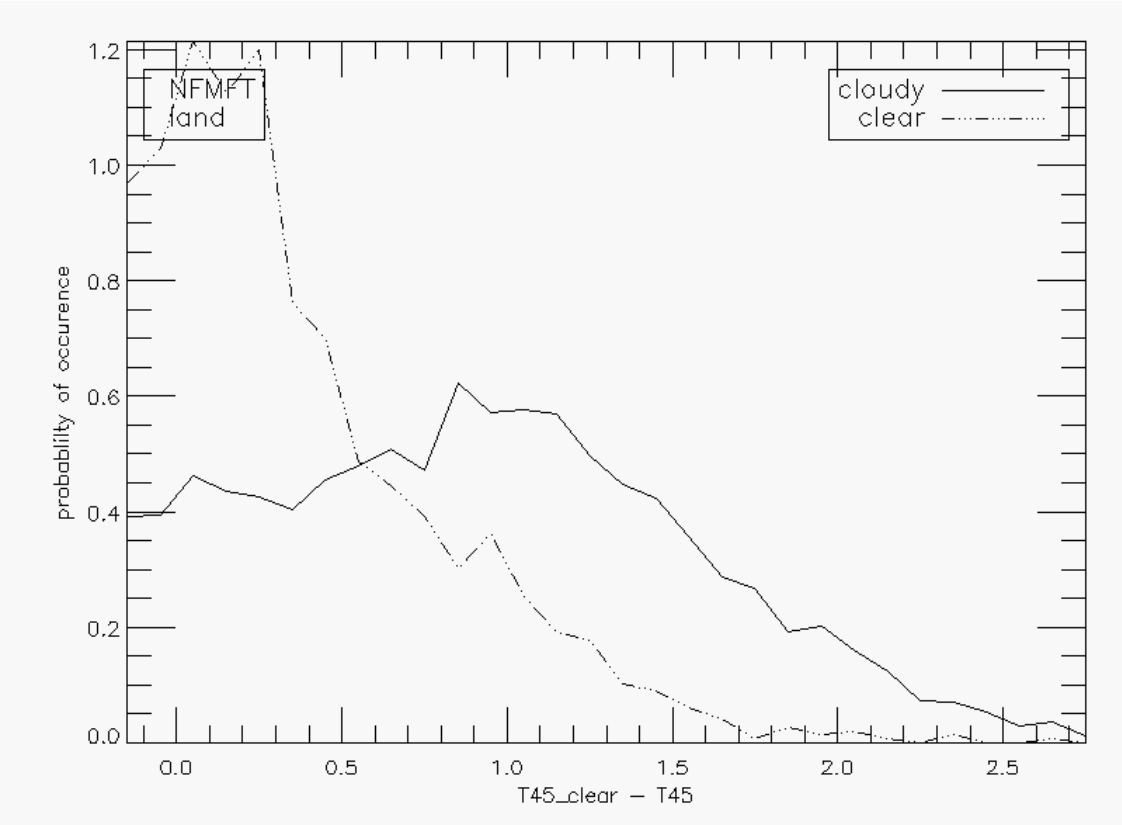

Figure 14 Same as Figure 13 for ice-free land regions.

1.11.1.2.6 Relative Four Minus Five Test (RFMFT)

The previous two split-window tests operated on the absolute difference between the observed and clear-sky BTD[11-12]. As its name implies, the Relative FMFT (RFMFT) operates on relative variations in the BTD[11-12]. While the basis for the PFMFT and NFMFT tests was the variation in BTD[11-12] for clear-sky conditions, the basis for the RFMFT is the variation in BTD[11-12] for cloudy conditions.

Figure 15 shows the variation in simulated BTD[11-12] for a single cirrus cloud viewed at nadir in a standard tropical atmosphere. The curves were generated by varying the cloud emissivity from zero (clear-sky) to unity. The three curves represent three different clouds with varying cloud temperatures and cloud microphysics. Typically these curves give maximum values of BTD[11-12] for visible (0.64 μm) optical depths of about 2. One obvious feature in Figure 15 is the rapid variation in BTD[11-12] with BT11 on either side of the maximum values of BTD[11-12]. In these simulations, BT11 will vary monotonically with cloud emissivity. Because cloud emissivity often varies significantly over small spatial scales, the correlation of BTD[11-12] with BT11 offers another signature of cloud that can be exploited in the ACM. The β parameter in Figure 15 is defined as:

$$\beta = \ln(1-\varepsilon_{12}) / \ln(1-\varepsilon_{11})$$

where ε_{11} and ε_{12} are the 11 and 12 micron emissivities.

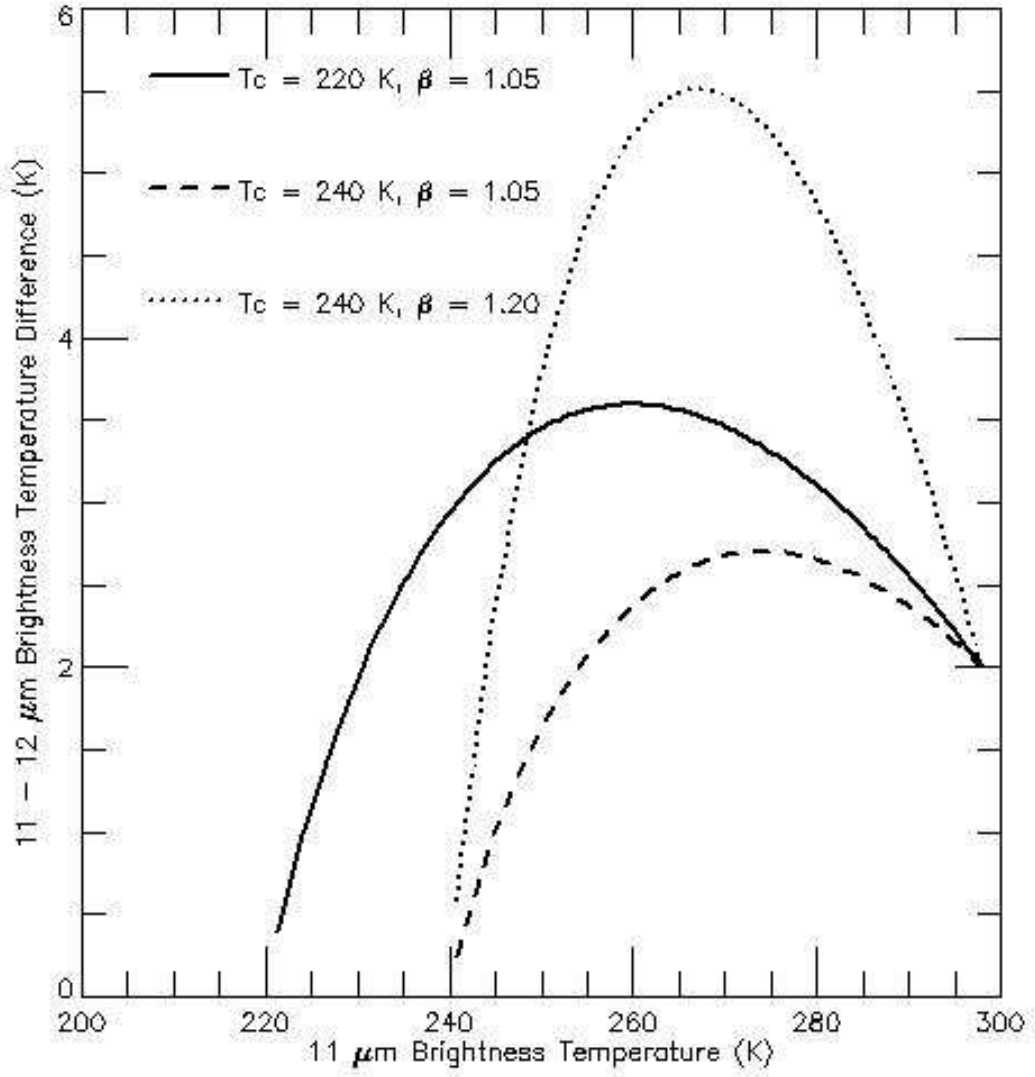

Figure 15 Variation of the 11 -12 μm brightness temperature difference as a function of the 11 μm brightness temperature computed for a single layer cirrus cloud for various cloud temperatures and cloud particle sizes. Surface temperature was 300K and the atmosphere was modeled using a standard tropical profile. (Figure taken from Heidinger and Pavolonis, 2009)

The metric used in the RFMFT is the difference in BTD[11-12] from a pixel and its neighboring warm center (NWC). The NWC point is defined as the warmest pixel (greatest BT11) in a 5x5 pixel array centered on the pixel being tested. The assumption here is that the NWC points represent the optically thinnest pixel in the local area.

Significant deviations from the BTD[11-12] at the NWC (positive or negative) should be indicative of cloud. Specifically, the metric used in the RFMFT is as follows:

$$\chi = abs(BTD_{11,12}^{nwc} - BTD_{11,12})$$

Taking thresholds on the absolute value of this difference ensures that large deviations in BTD[11-12] with respect to the NWC split window difference are captured regardless of sign.

Figure 16 and Figure 17 show the probability of occurrence of the RFMFT metric for clear and cloudy regions as determined by CALIPSO. As predicted by Figure 15, the RFMFT metric appears to offer skill at separating cloudy and clear pixels. While the PFMFT and NFMFT distributions looked quite different for land and ocean, the RFMFT distributions look very similar. This result may be due to lack of reliance on RTM calculations or due to robustness of the RFMFT metric.

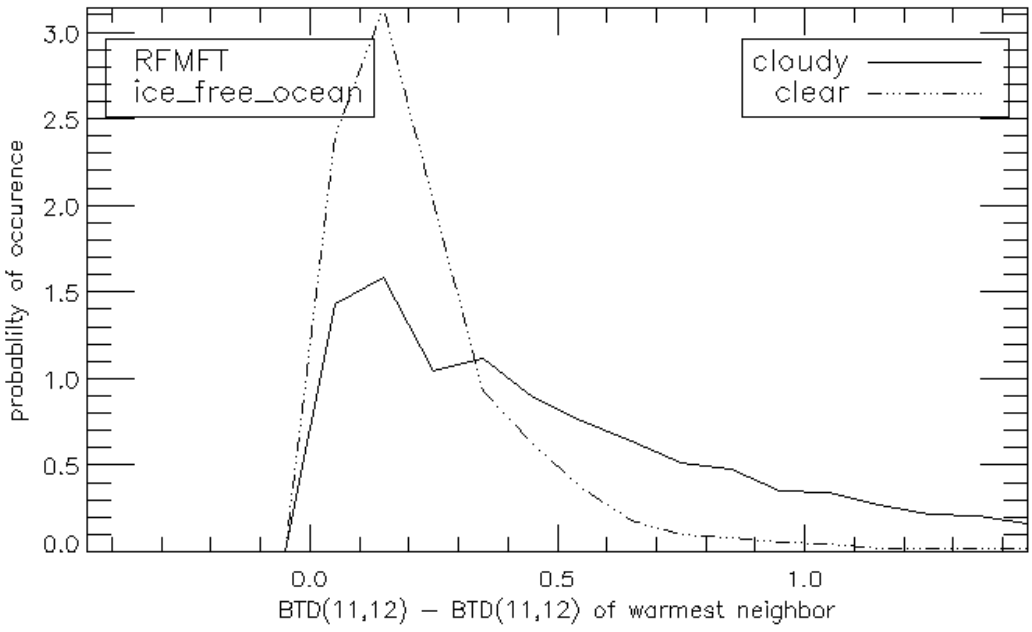

Figure 16 Probability distribution function (pdf) of the difference in the 11-12 μm brightness temperature difference observation minus the 11-12 μm brightness temperature difference observation from the neighboring warm center (NWC) for clear and cloudy pixels as determined by CALIPSO for ice-free ocean regions.

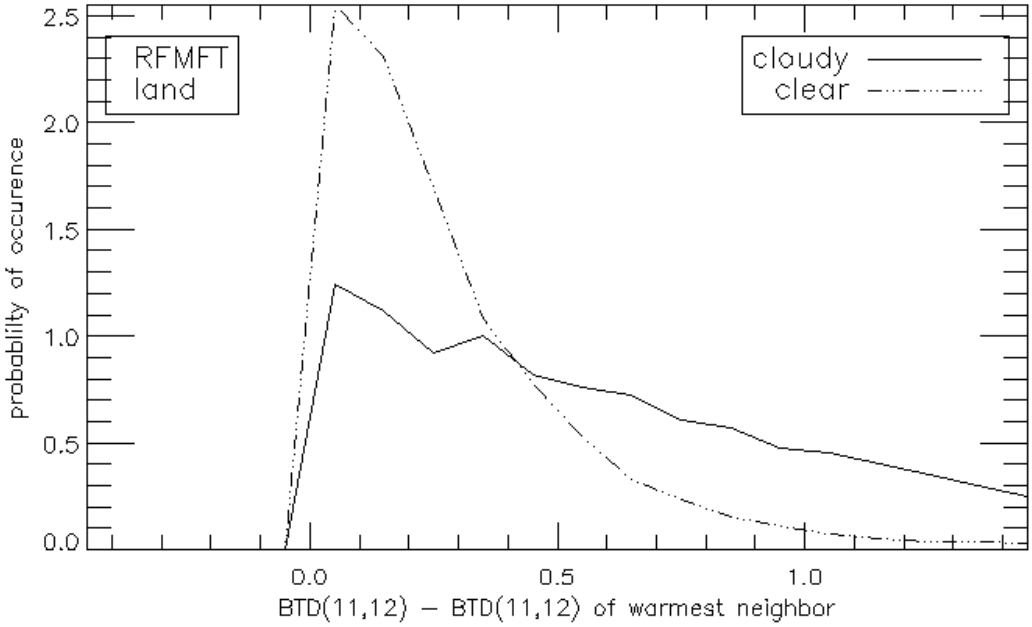

Figure 17 Same as Figure 16 for ice-free land regions.

As can be seen in the above figures, the majority of the influence of the RFMFT occurs with BTD[11-12] less than 1.0, the RFMFT is not applied to pixels with a BTD[11-12] of greater than one. Finally, due to potentially large biases of the surface temperature over land in the NWP models for extremely warm surfaces, the RFMFT test is not applied to land pixels with 11 micron BT of over 300K.

1.11.1.2.7 Cirrus Water Vapor Test (CIRH2O)

The CIRH2O test operates on the spatial correlation between an infrared window channel and an infrared water vapor channel. The physical basis is that spatial variation due to surface features should be present in the window channel, but not in the water vapor channel (which cannot see the surface due to the clear-sky atmospheric opacity). Spatial variations due to water vapor should be apparent in the water vapor channel but invisible in the window channel. In addition, the presence of upper tropospheric cloud in both channels should always result in a decrease in the brightness temperature. Therefore, spatial variations that are apparent and correlated in both the window and the water vapor channel are indicative of cloud. The use of spatial patterns in water vapor channels to detect cirrus is described by Krebs et al. (2007) for use in the Meteosat Second Generation Cirrus Detection Algorithm MeCiDA. MeCiDA operates on 15x15 arrays and does not look for correlations between channels.

The CIRH2O test operates on 3x3 arrays and uses Channel 10 for the window channel. The correlation is computed using the Pearson Correlation method and a threshold on the correlation of 0.7 was determined to be the optimal threshold for this test. Unlike the other tests, this threshold was determined via manual analysis of co-located SEVIRI and

CALIPSO data. In addition, a minimum amount of variability is required in both channels to prevent this test from falsely indentifying non-cloud features. The 3x3 standard deviations in both channels are required to exceed 0.5K before this test is applied. To avoid regions where the surface might be visible in the water channel, pixels where the slant path TPW falls below 0.30 cm are excluded. While this test uses 3x3 pixel arrays, its results apply only to the center pixel in the array. As stated above, one of the main features of this test is its insensitivity to surface effects. Therefore, there are no surface type dependent thresholds for this test.

1.11.1.2.8 Terminator Thermal Stability Test (TERM_THERM_STAB)

One of the most challenging region for cloud detection is in the terminator – the transition between day and night. In this region, the visible reflectances become unusable and the 3.9 μm channel becomes insensitive to cloud. Given the temporal stability of many cloud types (i.e., fog/low stratus), one solution to this conundrum is to exploit the temporal information provided by geostationary imagers. The TERM_THERM_STAB test is the solution developed for the ACM in the terminator region. The TERM_THERM_STAB logic is taken directly from the cloud mask run by EUMETSAT in the Nowcasting Satellite Application Facility (SAFNWC). This mask is described by Derrien et al. (2008). The SAFNWC mask employs three terminator specific techniques. We chose only to employ the temporal-differencing technique and ignored the "region growing" technique outlined in Derrien et al. (2008).

The TERM_THERM_STAB test operates on pixels with a solar zenith angle between 80 and 93 degrees. The test first looks at the cloud mask from the scene one hour earlier. If that pixel is Cloudy, then this test will return a positive result if certain spectral signatures are constant from the current scene compared to the scene one hour ago. The spectral signatures used over land differ from those used over ocean. Over land, the spectral signatures are that the Channel 14 BT change must be less than 1.0K and that the change in the Channel 14 – Channel 11 BTD must be less than 0.5 K. Over ocean the spectral signatures are that the Channel 14 BT change must be less than 1.0K and that the change in Channel 14 – Channel 15 BTD must be less than 0.6 K. Note that the original SAFNWC test also looks at the cloud-top temperature product, which is not done in our implementation.

1.11.1.3 Shortwave Infrared Cloud Detection Tests

1.11.1.3.1 4 μm Emissivity Test (EMISS4)

The 4μm emissivity test exploits the very high sensitivity of 4 μm observations (Channel 7) to the presence of cloud. Cloud detection tests in the 4 μm region often use brightness temperature differences computed from the 4 μm brightness temperature and the 11 or 12 μm brightness temperatures. The ACM employs the 4 μm emissivity, (e_4) which is computed using the following relationship.

$$e_4 = I_4 / I_{4,bb}$$

where I_4 is the 4μm observed radiance and $I_{4,bb}$, the 4μm blackbody radiance, which is calculated by substituting the 11 μm brightness temperature into the Planck function, while using the appropriate coefficients for the 4 μm channel. The ETROP test uses the following metric (χ) in the test:

$$\chi = (e_4 - e_{4,clear}) / e_{4,clear}$$

The value of $e_{4,clear}$ is an estimate of e_4 under cloud-free conditions and is computed as follows:

$$e_{4,clear} = I^{solar}_{4,clear} / I_{4,bb,clear}$$

where $I_{4,bb,clear}$ is calculated similar to $I_{4,bb}$, except using the clear sky 11 μm brightness temperature, $I^{solar}_{4,clear}$ is the clear-sky estimate of the 4 μm radiance that includes the effects of solar reflectance. $I^{solar}_{4,clear}$ is computed using the following relationship:

$$I^{solar}_{4,clear} = I_{4,clear} + (1 - e_{4,sfc}) t_{4,sfc} \mu_o F_o / \pi$$

e_{4sfc} is the 4 μm surface emissivity as provided by the SEEBOR emissivity database, $t_{4,sfc}$ is the transmission for the solar-surface-satellite path, μ_o is the cosine of the solar zenith angle, $I_{4,clear}$ is the clear sky radiance calculated by the RTM, and F_o is the integrated amount of energy in the 4 μm channel (ABI channel 7). The transmission for the solar-surface-satellite path, $t_{4,sfc}$, is calculated as follows:

$$t_{4,sfc} = trans^{\rho}_{4,rtm}$$

$trans_{4,rtm}$ is the atmospheric transmittance for channel 4 for the slant-path from the top-of-atmosphere to surface, determined by the RTM, and ρ is defined as:

$$\rho = 1.0 + \left(\frac{\cos(\theta_{sat})}{\cos(\theta_{sol})}\right)$$

where θ_{sat} is the local zenith angle and θ_{sol} is the solar zenith angle.

This particular metric was chosen to make a cloud detection test using the 4 μm channel that is largely insensitive to the solar viewing geometry. One of the main disadvantages of brightness temperature difference tests are that the observed values are impacted greatly by the solar geometry and the scene temperatures. Applying a constant brightness temperature threshold would therefore offer different sensitivity to the presence of cloud over different regions and times of day. This formulation does not remove the ambiguity that occurs in the 4 μm radiances during terminator conditions where the contribution of the observed radiance due to reflected sunlight is comparable to that due to emission. Because of that, the EMISS4 test is not applied in the glint regions as determined by the

derived glint mask. In addition, if the pixel is to warm (an 11 μm BT of 310 K), this test isn't performed.

This test has been made day/night independent, working through the terminator. As shown above, this is done by including solar energy when present in the computation of the 4 μm clear-sky radiances that are then used to compute the e_4_clear values. We divide by $e_{4,clear}$ to account for the elevated values during the day and to make this metric day/night insensitive. At night, when there is no solar component, $I^{solar}_{4,clear}$ simply becomes $I_{4,clear}$.

Figure 18 and Figure 19 show the distribution of the ETROP test metric, defined above, for clear and cloudy pixels over land and ocean. As expected, cloudy pixels give large positive values while clear-sky pixels provide values that cluster around zero. These figures show that cloudy results also provide negative values. These values typically occur for water phase clouds (i.e., fog) during the night and are the focus of the ULST test.

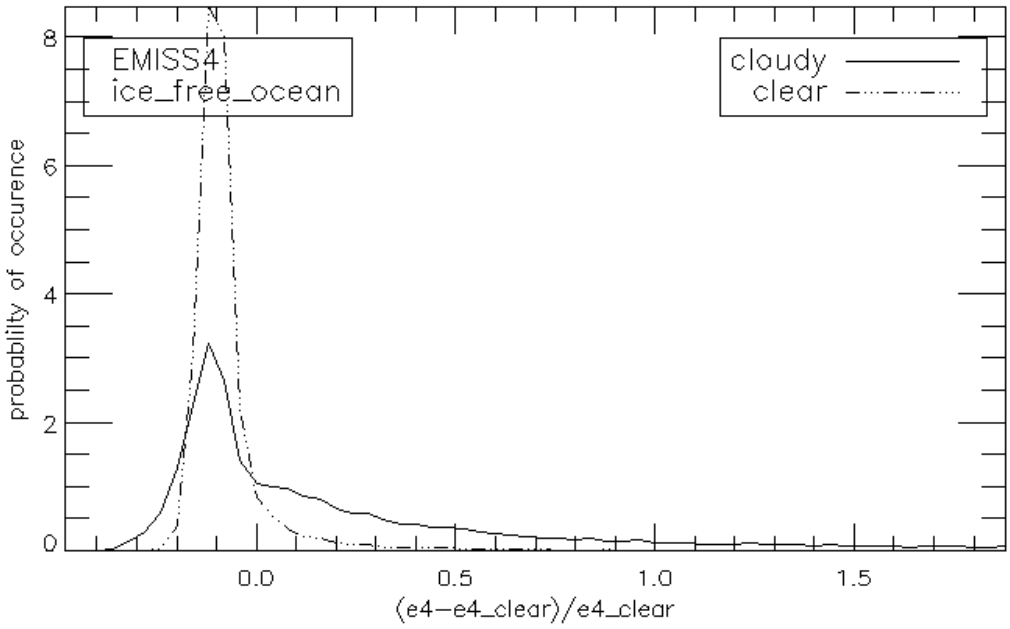

Figure 18 Probability distribution function (pdf) of the ratio of (e4-e4_clr) / e4 for clear and cloudy pixels as determined by CALIPSO for ice-free land regions. e4 is the 4 μm (Channel 7) derived emissivity and e4_clr is the channel 7 emissivity derived from the clear-sky computations.

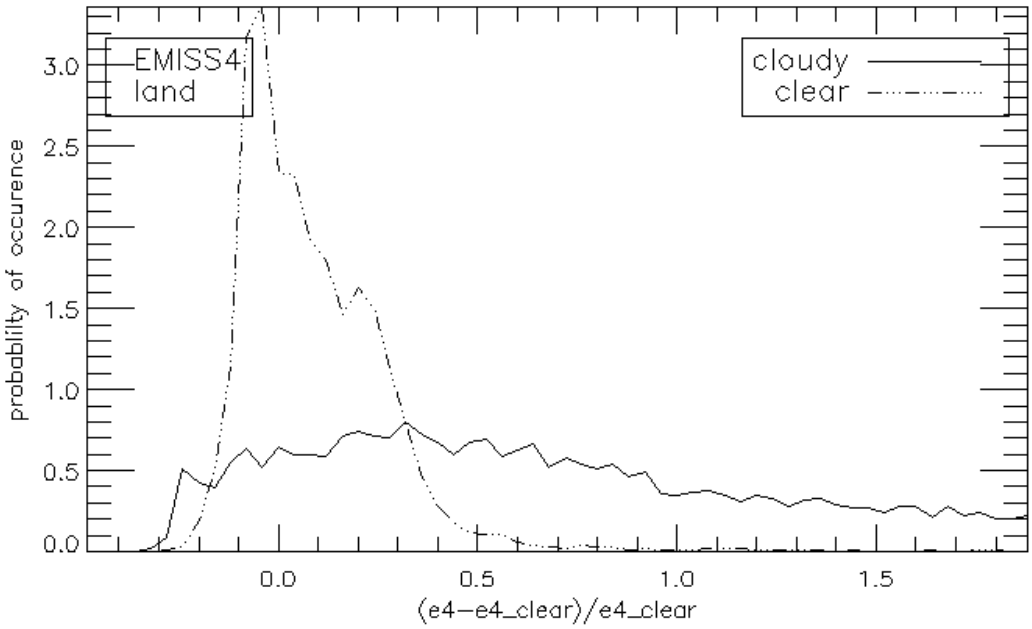

Figure 19 Same as Figure 18 for ice-free land regions.

1.11.1.3.2 ULST – Uniform Low Stratus Test

The uniform low stratus test (ULST) takes advantage of the fact that low uniform stratus clouds are more reflective (less emissive) than the surface in the 3.9 μm channel (Hunt 1973). The clear sky 3.9 μm emissivity is computed using the same formulation as given in the EMISS_4 explanation with the solar component neglected.

The ULST operates on the difference between $e_{4,clear}$, produced by the same manner as the EMISS_4 test, and e_4 only during nighttime hours. Figure 20 and Figure 21 show the distribution of the clear and cloudy values of $e_{4,clear} - e_4$ for land and ocean regions. The focus of the ULST is on pixels where the values of $e_{4,clear} - e_4$ are positive, which are due to low level and often uniform clouds such as stratus and fog. The ULST exists as a separate test from the EMISS_4 in order to provide flexibility to the fog detection algorithm run by the GOES-R AWG Aviation Team. In addition, the ULST test looks at a different metric than the EMISS_4 test and is only performed at night. This figure indicates that while the ULST will not detect a large amount of cloudiness, it should

reliably detect the specific cloud features (fog) for which it is designed.

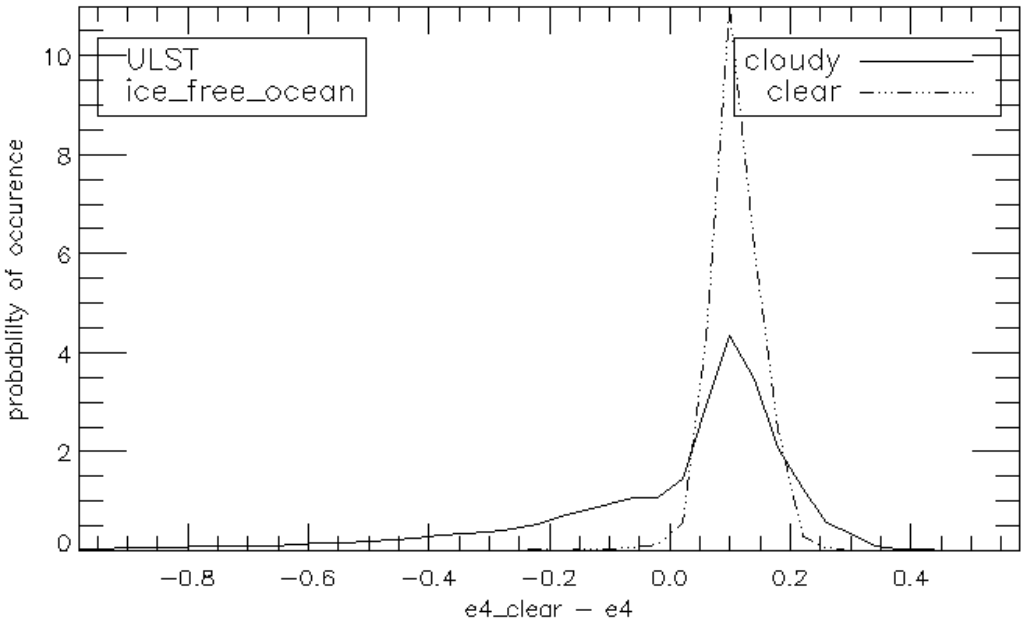

Figure 20 Probability distribution function (pdf) of the ratio of e4-e4_clr for clear and cloudy pixels as determined by CALIPSO for ice-free ocean regions. e4 is the 4 μm (Channel 7) derived emissivity and e4_clr is the channel 7 emissivity derived from the clear-sky computations

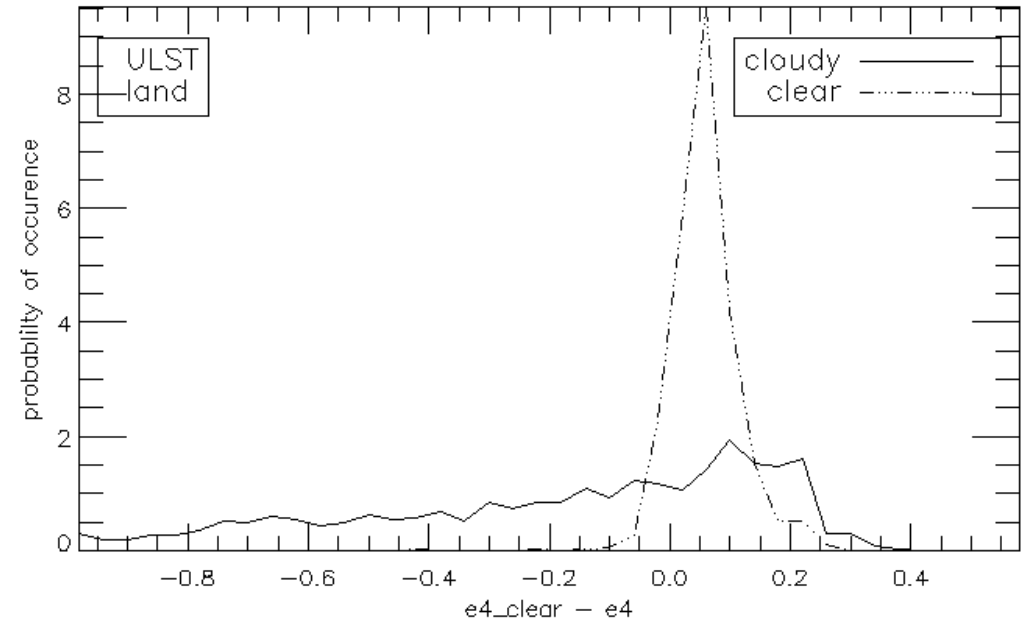

Figure 21 Same as Figure 20 for ice-free land regions.

Because of the sensitive nature of this test, pixels that are to warm (11 micron BT of greater than 290K), are cold surfaces (as determined by the cold surface masked described in section), have large measured 3.9 micron emissivities (.95 or greater), have high surface 3.9 micron emissivities (0.90 and greater) or have suspect clear sky emissivities (less than 0.85 or greater than 1.25) do not have this test performed.

1.11.1.4 Solar Reflectance Cloud Detection Tests

1.11.1.4.1 RGCT – Reflectance Gross Contrast Test

The Reflectance Gross Contrast Test (RGCT) works on the assumption that clouds exhibit larger values of the visible reflectance than clear sky. Currently, the ACM applies a threshold to the 0.65 μm reflectance (Channel 2) over land and water. This test is not applied over known snow/ice surfaces and is not applied when the solar zenith angle exceeds 80^o or for pixels located in sun glint regions, which are areas with glint angles of greater than 40^o. In addition, it is not applied through pixels where the reflected energy back to the imager goes through a large amount of the atmosphere, which occurs at solar zenith angles greater than 87^o. These restrictions seek to avoid the limb brightening affects that occur at large local zenith angles.

The metric used by the RGCT is the difference in the observed 0.65 μm reflectance and the computed clear-sky value. The clear-sky value is computed by modifying the assumed clear-sky 0.65 μm surface reflectance values to include the effects of gaseous absorption (water vapor and ozone) and the effects of Rayleigh and aerosol scattering. This computation is described in a later section. The source of the surface reflectance data over land is the MODIS white-sky albedo (Moody et al, 2008) ancillary dataset which is sampled to a resolution of 5 km for use in the ACM. Operationally this test will either use the clear sky composite produced by the Land AWG team or the global MODIS white-sky albedo ancillary dataset, as a backup. A nearest neighbor sampling method, namely the MODIS point with the closest distance to the imager point, is used to interpolate to each pixel. Over the ocean, a surface reflectance of 5% is assumed. It is important to note the effects of glint are not captured in this computation and the white-sky albedo product does not simulate the reflectance for a given viewing geometry. However, use of this product has proven to add skill over that provided by fixed land or surface-type based surface reflectance values.

Figure 22 and Figure 23 give the distributions of the difference of the observed minus the clear sky values of the 0.65 μm reflectance computed for clear and cloudy pixels as determined by CALIPSO. As expected, the cloudy distributions range over larger values than those seen for clear pixels, which indicate definite skill at unambiguous cloud detection. However, the CALIPSO cloudy distributions do indicate that many cloudy pixels have reflectance very near that predicted for clear conditions especially over the ocean. Whether this is due to true presence of very thin cloud or due to a difficulty in daytime cloud detection by CALIPSO is still to be determined.

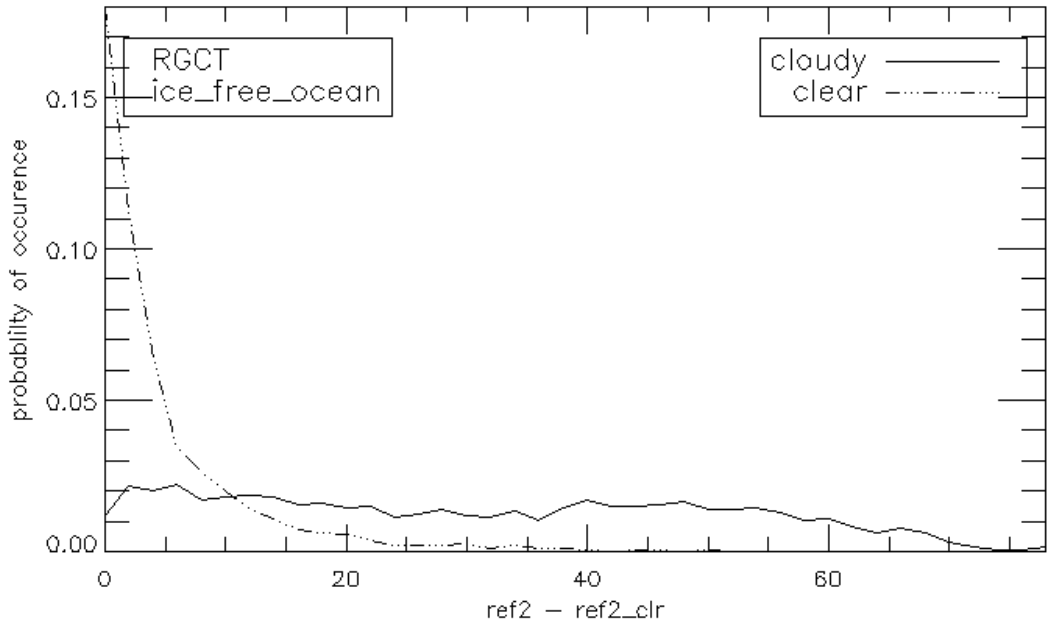

Figure 22 Probability distribution function (pdf) of the difference between the observed 0.65 µm (Channel 2) reflectance and the computed clear-sky value for ice-free ocean pixels.

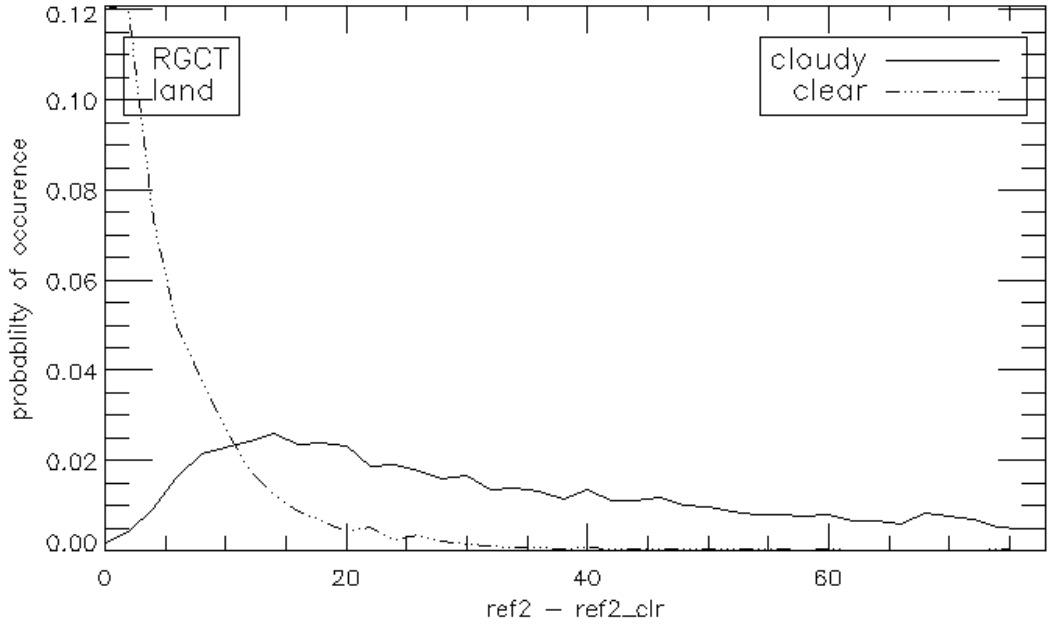

Figure 23 Same as Figure 22 for ice-free land pixels.

1.11.1.4.2 RVCT - Relative Visible Contrast Test

The Relative Visible Contrast Test (RVCT) is a solar-reflectance analog to the RTCT. The basic premise of the RVCT is that over a small region pixels that are much brighter than the darkest pixel in the neighborhood are likely cloudy. The RVCT metric used in the ACM is the observed 0.65 μm reflectance minus the minimum value observed over a 3x3 pixel array centered on the pixel being tested. The targeted cloud features of the RVCT are small scale clouds and cloud edges. However, care must be exercised to avoid the false detection of cloud in the presence of coasts and other strong surface reflectance gradients. Therefore the test is not applied over known snow/ice surfaces (based on ancillary data) or coastal regions, as the variability in the surface reflectance is too great. In addition, the RVCT has angular restrictions where the scattering is too great, where the scatting angle is larger than 90^o. Finally, the RVCT is not applied where the reflected energy back to the imager goes through a large amount of the atmosphere, which occurs at solar zenith angles greater than 83^o. The benefit of this test is that it is not dependent on knowledge of the surface reflectance.

Figure 24 and Figure 25 show the distribution of the RVCT metric computed for clear and cloudy pixels as determined by CALIPSO for ocean and land pixels. As expected, there is a separation of the clear and cloudy distributions with clear values being centered close to zero and cloudy values distributed over larger values. Therefore, it does appear that the RVCT offers skill in unambiguous cloud detection.

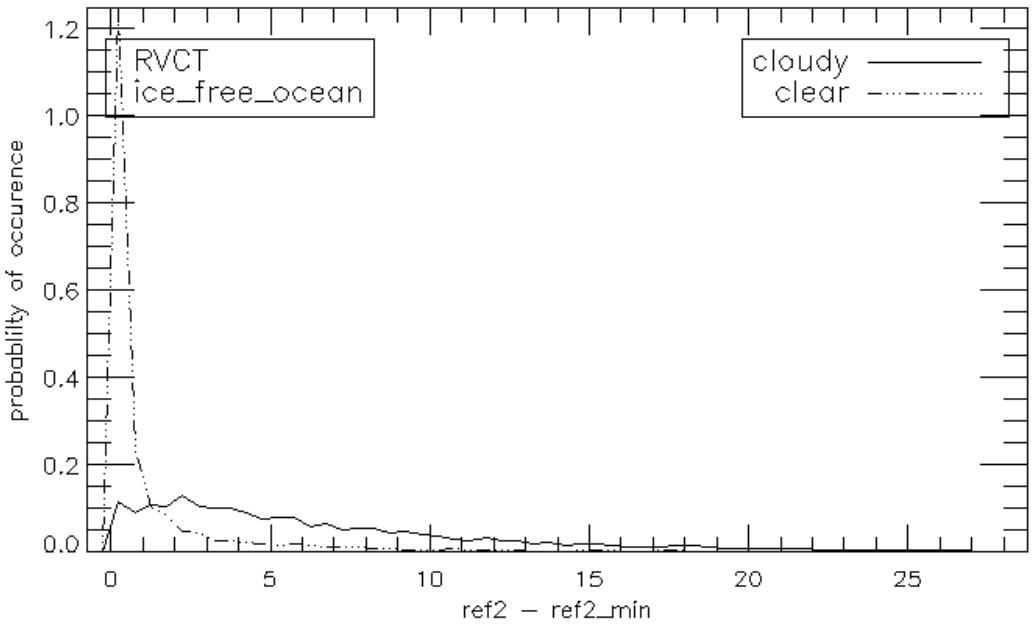

Figure 24 Probability distribution function (pdf) of the difference between the observed 0.65 μm (Channel 2) reflectance and the minimum value detected over a 3x3 pixel array for ice-free ocean pixels.

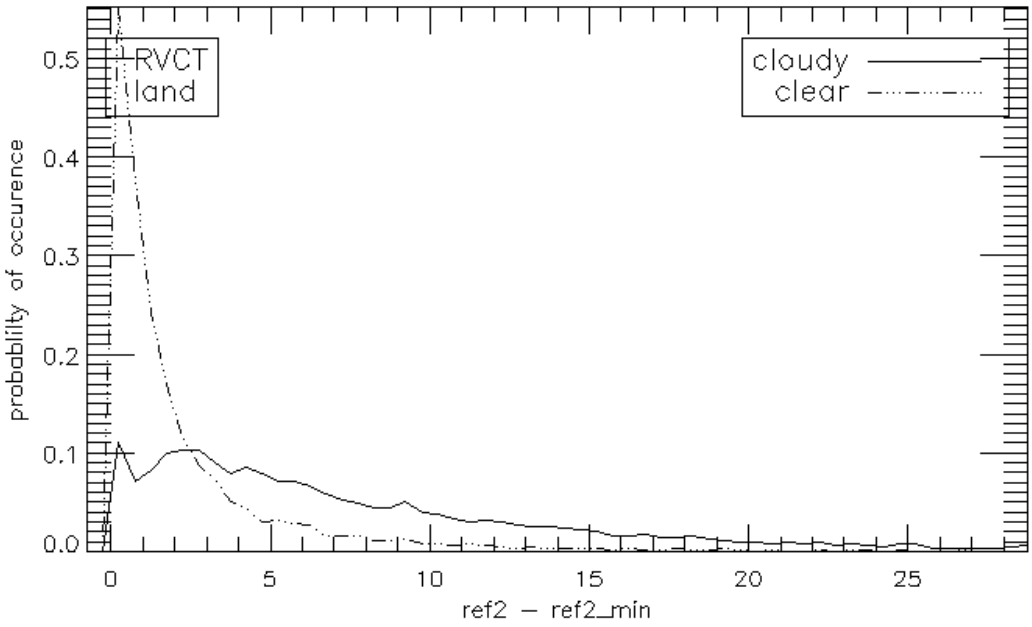

Figure 25 Same as Figure 24 for ice-free land regions.

1.11.1.4.3 NIRREF – Near Infrared Reflectance Test (1.6 μm)

Due to significant differences in the imaginary indices of the refraction index of water and ice in some regions of the near-infrared (NIR) spectrum, NIR reflectances are useful for detecting water cloud on top of snow and ice covered surfaces. The NIR channels, particularly the 1.6μm reflectance are useful in discriminating between snow and clouds, as snow has very low 1.6μm reflectance, while the 1.6μm reflectance of clouds remains high. Consequently, both cirrus and optically thick water clouds can be directly classified and distinguished from snow using the 1.6μm channel (Warren, 1982). In fact, the usefulness of the 1.6μm channel has been demonstrated on both the operational Landsat Thematic Mapper satellite (Dozier, 1989; Baglio, 1989) as well as the AVHRR instrument. In addition, because of the strong signal of snow in the 1.6μm reflectance, it is also used to calculate the Normalized Difference Snow Index (NDSI). Thus, the 1.6μm reflectance is a useful test for clouds over snow.

Should the 1.6 μm reflectance not be available and the 3.9 μm reflectance is available, this test can also use the 3.9 μm reflectance.

However, there are some drawbacks to this test, such as prior knowledge of which pixels contain snow and which are snow-free, information provided by the snow mask described in section 3.3.2. In addition, there are issues at surface elevations (over 1000 m) as well as coastal pixels, as defined by the coast mask; thus, this test is not performed in these areas. Finally, this test cannot be performed in high solar zenith angle regions.

For options, each pixel is tested to see if the pixel is snow, has a solar zenith angle of less than 80^o and a surface height of less than 1000m.

If the test uses the 1.6 μm reflectance, the NDSI is then calculated

$$NDSI = \frac{R_{0.64} - R_{1.6}}{R_{0.64} + R_{1.6}}$$

where $R_{0.64}$ is the 0.64 μm reflectance and $R_{1.6}$ is the 1.6 μm reflectance. The NDSI is tested to see if the pixel is below the maximum NDSI threshold of 0.5. If it is, the 1.6 μm reflectance for the pixel is tested to see if it is above the threshold for cloud over snow and to see if the pixel is not a coastline.

If the 1.6 μm channel is not available, then after checking the solar zenith angle, snow mask and surface height, the 3.9 μm reflectance is tested to see if the 3.9 μm reflectance is above the threshold for cloud over snow.

The threshold for both the 1.6 and 3.9 μm reflectance versions of the NIRREF test is 15%/

1.11.1.4.4 CIRREF – Cirrus Reflectance Test (1.38 μm)

The 1.38 μm channel on MODIS has been used successfully to detect thin cirrus (Ackerman et al., 2002). The 1.38 μm channel resides in a strong water vapor absorption band that masks the surface under most conditions. The ACM test is based on the MODIS (MOD35) test (Ackerman et al., 2002) and uses a 1.38 μm reflectance threshold of 5%. The test is applied to all pixels that have a solar zenith angle of less than 80^o, that are not in surface height, with a maximum surface height in the surrounding 3x3 box of less than 2000m, and are not snow. Simulated ABI data will be used to verify the operation of this test before launch.

1.11.1.5 Clear Sky Uniformity Tests

The clear-sky uniformity tests act as filters of the clear pixels to identify clear pixels that reside in regions of high spatial heterogeneity and reclassify them as probably clear. The assumption is that the presence of cloud will increase the local spatial heterogeneity beyond the values expected for clear sky. Currently, the ACM uses two tests for spatial heterogeneity which are described below.

1.11.1.5.1 Reflectance Uniformity Test (RUT)

The RUT is a daytime test based on the local standard deviation of the observed 0.65 μm reflectance computed for a 3x3 box surrounding each pixel. If the standard deviation is greater than a threshold, a non-clear result is obtained. The physical basis is the assumption that clear regions should exhibit relatively spatially uniform reflectivity over land and ocean. In an attempt to make the RUT independent of the surface reflectance, the RUT metric is the ratio of the 0.65 μm reflectance standard deviation divided by the computed clear-sky reflectance and is expressed as a fraction (0-1). Because of the non-uniformity of coasts and snow, this test is not applied on those pixels. In the case of RUT and TUT (below), the standard deviations are always computed using 3x3 pixel arrays. No attempt is made to adjust the resolutions to account for the actual pixel resolution, which is a function of zenith angle.

In the ACM, the RUT is applied to the 0.65 μm reflectance standard deviation computed over a 3x3 pixel array divided by the computed clear-sky 0.65 μm reflectance for daytime pixels with solar zenith angles out to 80.0 degrees. Figure 26 shows the variation of this quantity for land and ocean pixels plotted as a variation of the collocated CALIPSO cloud fraction. As stated above, the goal of the RUT is to separate truly clear pixels from those that are cloud contaminated. An appropriate threshold for the RUT is given by the value for CALIPSO cloud fractions of zero (the most clear of pixels). This analysis shows that the RUT, as formulated here, is indeed insensitive to the underlying surface reflectance. Based on the analysis in Figure 26, the ACM uses a threshold 0.20 of for the RUT for land and 1.0 for ocean pixels. In addition, the RUT is not performed on pixels with a solar zenith angle of greater than 80^{o}.

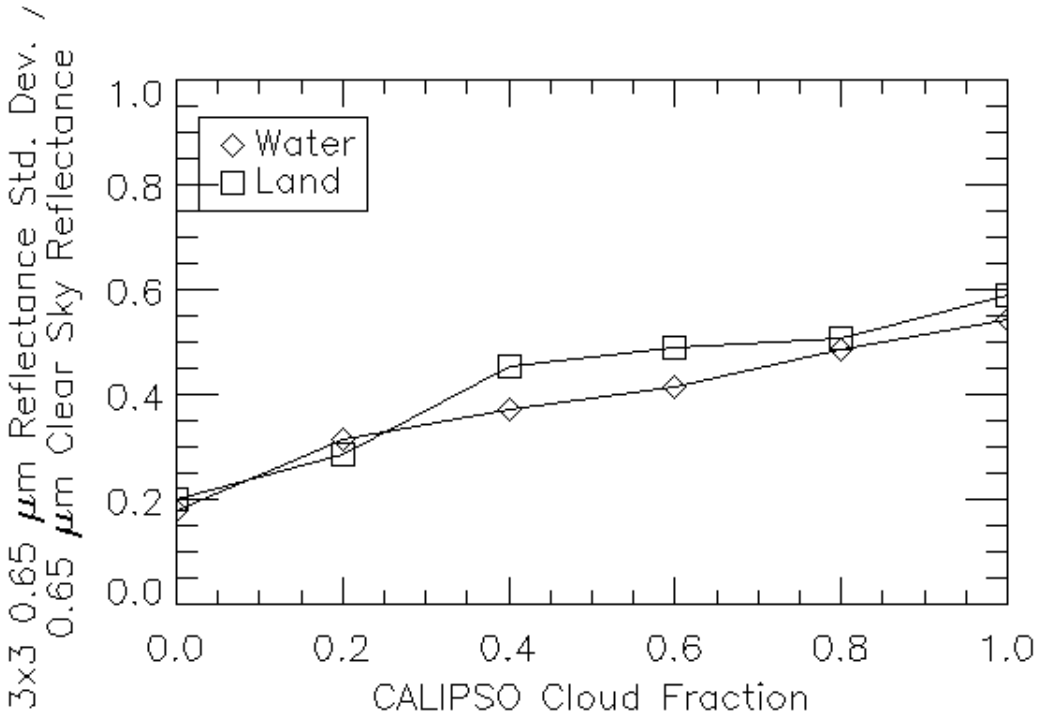

Figure 26 Variation of the standard deviation of the 0.65 μm reflectance computed over a 3x3 pixel array divided by the computed clear-sky reflectance as a function of the CALIPSO cloud fraction. Results are separated for land and ocean pixels.

1.11.1.5.2 Thermal Uniformity Test (TUT)

The thermal analog to the RUT is the TUT (Thermal Uniformity Test) and is based on the standard deviation of the observed 11 μm brightness temperature computed on a 3x3 box surrounding each pixel. If the standard deviation is greater than a threshold, a non-clear result is obtained. Again, because of the fact that coasts are inherently non-uniform, no coast pixels are used in this test. The thresholds used are increased by the value of $3.0*\Gamma*Z\_std$ where Γ is the lapse rate (7.0 K/km) and Z_std (km) is the 3x3 standard deviation of the surface elevation. The factor 3 accounts for the fact we are assuming a 3-σ departure from the mean elevation.

Figure 27 shows the variation of the 3x3 11 μm brightness temperature standard-deviation as a function of CALIPSO cloud fraction. Based on the goal of separating truly clear pixels from those with cloud contamination, thresholds of 0.6 for water and 1.1 for land pixels were chosen as the TUT thresholds.

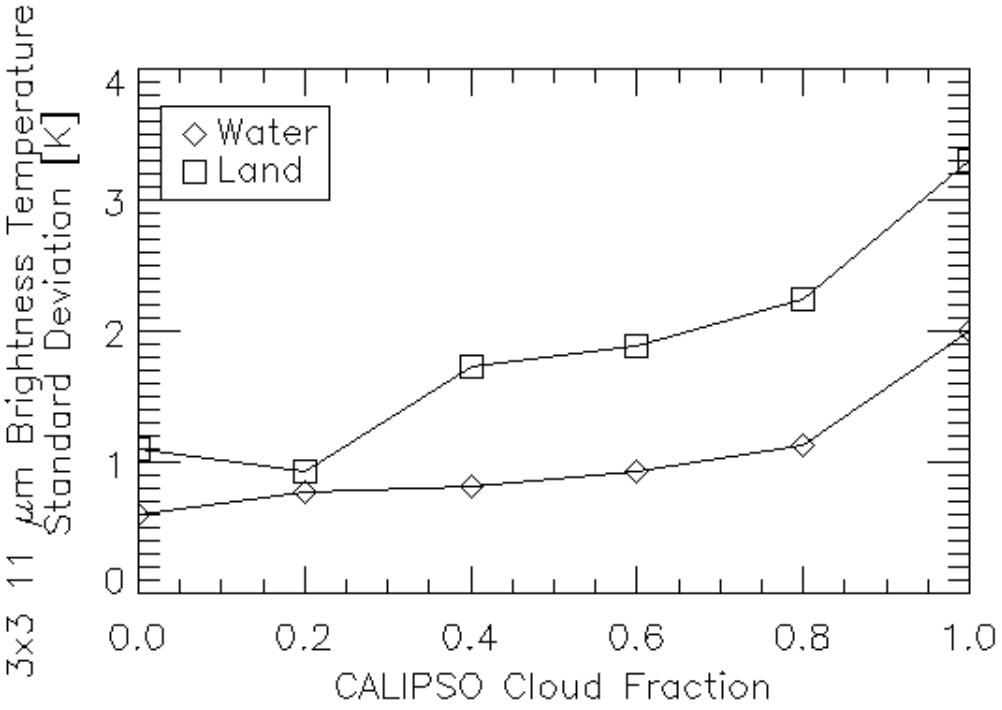

Figure 27 Variation of the standard deviation of the 11 μm brightness temperature computed over a 3x3 pixel array as a function of the CALIPSO cloud fraction. Results are separated for land and ocean pixels.

1.11.1.6 Clear-sky Restoral Tests

The function of the clear-sky restoral tests is to "restore" probably clear pixels to the clear condition. These tests are used primarily to identify probably clear and probably cloudy pixels. In and of itself, spatial heterogeneity is not an unambiguous indication of cloud. For example, thermal fronts on the ocean surface will present gradients in the 11 μm brightness temperature on the order of are seen in cloud edges. Therefore, this test assumes that probably-clear pixels that occur in regions where no cloud detection test was able to detect cloud should be classified as clear. For the current version of this test, these regions are defined as a 5x5 box around each pixel is considered. It is important to note that while the results of this test and of the clear-sky uniformity tests are included in the output users can ignore the clear-sky restoral results, if desired.

1.11.1.6.1 Probably-Cloudy Restoral Tests

The purpose of the Probably Cloudy Restoral test is to classify cloud edges as being probably cloudy. This knowledge is useful for subsequent applications that need to ascertain the confidence of whether a pixel is truly cloud filled. For this test, if a clear or probably clear pixel exists within the 3x3 pixel array centered on a cloudy pixel, that cloudy pixel is reclassified as probably cloudy.

1.11.2 Radiative Transfer Computations for Channel 2

As described above, the RGCT test operates on the observed Channel 2 reflectance and an estimate of its value under clear conditions. This section describes that computation of the clear-sky Channel 2 reflectance. Note, future implementations of the AIT framework may include versions of the CRTM that provide this functionality.

1.11.2.1 Rayleigh Scattering

The Rayleigh or molecular scattering optical is taken from the cloud mask threshold include file and is not computed during execution. For ABI, we have estimated that the total in-band to Channel 2 Rayleigh optical depth is approximately 0.05. The Rayleigh phase function is used to account for the angular distribution of the Rayleigh scattering.

$$P_{Ray} = 0.75(1+\mu^2)$$

where μ is the cosine of the scattering angle where scattering angle is defined by the solar and viewing geometries.

1.11.2.2 Aerosol Scattering

To model the aerosol scattering, a Henyey-Greenstein phase function was assumed as illustrated below.

$$P_{aer} = (1+g_{aer}^2) \Big/ (1+g_{aer}^2 - 2g_{aer}\mu)^{3/2}$$

In the above equation, g_{aer} is the asymmetry parameter. The single scatter albedo ($\omega_{o,aer}$), g_{aer} and total column aerosol optical depth, τ_{aer}, are provided in the cloud mask threshold include files.

1.11.2.3 Gaseous Absorption

The main absorbing gases in Channel 2 are water vapor and ozone. The total column optical depths (t) are computed using polynomial regressions based on the total precipitable water (TPW) and total column ozone (TOZONE).

$$\tau_{h_2o} = a + b(TPW) + c(TPW^2)$$

$$\tau_{o_3} = a + b(TOZONE) + c(TOZONE^2)$$

The coefficients (a,b,c) for the water vapor and ozone optical depth regressions were computed using MODTRAN4 and the assumed ABI Channel 2 spectral response functions. For use in this routine, the ozone and water vapor optical depths are combined in one gaseous optical depth, τ_{gas}.

$$\tau_{gas} = \tau_{h_2o} + \tau_{o_3}$$

1.11.2.4 Computation of Clear-sky Reflectance

The computation of the clear-sky Channel 2 reflectance is done by combining a single scattering approximation coupled with an isotropic two-stream approximation. This formulation is a modified version of that used by the MODIS Atmospheres Science Team and described by Wang and King (1997).

To compute the clear-sky reflectance, several intermediate terms are needed. First, a total optical depth, τ_{total}, is computed from the Rayleigh, aerosol and gas optical depths.

$$\tau_{total} = \tau_{Ray} + \tau_{aer} + \tau_{gas}$$

In addition, a total optical depth for isotropic scattering computed as follows

$$\tau_{iso,total} = \tau_{Ray} + (1 - g_{aer})\tau_{aer} + \tau_{gas}$$

where the aerosol optical depth is scaled by $1 - g_{aer}$. The effective single scatter albedo, ϖ_o, of the entire column is computed as

$$\varpi_o = (\varpi_{o,aer}\tau_{aer} + \tau_{ray}) \Big/ \tau_{total}$$

and the effective phase function, P, of the entire column is computed as

$$P = (\varpi_{o,aer}\tau_{aer}P_{aer} + \tau_{Ray}P_{Ray}) \Big/ \tau_{scat,total}$$

where $\tau_{scat,total}$ is the total scattering optical depth.

$$\tau_{scat,total} = \tau_{Ray} + \omega_{o,aer}\tau_{aer}.$$

The Channel 2 clear-sky reflectance, $R_{2,clear}$ is computed from three terms. The first term, R_a, accounts for the single scattering contribution of the atmosphere. R_a is computed using the following relation

$$R_a = \varpi_o P \Big/ (4m\mu_v\mu_o(1 - T_{ss}))$$

where m is the airmass factor ($1/\mu_v + 1/\mu_o$), and T_{ss} is the single-scattering transmission term computed as

$$T_{ss} = e^{-(\tau_{total}/\mu)}.$$

The second term, R_b, accounts for the contribution of reflectance scattered in the atmosphere and then scattered off the surface and is computed as follows

$$R_b = \tau_{iso,scat,total} \Big/ (2\mu_o)\, T_{iso,total,view}\alpha_{sfc}$$

where α_{sfc} is the surface albedo and $T_{iso,total,view}$ is the transmission term computed along the viewing direction assuming isotropic scattering.

$$T_{iso,total,view} = e^{-(\tau_{iso,total}/\mu)}$$

The third term, R_c, is the contribution of reflectance scattered off the surface from the direct solar beam and then scattered in the atmosphere. This term is given by

$$R_c = \tau_{iso,scat,total} \Big/ (2\mu_v)\, T_{iso,total,sun}\alpha_{sfc}$$

where

$$T_{iso,total,sun} = e^{-(\tau_{iso,total} / \mu_o)}.$$

The final clear-sky Channel 2 reflectance is computed simply as

$$R_{2,clear} = 100(R_a + R_b + R_c)$$

where the factor converts the reflectance to a percentage.

1.11.2.5 Renormalization of Reflectances in the Terminator Region.

Following a method given by Li and Shibata (2006), the ACM renormalizes reflectance values in the terminator region. This is performed when the solar zenith angle value is greater than a value stored in the thresholds file. This value is currently set to 60.0 degrees. The new normalized reflectance is given by

$$R = \mu R_\mu \frac{24.35}{2\mu + (498.5225\mu^2 + 1)}$$

where R_μ is the standard reflectance, and μ is the cosine of the local zenith angle. This equation corresponds to Eq (9) in Li and Shibata (2006). The goal of this renormalization is to improve accuracy for values of the solar zenith angle near 90 degrees.

1.11.3 Mathematical Description

1.11.3.1 Computation of Binary Cloud Mask

The main product of the ACM is the binary cloud mask. A clear classification is given to pixels where the 4 level cloud mask is clear or probably clear. A cloudy classification is given to pixels that the 4 level cloud mask indicates cloudy or probably cloudy. This computation is used in the validation methodology.

1.11.3.2 Computation of 4-level Mask

As stated above, the official outputs of the ACM are the binary (yes/no) decisions for each test. The final 4-level cloud mask is determined solely from the individual yes/no decisions. The current logic to derive the final 4-level cloud mask is given by the figure below. Currently, it takes only one positive result of any cloud mask test to produce a cloudy or probably cloudy result.

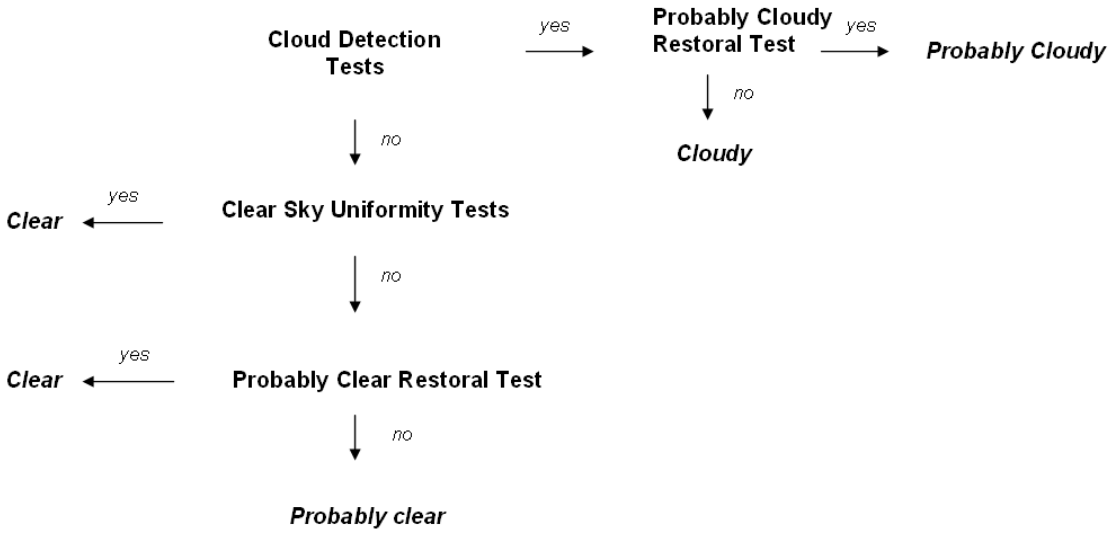

Figure 28 Schematic illustration of the logic employed to derive a 4-level cloud mask (clear, probably clear, probably cloudy and cloudy) from the individual tests results.

1.11.3.3 Computation of Thresholds for Cloud Mask Tests

As shown in Sections 3.4.2, the cloud mask tests used in the ACM do provide some skill at separating clear from cloudy pixels. This section explains how specific thresholds were selected. As stated above, the philosophy of the ACM is to use multiple tests that are sensitive to different characteristics of cloud to achieve the specified performance. An inherent assumption is that the thresholds for each test are set conservatively to ensure a minimal rate of false detection. No test is expected to detect all clouds nor is any one test allowed to have significant false detection rates.

To demonstrate the impact of threshold selection on the performance of the cloud mask test, Figure 29 shows the variation of false and true cloud detection rates for the ETROP test over the ice-free ocean. Figure 29 is derived from the pdfs shown in Figure 2. True cloud detection rate is defined as the percentage of all pixels that are correctly detected as cloud. False cloud detection rate is defined as the percentage of pixels that are falsely detected as cloud. The threshold in the ETROP is the derived Channel 14 emissivity referenced to the Tropopause. As the threshold increases, the false cloud rate and true cloud rate decrease. For a threshold set to a value on the left side of the figure (say -0.5), the true and false cloud rates sum to 100%. For threshold values large enough that no clouds are detected, both the true and false cloud rates are zero.

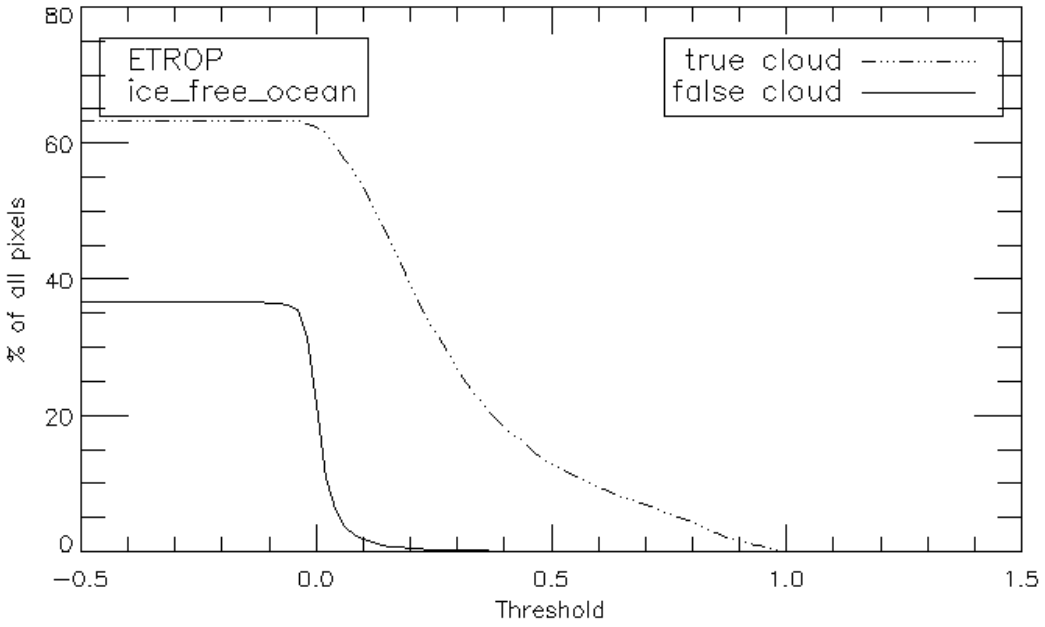

Figure 29 Illustration of the variation of true cloud and false cloud detection rates for the ETROP test applied over ice-free ocean. True cloud detection rate is defined as the percentage of all pixels that are correctly detected as cloud. False cloud detection rate is defined as the percentage of pixels that are falsely detected as cloud. The threshold in the ETROP is the derived Channel 14 emissivity referenced to the Tropopause. As the threshold increases, the false cloud rate and true cloud rate decrease. For a threshold set to value on the left side of the figure, the true and false cloud rates sum to 100%. The goal of the ACM is to minimize false detection while maintaining sufficient true detection rates.

The goal of the ACM is to minimize false detection while maintaining sufficient true detection rates. As Figure 29 shows, there is a range in ETROP threshold where the false cloud rate approaches zero and the true cloud rate remains well-above zero. In the ACM, the threshold is selected by its value of false cloud detection rate. In order to select the optimal false cloud detection rate, the Probability of Correct Detection (POD) for the combined binary mask was computed as a function of the allowable maximum false cloud detection rate. POD is computed using the following relationship.

POD = (Number of Correct Cloud Decision + Number of Correct Clear Decisions) / Number of Total Decisions

As described later, the overall binary cloud mask is given a clear value if no test detects cloud and a value indicative of cloud if any test detects cloud. Figure 30 shows this computation generated separately for land and ocean pixels based on all tests combined. Based on this analysis, a threshold of 2% on the maximum allowable false cloud detection rate maximizes the POD value (*which is the official metric of performance for the binary cloud mask*). Table 3 shows the thresholds for land, ocean and snow/ice surfaces computing using this procedure.

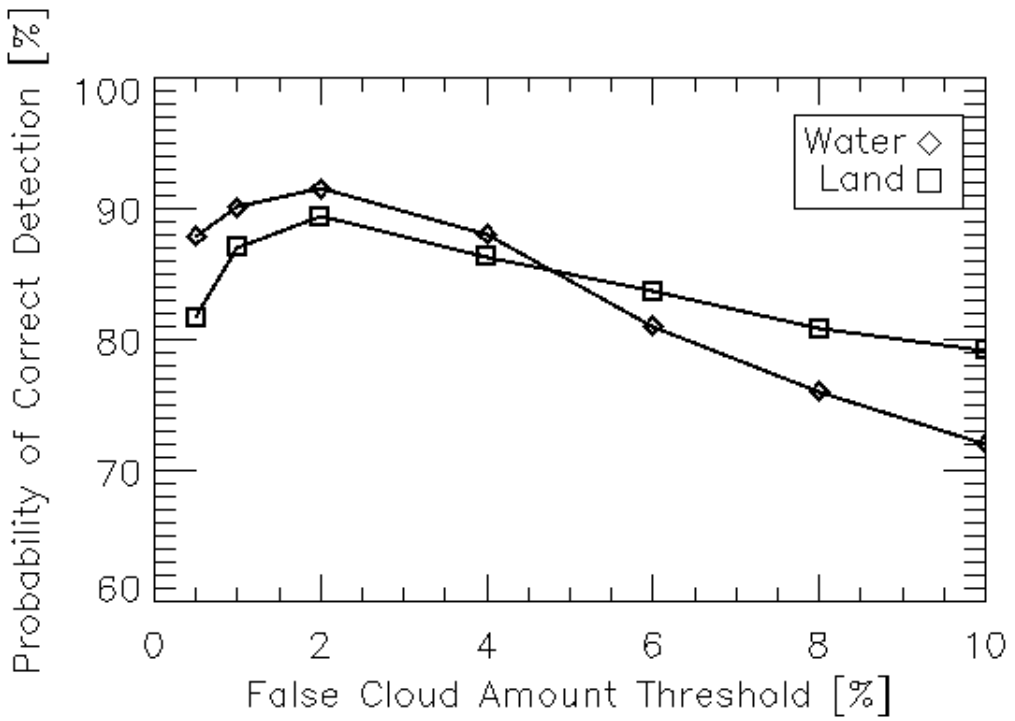

Figure 30 Illustration of the effect of the false cloud amount threshold applied to each cloud mask test on the overall Probability of Correct Detection Metric (POD). The current F&PS specification on POD is 87%. Maxima POD value are achieved when a maximum false cloud detection rate of 2% is used when deriving the thresholds for each test.

Table 3. CALIPSO-derived Thresholds from ACM. Thresholds represent the values that provide a maximum false cloud detection rate of 2%.

Cloud Mask Test	Ocean	Land	Snow/Ice
ETROP	0.10	0.30	0.4
ETROP-LRC	0.28	0.30	0.4
RTCT	3.2	4.1	N/A
PFMFT	0.8	2.5	1.0
NFMFT	-1.0	-2.0	-5.0
RFMFT	0.7	1.0	N/A
TEMPIR	2.0	2.0	2.0
EMISS_4	0.10	0.46	0.4
ULST	0.12	0.10	0.12
RGCT	11.0	19.0	N/A
RVCT	8.0	10.5	N/A
NIRREF	N/A	N/A	1.50
TUT	0.6	1.1	land or ocean

			thresh, depending on land mask
RUT	0.2	1.0	N/A

1.11.4 Algorithm Output

The following section describes the three sets of output from the ACM algorithm. To meet 15 minute refresh requirement, the clear sky mask only needs to be run once every 15 minutes.

1.11.4.1 Output

In addition to the binary (yes/no) cloud mask, the final output of the ACM consists of a 4-level cloud mask. The cloud mask values and a description of their meaning are given below in Table 4.

*Table 4. Cloud mask values and their descriptions. *The ACM is written to be insensitive to the order of the numerical values of the cloud mask and the values are stored in a static structure. Switching this order (for example to the JPSS convention) poses no problems.*

Cloud Mask Value	Numerical Value*	Description
Clear	3	Pixels that passed no test for cloud and failed a test for spatial heterogeneity
Probably clear	2	Pixels that passed no test for cloud but passed tests for spatial heterogeneity
Probably cloudy	1	Pixels that passed a test for cloud and passed a test for cloud edges
Cloudy	0	Pixels that passed a test for cloud and failed a test for cloud edges

The algorithm also produces four bytes of output which are comprised of bits holding the test results (no = 0, yes = 1) for each of the various tests and flags that are used to compute the 4-level cloud mask as an intermediate/diagnostic product and are required inputs for other algorithms. This output is shown and described in Table 5.

Table 5. Cloud mask tests and flags and their descriptions.

Byte	Bit	Description
Ancillary Data Flags		
1	1	Cloud mask attempted flag
1	2	Day/night flag
1	3	Terminator flag
1	4	Land/Ocean flag
1	5	Coast/No Coast flag
1	6	Glint / No Glint flag

1	7	Desert / no desert flag
1	8	Snow / no snow flag
2	1	Cold Surface
Clear-Sky Spatial Uniformity Tests		
2	2	RUT – Reflectance (0.63 μm) Uniformity Test
2	3	TUT – Thermal (11 μm BT) Uniformity Test
Infrared Cloud Detection Tests		
2	4	RTCT – Relative Thermal Contrast Test
2	5	ETROP – Emissivity at Tropopause Test
2	6	PFMFT – Positive FMFT (Split-Window BTD) Test
2	7	NFMFT – Negative FMFT (Negative Split-Window BTD) Test
2	8	RFMFT – Relative FMFT (Split-Window BTD) Test
3	1	CIRH20 – Cirrus Water Vapor Test
3	2	TEMPIR - Temporal IR Test
3	3	TERMIR – Terminator Temporal IR Test
Solar Reflectance Cloud Detection Tests		
3	4	RGCT – Reflectance Gross Contrast Test
3	5	RVCT – Relative Visible Contrast Test
Shortwave Solar Reflectance Cloud Detection Tests		
3	6	NIRREF – Near-IR Snow Test (1.6 μm)
3	7	CIRREF- Near IR Cirrus Test (1.38 μm)
Shortwave IR Thermal Tests		
3	8	EMISS4 – 4 μm Emissivity Test
4	1	ULST – Uniform Low Stratus Test
Restoral Tests		
4	2	PCLR – Probably clear restoral test
4	3	PCLD – Probably cloudy test
Extra bits		
4	4	blank
4	5	blank
4	6	blank
4	7	blank
4	8	blank

1.11.4.2 Quality Flags

In addition to the algorithm output, a pixel level quality flag will be output. The values will be assigned as follows:

Flag Value	Description
0	Valid, good quality cloud mask
1	Invalid pixel due to space view
2	Invalid pixel due to being outside of sensor zenith range
3	Invalid earth pixel due to bad data (bad or missing 11 μm BT or bad/missing clear sky 11 μm BT)
4	Reduced quality Cloud mask (bad 3.9μm pixel)

5	Reduced quality 0.64 μm tests
6	Reduced quality due to other bad channels (excluding 0.64, 3.9 or 11 μm)

The quality flag is initialized to invalid (1) for all pixels. If the pixel is determined to be a space pixel, the quality flag remains "invalid due to space pixel" (1). If the pixel is an earth pixel with a local zenith angle of greater than 70 degrees, the quality flag is set to "Invalid pixel due to being outside of sensor zenith range" (2). If the pixel is an earth pixel with a local zenith angle of less than 70, but has an invalid 11 μm brightness temperature or invalid 11 μm clear sky brightness temperature, the pixel is considered "Invalid earth pixel due to bad data" (3). If neither of these criteria are met, then the quality flag for the pixel is set to "Valid" (0).

After all of the cloud mask tests have been completed, two further tests on the quality of the cloud mask are performed. The first is to check if there is valid 3.9 μm data by checking the bad pixel flag. If the 3.9 μm is not valid for a given pixel, then the quality flag is set to "Reduced quality" (4). Should the 3.9 μm be good, and the pixel is a daytime pixel, a further check of the visible channels is performed. If the pixel is a daytime pixel and the clear sky 0.64 μm reflectance for that channel is missing or the 0.64 micron channel bad pixel flag is set to "bad," then the ACM quality flag is set to "Reduced quality 0.64 μm tests" (5). If other channel is bad, the quality flag is set to (6).

1.11.4.3 Metadata

In addition to the algorithm output and quality flags, the following will be output to the file as metadata for each file:

- Percent of pixels that are clear
- Number of cloud mask categories (4 cloud mask categories: Clear, Probably Clear, Probably Cloudy and Cloudy)
- For each cloud mask category, the following information is required:
    - Count of pixels for the cloud mask category
    - Definition of cloud mask category
- Total number of cloud mask points
- Terminator mark or determination
- Minimum, Maximum and Mean observation-calculation for all-sky (Channels 7-16)
- Minimum, Maximum and Mean observation-calculation for clear-sky (Channels 7-16)
- Standard deviation between observation and calculation for all-sky (Channels 7-16)
- Standard deviation between observation and calculation for clear-sky (Channels 7-16)

2 Test Data Sets and Outputs

2.1 Simulated/Proxy Input Datasets

As described below, the data used to test the ACM included SEVIRI observations collocated with CALIPSO data and with MODIS granules. Data from August 2006 (summer), February 2007 (winter), April 2007 (spring) and October 2007 (fall) were used to span the entire SEVIRI domain and encompass a full range of conditions. The rest of this section describes the proxy and validation data sets used in assessing the performance of the ACM. Table 6 shows the channel mapping between the proxy dataset (SEVIRI) and ABI:

Table 6. ABI and SEVIRI channel numbers with associated wavelengths for ABI

ABI Channel Number	*SEVIRI Channel Number*	*Wavelength (μm)*
2	1	0.64
4	n/a	1.38
5	3	1.61
7	4	3.9
9	n/a	7.0
10	6	7.4
11	7	8.5
14	9	11.2
15	10	12.3

2.1.1 SEVIRI Data

SEVIRI provides 11 spectral channels with a nadir spatial resolution of 3 km and a temporal resolution of 15 minutes. SEVIRI provides the best source of data currently for testing and developing the ACM. The figure shown below is a full-disk SEVIRI image from 12 UTC on August 10, 2006. Except for the 1.38 μm channel, SEVIRI provides an adequate source of proxy data for testing and developing the ACM. The SEVIRI data was provided by the UW SSEC Data Center.

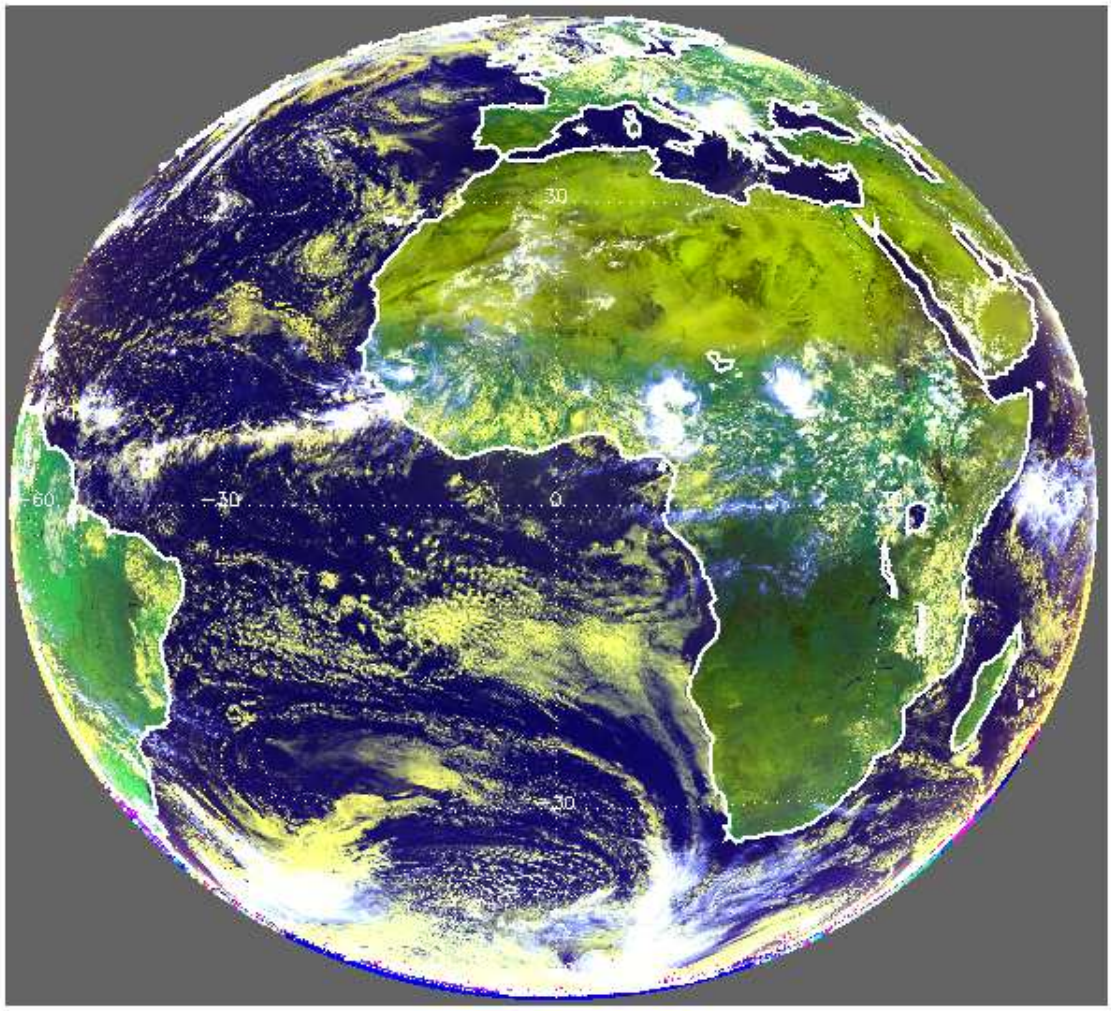

Figure 31 Fulldisk 0.63, 0.86 and 11 μm false color image from SEVIRI for 12 UTC on August 10, 2006.

2.1.2 CALIPSO Data

With the launch of CALIPSO and CloudSat into the Earth Observing System (EOS) A-Train in April 2006, the ability to conduct global satellite cloud product validation increased significantly. Currently, CALIPSO cloud detection results are used to validate the cloud detection of the ACM. The CALIPSO data used here are the 1 km cloud layer results (Vaughan et al., 2005).

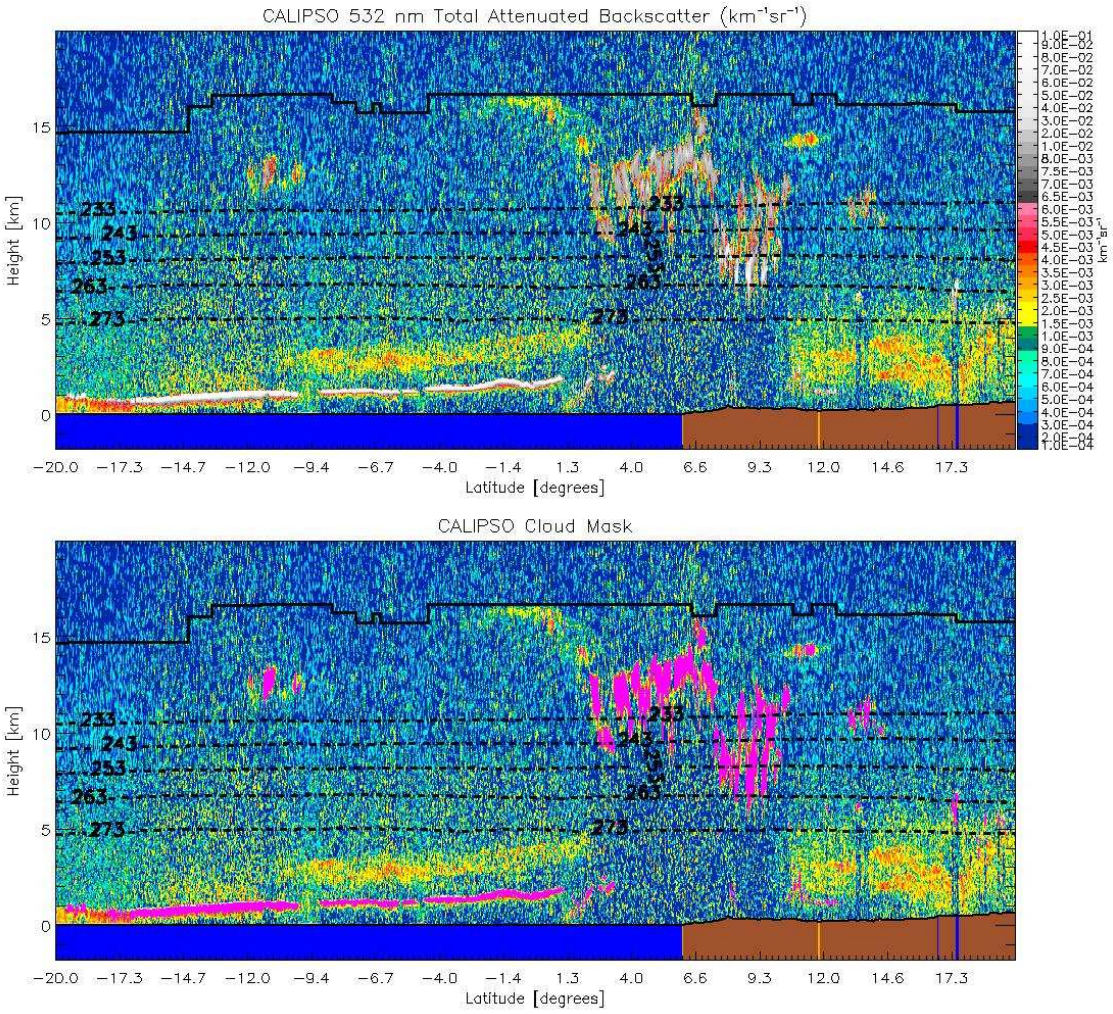

Figure 32 Illustration of CALIPSO data used in this study. Top image shows a 2D backscatter profile. Bottom image shows the detected cloud layers overlaid onto the backscatter image. Cloud layers are colored magenta. (*Image courtesy of Michael Pavolonis/NOAA***)**

The individual CALIPSO results within each SEVIRI pixel were averaged to give a cloud fraction for each SEVIRI pixel. This cloud fraction is compared to the 4-level ACM results in the next sections. Using the CALIPSO cloud fraction product, only pixels that coincide with at least four CALIPSO laser shots are used for evaluation. The error is estimated as the percentage of pixels for each cloud mask category that falls outside the following ranges of CALIPSO cloud fraction: the requirements state that this is a "Clear-

sky" mask, and as such, the probably clear and clear pixels are called "Clear" and probably cloudy and cloudy pixels are called "Cloud." In addition, for the analysis with CALIPSO, only cloud fractions equal to 100% were considered as cloud while all other conditions were considered clear pixels by CALIPSO.

2.2 Output from Simulated/Proxy Inputs Datasets

The ACM was generated using the SEVIRI data from the entire month of August 2006 as well as 2 weeks in February 2007 (winter), April 2007 (spring) and October 2007 (fall) were used to span the entire SEVIRI domain and encompass a full range of conditions. During both the TRR and subsequent tests, comparisons between the online (Framework) and offline (Cloud AWG) output of the ACM, when the same inputs were used, showed an exact match of the Clear Sky Mask. These tests were conducted under different conditions using the same input for both the online and offline tests. Figure 33 shows the ACM 4-level mask with the clear value replaced by the surface temperature. This image is for 12 Z on August 10, 2006 and corresponds to the false-color image shown in Figure 31. The CALIPSO and SST analyses were then applied to the ACM results and used to generate the performance estimates provided below.

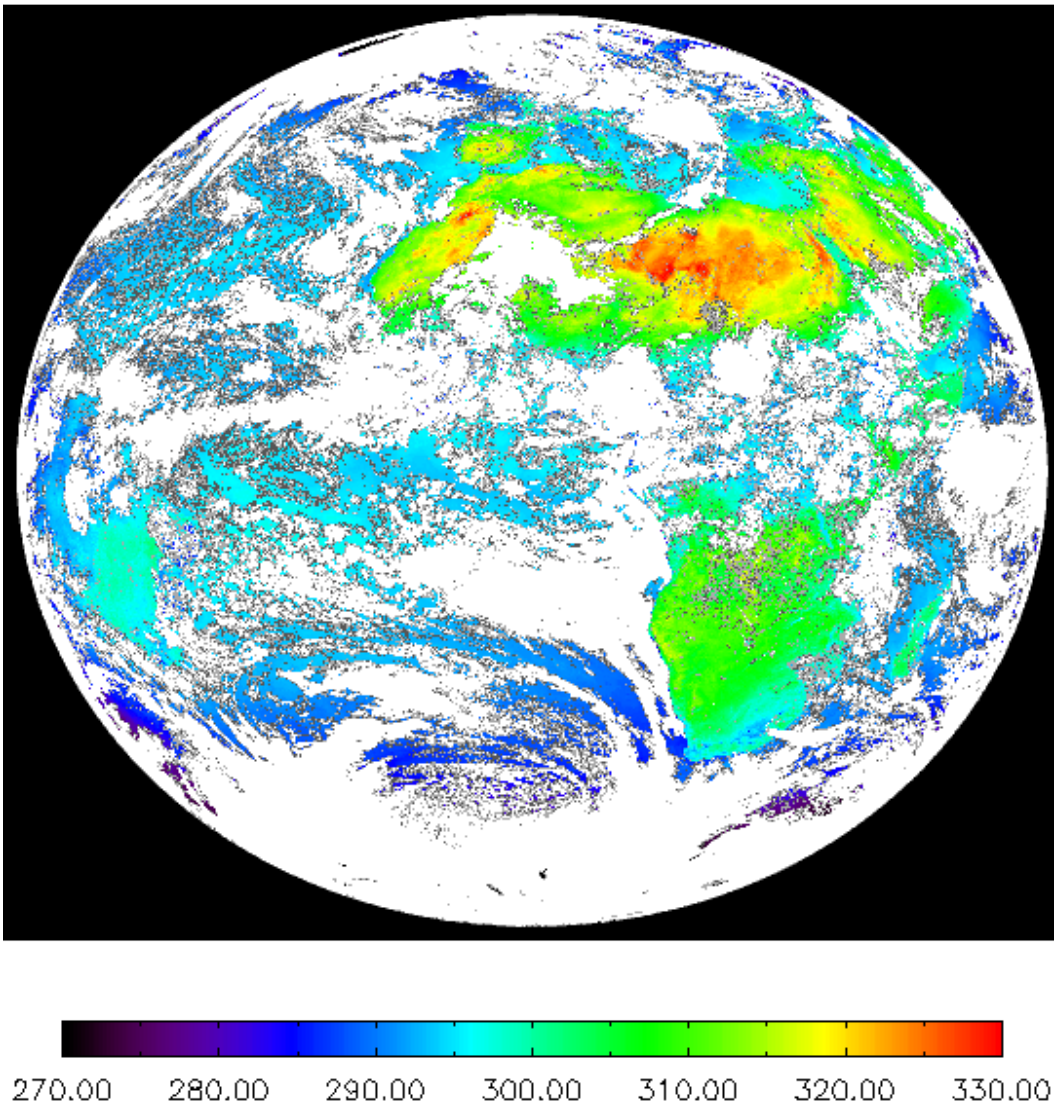

Figure 33 Example ACM 4-level cloud mask from 12 UTC August 10, 2006 produced from SEVIRI on MET-8. Where clear, the derived surface temperature is shown with the units of K.

2.2.1 Precisions and Accuracy Estimates

To estimate the performance and accuracy of the ACM, we have used the MODIS Cloud Mask product (MOD35/MYD35) and CALIPSO data as described above. This section will present our analysis methodology for estimating the precision and accuracy. The next section will provide the quantitative results in terms of the MRD specifications.

2.2.1.1 CALIPSO Analysis

The CALIPSO/CALIOP data (hereafter referred to as CALIPSO) provides unique information on the cloud fraction, which can be used to validate the ACM. To do this analysis, a collocation tool has been developed to determine the relevant information provided by CALIPSO for each collocated SEVIRI pixel. This tool has been applied to all SEVIRI data for the datasets specified in section 4.1. For each SEVIRI pixel that is collocated with CALIPSO data, the following information is available.

- Time difference between SEVIRI and CALIPSO
- Number of cloud layers observed by CALIPSO
- Cloud fraction

In addition to the above information, the SEVIRI 11 μm radiances and the computed clear-sky radiances to estimate the cloud emissivity assuming the cloud existed at the height given by CALIPSO. The analysis shown in this section provides the performance of the ACM based on cloud height (Z_c) and emissivity (e_c) as provided by CALIPSO. The height bins were set to a width of 1 km thick and range from 0 to 20 km. The cloud emissivity bins were to a width of 0.1 and range from -0.2 and 1.2. Emissivity less than 0 imply the observed radiance was less than the clear-sky radiance and emissivities greater than 1.0 implies that the observed radiance was greater than the blackbody emission at the CALIPSO cloud temperature.

The results of comparing the CALIPSO cloud fraction to values of the ACM at the pixel-level are shown in the figures below. Figure 34 shows the distribution of cloudy points in Z_c-e_c space from the 8-weeks of data from 4 seasons. The sample size is roughly 32000 pixels. As stated above, these points occurred during periods of co-incidence between SEVIRI and CALIPSO. Figure 34 shows that low clouds were dominant over this period with a secondary peak of high thin cirrus. It is important to note the CALIPSO emissivity calculation is very uncertain for low clouds. However, low emissivities always imply observed radiances that are very close to the assumed clear-sky values.

Figure 35 shows the distribution in Z_c-e_c space of the clouds detected by CALIPSO that were missed by the ACM. The values in Figure 35 show the fraction of missed clouds computed from the number of missed clouds divided by the total number of cloudy pixels in each Z_c-e_c bin. The total number of cloudy pixels in each Z_c-e_c bin is shown in Figure 34. This analysis reveals that the ACM performs well for all clouds with $e_c > 0.2$ except for very low clouds ($Zc < 1$ km). The highest rate of missed clouds (71%) occurs for

values of $e_c < 0.2$ and for Zc < 2 km. The ACM also misses some high clouds for values of $e_c < 0.1$.

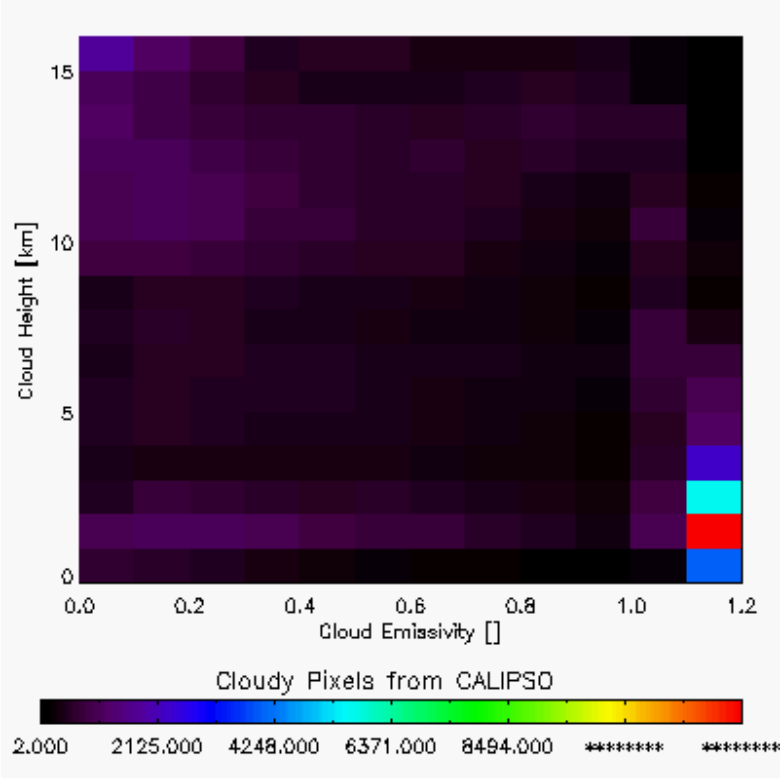

Figure 34 Distribution of cloudy pixels determined by CALIPSO displayed as a function of CALIPSO-derived cloud height and cloud emissivity. Data observed during simultaneous SEVIRI and CALIPSO periods over 8 weeks from 4 seasons in 2006 and 2007.

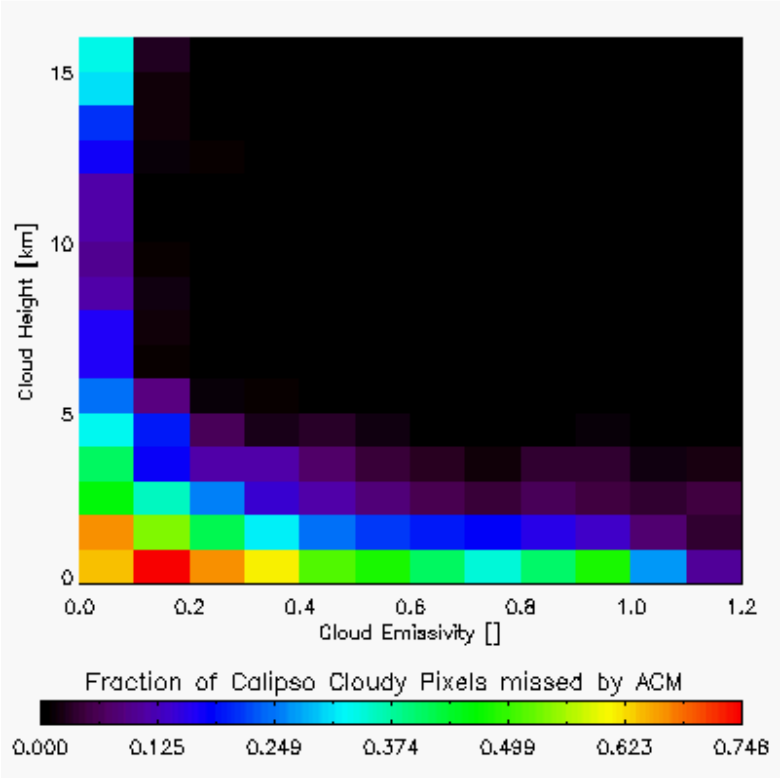

Figure 35 CALIPSO-derived height and emissivity distribution of pixels that were cloudy as observed by CALIPSO but classified as clear by the ACM. Values are fractions of missed cloudy pixels over the total number of CALIPSO-derived cloudy pixels in each Zc-ec bin. Light gray indicates no data.

Table 7 shows the probability of correct detection (POD) for the binary ACM results compared to CALIPSO. False cloud is the percentage of falsely detected cloud pixels while false clear is the percentage of falsely detected clear pixels.

The number of correct cloud decisions is computed as the number of pixels where ACM gave a cloudy results and the CALIPSO cloud fraction was greater than 0.8. The number of correct clear decisions was computed as the number of pixels where ACM gave a clear decision and the CALIPSO cloud fraction was less than 0.2

Table 7. Computed POD numbers for the 8 weeks of SEVIRI/CALIPSO taken over 4 seasons during 2006 – 2007.

	POD	False Cloud	False Clear
Ocean-Day	91.9%	4.1%	4.0%
Ocean-Night	89.4%	3.3%	7.2%
Ocean	90.9%	3.8%	5.4%
Land-Day	93.9%	4.6%	1.4%
Land-Night	89.5%	2.2%	8.3%
Land	92.2%	3.7%	4.1%
Total (Land/Ocean + Day/Night)	91.4%	3.7%	4.9%

2.2.1.2 MODIS Analysis

As stated above, CALIPSO provides our source of cloudiness information that is used to derive and verify the ACM. To complement the CALIPSO analysis, the ACM was also compared to the official NASA Goddard MODIS cloud mask, which is also known as MYD35 (Ackerman et al., 1988; Ackerman et al., 2002). The MYD35 provides a 4-category cloud mask at a spatial resolution of 1 km. It has become a widely-used cloud mask for many MODIS applications.

To compare the ACM results to MODIS, the ACM was processed through using MODIS granules for a single day. Because the input to the ACM for this analysis was the MODIS imagery, the analysis was able to compare the MYD35 output and the output of the ACM directly. Figure 36 shows a direct comparison of the ACM applied to MODIS as compared to the MYD35 results. Regions that are white represent regions where both MYD35 and the ACM gave cloudy results. Regions that are blue or green represent areas where both MYD35 and the ACM gave clear results. Regions that are red are those where MYD35 gave cloudy results and the ACM gave a clear result. Finally, cyan regions are those where the ACM detected cloud and the MYD35 did not. There does appear to be a general preference for the ACM to detect more cloud than MYD35 in the presence of small scale cloudiness and cloud edges. When doing an analysis over the entire granule and assuming that MYD35 is correct, a POD of 0.97 is computed. This value is above the F&PS specification of 87%. The cloud fractions are also in rough agreement. The ACM was run over the course of a day, resulting in a total POD with MODIS of 91%. While this was just a single day, the results covered a wide range of conditions and land types.

In summary, while any passive satellite product cannot be considered a source of validation for another passive satellite product, the MYD35 comparison does provide evidence that the ACM is performing well and as expected. This analysis is being applied to many MODIS and SEVIRI datasets and more robust statistics will be generated.

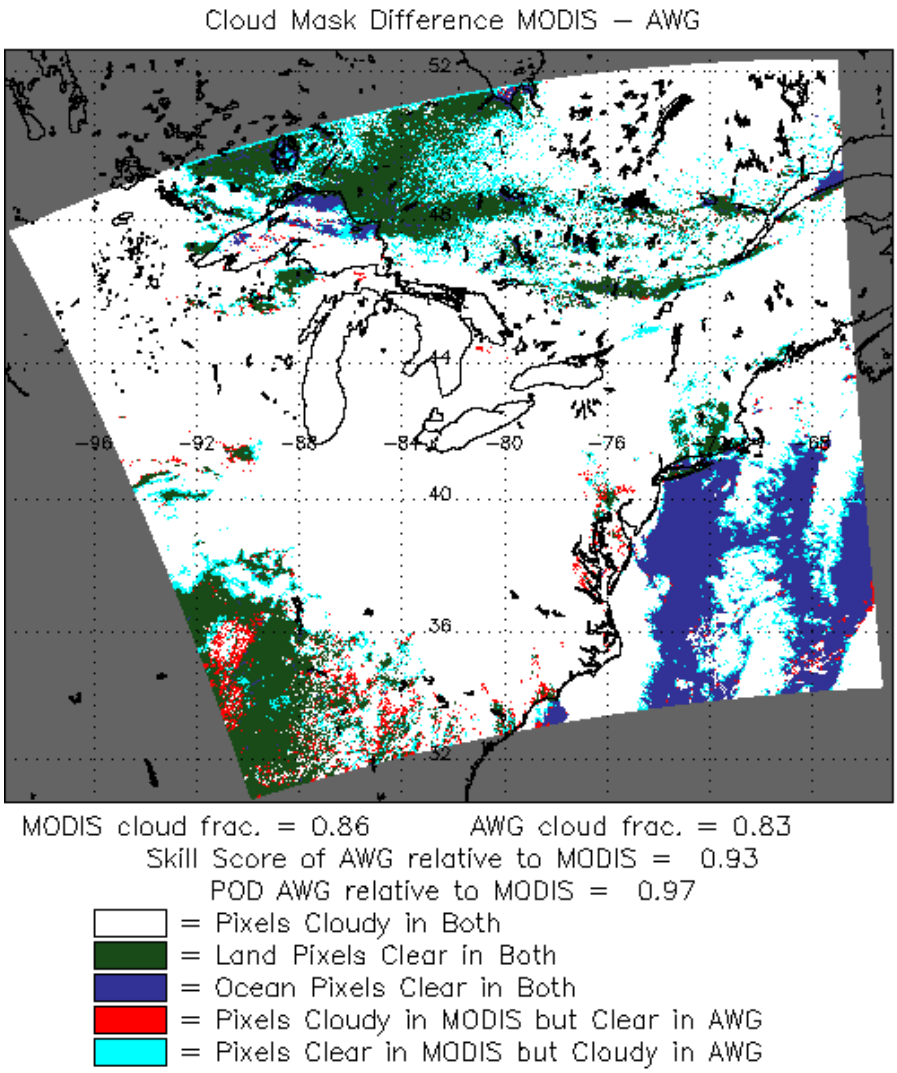

Figure 36 Comparison of MODIS (MYD035) and the ACM applied to SEVIRI data on June 13, 2008 at 18:25 UTC. Legend of images contains POD and skill scores computed for all pixels.

2.2.1.3 EUMETSAT CM Comparison Analysis

Because SEVIRI was being used as a proxy dataset, another source of comparison is the EUMETSAT Meteorological Product Extraction Facility (MPEF) Cloud Mask product (Lutz, 1999) can be performed. This cloud mask is the official real-time cloud mask for SEVIRI from EUMETSAT. A similar comparison to that done above for MODIS was done using two days worth (one summer, one winter) of SEVIRI data. Figure 37 shows the result of one image from this analysis.

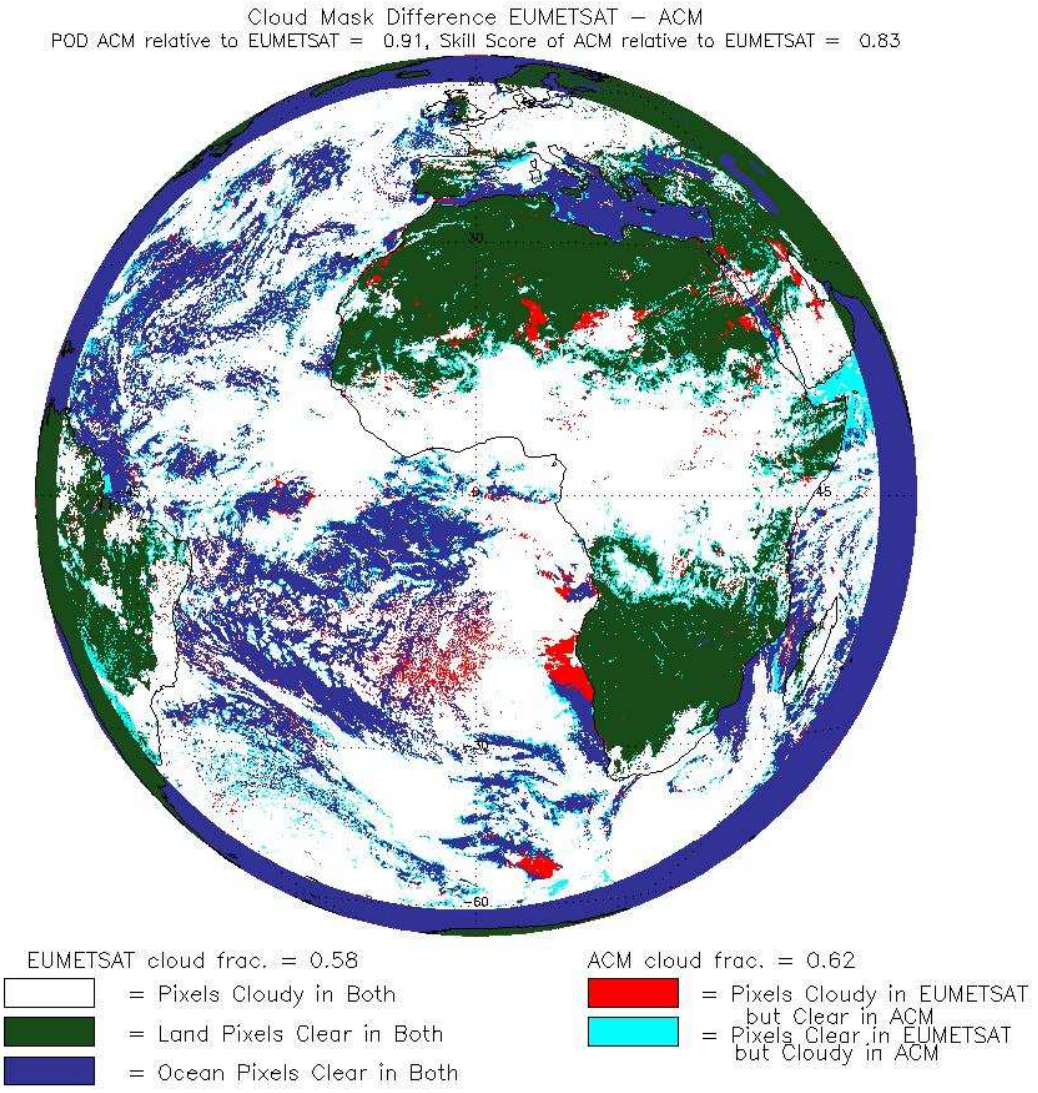

Figure 37. Comparison of EUMETSAT MPEF and the ACM applied to SEVIRI data on August 3, 2006 at 12:00 UTC. Legend of images contains POD and skill scores computed for all pixels.

As before, regions that are white represent regions where both EUMETSAT/MPEF and the ACM gave cloudy results. Regions that are blue or green represent areas where both MPEF and the ACM gave clear results. Regions that are red are those where MPEF gave cloudy results and the ACM gave a clear result. Finally, cyan regions are those where the ACM detected cloud and the MPEF did not.

When doing an analysis over the entire image and assuming that MPEF cloud mask is correct, a POD of 0.91 is computed, above the required 87% POD as specified in the F&PS. In addition, the cloud fractions between the two are also in rough agreement. Over the course of two days (Aug 3, 2006 and Feb 3, 2007), from over 2E9 points of comparison, the resulting total POD with EUMETSAT was 87.5%. While this is just over the requirements in the F&PS, it should be noted that we noted several regions of

probably false cloud detections in the MPEF product. One of these areas is off the coast of Nambia shown below in

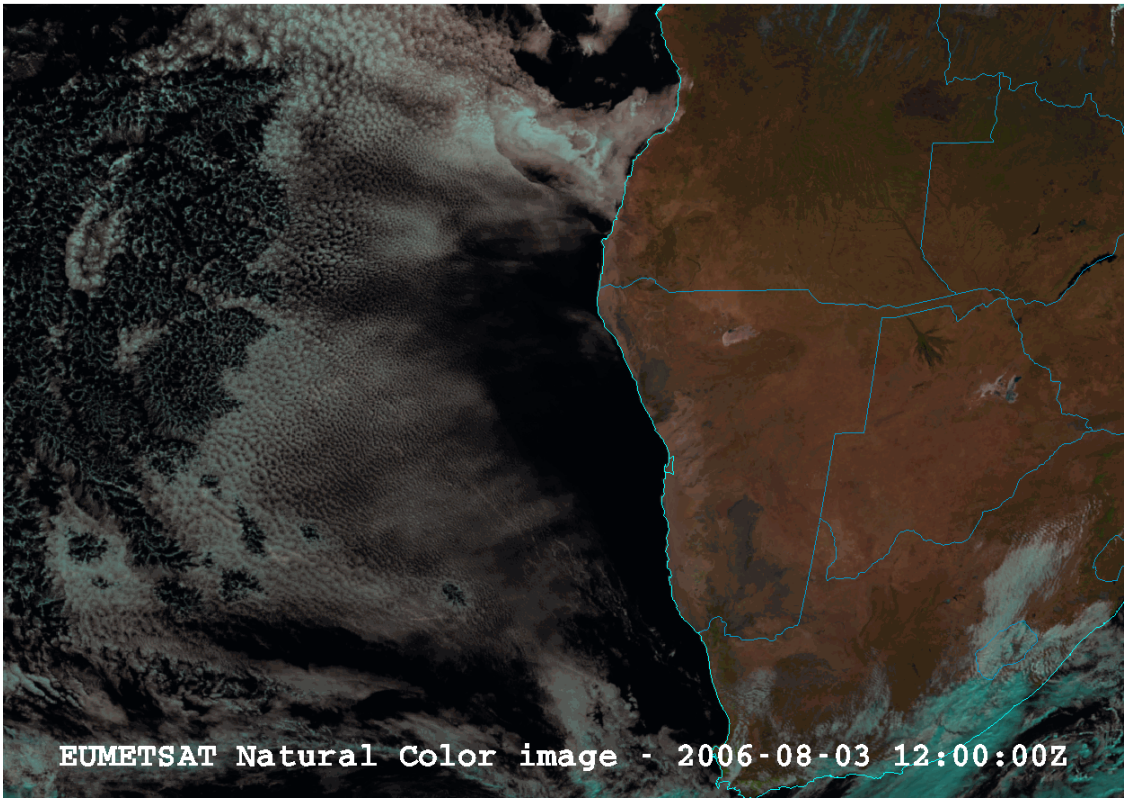

Figure 38. SEVIRI "True" color (0.64, 0.86, 1.61μm) image from on August 3, 2006 at 12:00 UTC.

As can be seen from the EUMETSAT/SEVIRI "natural" color image, there are no clouds off the coast of Nambia. However, the MPEF cloud mask marks the area as clear, while the ACM marks the area as clear. Similar cases of disagreement between the ACM and other successful operational masks like MPEF are also seen. This highlights the difficulty in validating one mask with another and helps explain our reliance on CALIPSO for quantitative validation.

2.2.2 Error Budget

The F&PS states that the probability of correct detection (POD) for the ACM should be greater than 87%. The F&PS specification applies to the binary mask. The results of the binary cloud mask are presented in the Table 6 where the CALIPSO 1km Cloud Layer product is assumed to be the truth. From this analysis, the ACM is meeting threshold performance for land and ocean regions for all solar viewing geometries (day and night).

As described earlier, there is reason to believe that CALIPSO is overestimating the amount of missed clouds by the ACM especially during the day. Therefore, to complement the CALIPSO analysis, a comparison was made between the ACM and the MODIS cloud mask (MYD35) on collocated SEVIRI and MODIS pixels. For the scene

shown and for other scenes, the POD numbers for the ACM relative to MODIS exceed the goal values set up in the F&PS.

The most important metric of the ACM is that it delivers useful information on the presence of cloud to downstream algorithms. To do that, we have worked on incorporating tests from both other AWG teams as well incorporating tests from other cloud masks, such as the MODIS (MOD/MYD35) and EUMETSAT cloud mask groups.
.

3 Practical Considerations

3.1 Numerical Computation Considerations

The ACM is implemented sequentially. Because some cloud detection tests rely on the values of the ancillary data flags, the ancillary data flags need to be computed first. All tests are applied before the final cloud mask is determined. The ACM is currently implemented into the AIT Framework and uses its numerical routines for processing.

3.2 Programming and Procedural Considerations

The ACM requires knowledge of spatial uniformity metrics that are computed for each pixel using pixels that surround it. In addition, the temporal tests require information from the previous image. Beyond this reliance, the ACM is purely a pixel by pixel algorithm.

3.3 Quality Assessment and Diagnostics

The following procedures are recommended for diagnosing the performance of the ACM.

- Monitor the percentage of pixels falling into each ACM cloud mask values. These values should be quasi-constant over a large area.
- Derive a surface temperature from all pixels of the ACM. Compute the distributions of the observed – background surface temperature for each ACM value.
- Periodically image the individual test results to look for artifacts or non-physical behaviors.
- Maintain a close collaboration with the other teams using the ACM in their product generation.

3.4 Exception Handling

The ACM includes checking the validity of each channel before applying the appropriate test. The ACM also expects the main processing system (i.e., the AIT Framework) to flag any pixels with missing geolocation or viewing geometry information.

The ACM does check for conditions where the ACM cannot be performed. If the 11 μm channel measured or clear sky BT is saturated or missing, there is no attempt at processing the cloud mask, as it is a key channel in numerous tests for the ACM. If other

channels are saturated or missing, the corresponding test is not performed. A quality flag is set, which indicates the quality of the cloud mask for that particular pixel. The conditions for the quality flags are described in Section 1.11.4.2.

3.5 Algorithm Validation

This section is to be completed upon submission of validation plan.

4 ASSUMPTIONS AND LIMITATIONS

The following sections describe the current limitations and assumptions in the current version of the ACM.

4.1 Performance

The following assumptions have been made in developing and estimating the performance of the ACM. The following list contains the current assumptions and proposed mitigation strategies.

1. NWP data of comparable or superior quality to the current 6 hourly GFS forecasts are available. (Use longer range GFS forecasts or switch to another NWP source – ECMWF).

2. RTM calculations are available for each pixel. (Use reduced vertical or spatial resolution in driving the RTM).

3. High quality snow maps are available. (Use snow information from NWP).

4. Background snow-free surface reflectances will be available. (Use pre-computed reflectances stored as function of surface type).

5. All of the static ancillary data is available at the pixel level. (Reduce the spatial resolution of the surface type, land mask and or coast mask).

6. The processing system allows for processing multiple pixels at once for applying the spatial uniformity tests. (No mitigation possible)

7. The processing systems allows for ingesting previous output for applying the temporal tests. (Make temporal tests optional)

4.2 Assumed Sensor Performance

It is assumed that the ABI sensor will meet its current specifications. However, the ACM will be dependent on the following instrumental characteristics:

- The spatial uniformity tests in ACM will be critically dependent on the amount of striping in the data.
- Unknown spectral shifts in some channels will cause biases in the clear-sky RTM calculations that may impact the performance of the ACM.
- Errors in navigation from image to image will affect the performance of the temporal tests.

4.3 Pre-Planned Product Improvements

This section contains the potential future enhancements to the algorithm, the limitations they will mitigate, and possible and useful related information and links.

The ACM serves many other applications. Its development is therefore tied to the development and feedback from the other algorithms. At this point, it is therefore difficult to predict what the future modifications will be. However, the following list contains our current best guess of the future ACM modifications.

4.3.1 Optimization for Ocean Applications

The cloud detection accuracy requirements of the SST and aerosol applications over the ocean are very strict. It is recognized that specialized tests for these applications will be necessary. Coordination with the Ocean Application Team regarding the ACM algorithm and output is being done to incorporate their experience and to ensure the ACM is adequate for their needs.

4.3.2 Optimization for Land Applications

The ACM performance over land also needs to be optimized for the Land Application Team's algorithms. Coordination with the Land Application Team regarding the ACM algorithm and output is being done to allow for their feedback and to ensure the ACM is adequate for their needs.

REFERENCES

Ackerman, S.A., K.I. Strabala, W.P. Menzel, R.A. Frey, C.C. Moeller and L.E. Gumley, 1998: Discriminating clear sky from clouds with MODIS. J. Geophys. Res., **103**, 32139-32140.

Ackerman, S. A., Strabala, K. I., Menzel, W. P., Frey, R. A., Moeller, C. C., Gumley, L. E., Baum, B., Wetzel-Seeman, S., and Zhang, H.: Discriminating clear sky from clouds with MODIS Algorithm Theoretical Basis Document (MOD35), Tech. Rep. ATBD-MOD-06, University of Wisconsin-Madison, 2002

Baglio, J.V., and Holroyd, E.W., 1989. Methods for operational snow cover area mapping using the advanced very high resolution radiometer: San Juan Mountains Test Study, Research Technical Report, U.S. Geological Survey, Sioux Falls and U.S. Bureau of Reclamation, Denver.

Derrien M., and H. Le Gleau, MSG/SEVIRI cloud mask and type from SAFNWC, International Journal of Remote Sensing 26 (2005), pp. 4707–4732.

Dozier, J., 1989. "Remote sensing of snow in visible and near-infrared wavelengths," Theory and Applications of Optical Remote Sensing, G. Asrar, ed., John Wiley and Sons, New York.

Dybbroe, A., K.G. Karlsson, and A. Thoss, 2005: NWCSAF AVHRR Cloud Detection and Analysis Using Dynamic Thresholds and Radiative Transfer Modeling. Part I: Algorithm Description. *J. Appl. Meteor.*, **44**, 39–54.

Dybbroe, A., K.G. Karlsson, and A. Thoss, 2005: NWCSAF AVHRR Cloud Detection and Analysis Using Dynamic Thresholds and Radiative Transfer Modeling. Part II: Tuning and Validation. *J. Appl. Meteor.*, **44**, 55–71.

GOES-R Series Ground Segment (GS) Project Functional and Performance Specification (F&PS) [G417-R-FPS-0089]

GOES-R Level 1 Requirements Document (L1RD)

GOES-R Series Mission Requirements Document (MRD) [P417-R-MRD-0070]

GOES-R Acronym and Glossary (P417-R-LIST-0142)

GOES-R Algorithm Interface and Ancillary Data Description Document (AIADD)

Hann, S. L. L. Strow, and W. W. McMillan, 1996: Atmospheric infrared fast transmittance models: A comparison of two approaches, Proceedings of SPIE, 2830, 94-105.

Hansen, M., R. DeFries, J.R.G. Townshend, and R. Sohlberg (1998), UMD Global Land Cover Classification, 1 Kilometer, 1.0, Department of Geography, University of Maryland, College Park, Maryland, 1981-1994.

Hunt, G. E., 1973: Radiative properties of terrestrial clouds at visible and infrared thermal window wavelengths. Quart. J. Roy. Meteor. Soc., 99, 346–369.

Inoue, T., 1985: On the temperature and effective emissivity determination of semi-transparent clouds by bi-spectral measurements in the 10 micron window region. J. Meteor. Soc. Japan, 63 (1), 88–89.

Inoue, T., 1987: A cloud type classification with NOAA 7 split window measurements. J. Geophys. Res., 92, 3991-4000.

Krebs, W., Mannstein, H., Bugliaro, L., and Mayer, B.: Technical note: A new day- and night-time Meteosat Second Generation Cirrus Detection Algorithm MeCiDA, Atmos. Chem. Phys., 7, 6145-6159, doi:10.5194/acp-7-6145-2007, 2007.

Li, J. and K. Shibata, 2006: On the Effective Solar Pathlength. Journal of the Atmospheric Sciences 2006 63:4, 1365-1373

Lutz H. J., (1999) Cloud Processing for Meteosat Second Generation. EUMETSAT Tech. Department Tech. Memo. No.4, pp 26;

Moody, E.G., M.D. King, C.B. Schaaf, and S. Platnick, 2008: MODIS-Derived Spatially Complete Surface Albedo Products: Spatial and Temporal Pixel Distribution and Zonal Averages. J. Appl. Meteor. Climatol., 47, 2879–2894.

Pavolonis, M. J., 2009: Advances in extracting cloud composition information from spaceborne infrared radiances: A robust alternative to brightness temperatures. Part II: Proof of concept. Submitted to *J. Atmos. Sci.*

Prabhakara, C., R. S. Fraser, G. Dalu, M. C. Wu, and R. J. Curran, 1988: Thin cirrus clouds: Seasonal distribution over oceans deduced from Nimbus-4 IRIS. J. Appl. Meteor., 27, 379–399.

Seemann, S.W., E. E. Borbas, R. O. Knuteson, G. R. Stephenson, H.-L. Huang, 2007: Development of a Global Infrared Land Surface Emissivity Database for Application to Clear Sky Sounding Retrievals from Multi-spectral Satellite Radiance Measurements. Journal of Applied Meteorology and Climatology, accepted April 2007.

Stowe, L.L., P.A. Davis, and E.P. McClain, 1999: Scientific Basis and Initial Evaluation of the CLAVR-1 Global Clear/Cloud Classification Algorithm for the

Advanced Very High Resolution Radiometer. J. Atmos. Oceanic Technol., 16, 656–681.

Vaughan, M. A., Winker, D. M., and Powell, K. A.: CALIOP algorithm theoretical basis document. Part 2: Feature detection and layer properties algorithm, PC-SCI-202, Release 1.01, 87 pp., http://www-calipso.larc.nasa.gov/resources/project documentation.php, 2005.

Wang, M., & King, M. D. (1997). Correction of Rayleigh scattering effects in cloud optical thickness retrievals. *Journal of Geophysical Research-Atmospheres*, 102(D22), 25915-25926

Warren, S., 1982. Optical properties of snow, Reviews of Geophysics and Space Physics, 20, 67.

Wu, Xiangqian, W. Paul Menzel, and Gary S. Wade, 1999: Estimation of Sea Surface Temperatures Using GOES-8/9Radiance Measurements. Bulletin of the American Meteorological Society Volume 80, Issue 6 (June 1999) pp. 1127–1138

Appendix 1: Common Ancillary Data Sets

1. COAST_MASK_NASA_1KM

a. Data description

Description: Global 1km land/water used for MODIS collection 5.
Filename: coast_mask_1km.nc
Origin: Created by SSEC/CIMSS based upon NASA MODIS collection 5.
Size: 890 MB.
Static/Dynamic: Static

b. Interpolation description

The closest point is used for each satellite pixel:

1) Given ancillary grid of large size than satellite grid
2) In Latitude / Longitude space, use the ancillary data closest to the satellite pixel.

2. DESERT_MASK_CALCLTED

a. Data description

Description: Desert mask calculated using LAND_MASK_NASA_1KM and SFC_TYPE_AVHRR_1KM
Filename: N/A
Origin: N/A
Size: N/A
Static/Dynamic: N/A

b. *Interpolation description*

The interpolation is based on the surface type and land mask. No direct interpolation is used in the desert mask calculation, but it is reliant on the interpolation found in its dependencies.

The procedure of desert mask calculation is:
Desert mask is first initialized to “no desert”, then the land mask is checked. In the case of LAND, the surface type is then checked. The

desert mask is set as “NIR Desert” if the surface type is “wooded_grass_sfc”, “closed_shrubs_sfc”, “open_shrubs_sfc”, “grasses_sfc”, or “croplands_sfc”, and is set as “bright_desert” if surface type is “bare_sfc”.

3. LAND_MASK_NASA_1KM

a. Data description

Description: Global 1km land/water used for MODIS collection 5
Filename: lw_geo_2001001_v03m.nc
Origin: Created by SSEC/CIMSS based on NASA MODIS collection 5
Size: 890 MB.
Static/Dynamic: Static

b. Interpolation description

The closest point is used for each satellite pixel:

1) Given ancillary grid of large size than satellite grid
2) In Latitude / Longitude space, use the ancillary data closest to the satellite pixel.

4. NWP_GFS

a. Data description

Description: NCEP GFS model data in grib format – 1 x 1 degree (360x181), 26 levels
Filename: gfs.tHHz.pgrbfhh
Where,
HH – Forecast time in hour: 00, 06, 12, 18
hh – Previous hours used to make forecast: 00, 03, 06, 09
Origin: NCEP
Size: 26MB
Static/Dynamic: Dynamic

b. Interpolation description

There are three interpolations are installed:

NWP forecast interpolation from different forecast time:

Load two NWP grib files which are for two different forecast time and interpolate to the satellite time using linear interpolation with time difference.

Suppose:

T1, T2 are NWP forecast time, T is satellite observation time, and T1 < T < T2. Y is any NWP field. Then field Y at satellite observation time T is:

$$Y(T) = Y(T1) * W(T1) + Y(T2) * W(T2)$$

Where W is weight and

$$W(T1) = 1 – (T-T1) / (T2-T1)$$
$$W(T2) = (T-T1) / (T2-T1)$$

NWP forecast spatial interpolation from NWP forecast grid points. This interpolation generates the NWP forecast for the satellite pixel from the NWP forecast grid dataset.

The closest point is used for each satellite pixel:

1) Given NWP forecast grid of large size than satellite grid
2) In Latitude / Longitude space, use the ancillary data closest to the satellite pixel.

NWP forecast profile vertical interpolation

Interpolate NWP GFS profile from 26 pressure levels to 101 pressure levels

For vertical profile interpolation, linear interpolation with Log pressure is used:

Suppose:

y is temperature or water vapor at 26 levels, and y101 is temperature or water vapor at 101 levels. p is any pressure level between p(i) and p(i-1), with p(i-1) < p <p(i). y(i) and y(i-1) are y at pressure level p(i) and p(i-1). Then y101 at pressure p level is:

$$y101(p) = y(i-1) + \log(p[i] / p[i-1]) * (y[i] – y[i-1]) / \log (p[i] / p[i-1])$$

5. SFC_ELEV_GLOBE_1KM

a. *Data description*

Description: Digital surface elevation at 1km resolution.
Filename: GLOBE_1km_digelev.nc
Origin: NGDC
Size: 1843.2 MB
Static/Dynamic: Static

b. *Interpolation description*

The closest point is used for each satellite pixel:

1) Given ancillary grid of large size than satellite grid
2) In Latitude / Longitude space, use the ancillary data closest to the satellite pixel.

6. SFC_EMISS_SEEBOR

a. *Data description*

Description: Surface emissivity at 5km resolution
Filename: global_emiss_intABI_YYYYDDD.nc
Where, YYYYDDD = year plus Julian day
Origin: UW Baseline Fit, Seeman and Borbas (2006).
Size: 693 MB x 12
Static/Dynamic: Dynamic

b. *Interpolation description*

The closest point is used for each satellite pixel:

1) Given ancillary grid of large size than satellite grid
2) In Latitude / Longitude space, use the ancillary data closest to the satellite pixel.

7. SNOW_MASK_IMS_SSMI

a. *Data description*

Description: Snow/Ice mask, IMS – Northern Hemisphere, SSM/I – Southern Hemisphere
4km resolution – the 25 km SSM/I has been oversampled to 4km
Filename: snow_map_4km_YYMMDD.nc
Origin: CIMSS/SSEC
Size: 39 MB.
Static/Dynamic: Dynamic

b. *Interpolation description*

The closest point is used for each satellite pixel:

1) Given ancillary grid of large size than satellite grid
2) In Latitude / Longitude space, use the ancillary data closest to the satellite pixel.

8. SUNGLINT ANGLE

a. Data description

Description: Sunglint Angle Calculation
Filename: N/A
Origin: N/A
Size: N/A
Static/Dynamic: N/A

b. Description

```
//Calculating sunglint angle
float32 SunGlintAng(float32 SOLZA, float32 SENZA, float32 SOLAZ,
float32
SENAZ)
{
   float32 SunGlintA = Missing_Value;
   float32 DegreeToRadiance = 3.1415926/180.0;
   float32 RadianceToDegree = 180.0/3.1415926;
   float32 Temp1 =
cos(SOLZA*DegreeToRadiance)*cos(SENZA*DegreeToRadiance);
   float32 Temp2 =
sin(SOLZA*DegreeToRadiance)*sin(SENZA*DegreeToRadiance);
```

```
    float32 Temp3 = cos((180.0-(SOLAZ-SENAZ))*DegreeToRadiance);
    SunGlintA = acos(Temp1+Temp2*Temp3)*RadianceToDegree;

 return SunGlintA;
}
```

9. LRC

a. Data *description*

Description: Local Radiative Center Calculation
Filename: N/A
Origin: NOAA / NESDIS
Size: N/A
Static/Dynamic: N/A

b. Interpolation *description*

It should be first noted that the original description of the local radiative center calculation was done by Michael Pavolonis (NOAA/NESDIS) in section 3.4.2.2 of 80% GOES-R Cloud Type Algorithm Theoretical Basis Document. This description takes several parts of the original text as well as two of the figures from the original text in order to illustrate the gradient filter. In addition, the analysis performed by Michael Pavolonis (NOAA/NESDIS) regarding the number of steps taken is also shown in the LRC description. This description gives an overview and description of how to calculate the local radatitive center. The authors would like to recognize the effort that was done by Michael Pavolonis in the development of this algorithm.

The local radiative center (LRC) is used in various GOES-R AWG algorithms as a measure of where the radiative center for a given cloud is located, allowing for the algorithm to look at the spectral information at an interior pixel within the same cloud while avoiding the spectral information offered by pixels with a very weak cloud radiative signal. A generalized definition of the LRC is that, for a given pixel, it is the pixel location, in the direction of the gradient vector, upon which the gradient reverses or when the input value is greater than or equal to the gradient stop value is found, whichever occurs first.
Overall, this use of spatial information allows for a more spatially and physically consistent product. This concept is also explained in Pavolonis (2010).

The gradient vector points from low to high pixels of the input, such that the vector is perpendicular to isolines of the input value. This concept is best illustrated with a figure. Figure 1, which is of $\square_{stropo}(11\square m)$, is the actual gradient vector field, thinned for the sake of clarity. As can be seen, the vectors in this image point from cloud edge towards the optically thicker interior of the cloud. This allows one to consult the spectral information at an interior pixel within the same cloud in order to avoid using the spectral information offered by pixels with a very weak cloud radiative signal.

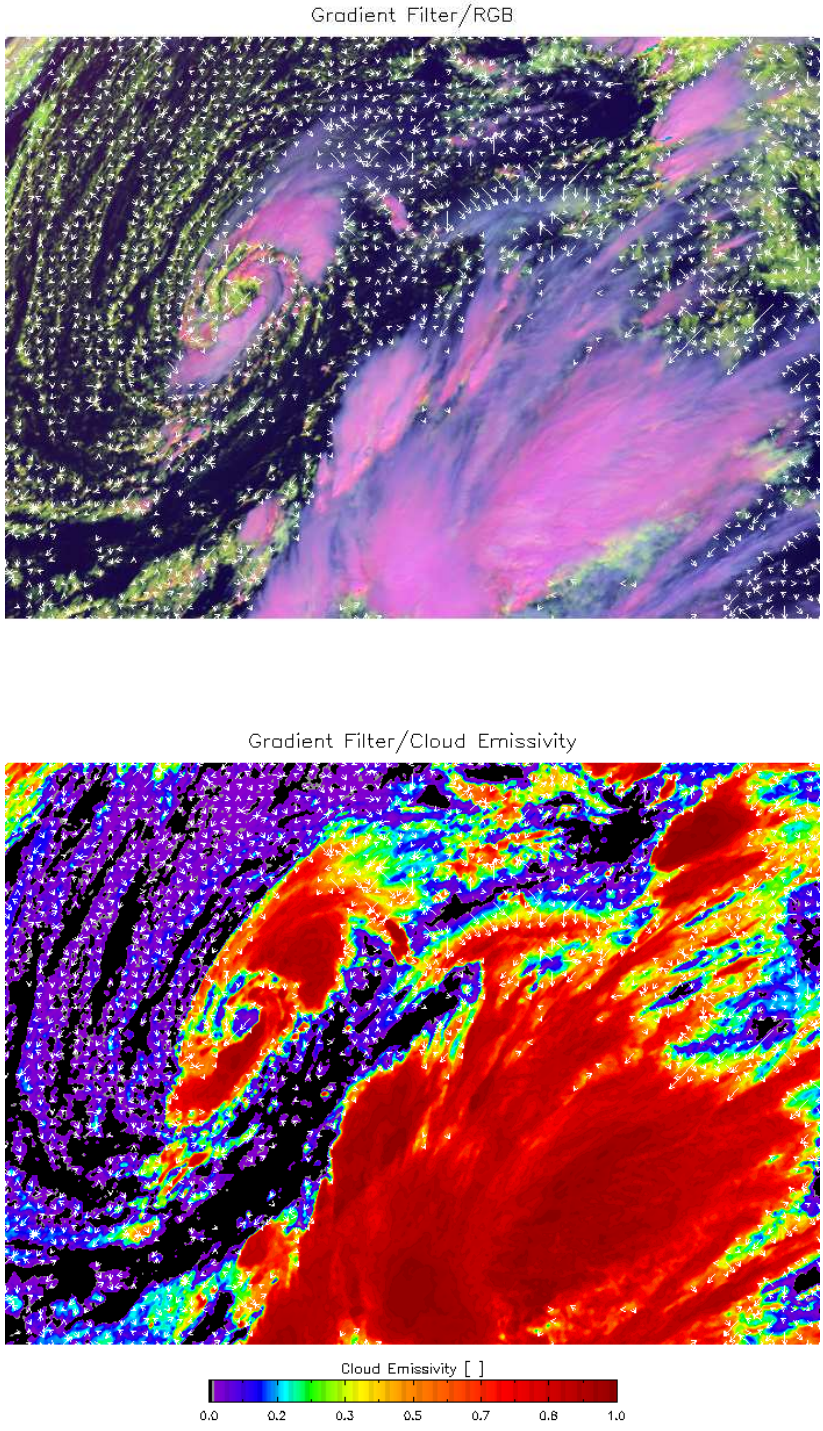

Figure 39: The gradient vector with respect to cloud emissivity at the top of the troposphere is shown overlaid on a false color RGB image (top) and the actual cloud emissivity image itself (bottom). The tail of the arrow indicates the reference pixel location.

While the above was a generalized description of the gradient filter, we next describe the method for calculating the LRC (the gradient vector).

The LRC subroutine (also known as the gradient filter) uses the following inputs

1. The value on which the gradient is being calculated on (Grad_Input)
2. The number of elements in the current segment
3. The number of lines in the current segment
4. LRC Mask for the current segment
5. The minimum allowed input value (Min_Grad)
6. The maximum allowed input value (Max_Grid)
7. The gradient stop value (Grad_Stop)

The input values to the LRC routine are typically either the 11□m troposphere emissivity, □$_{stropo}$(11□m), the nadir corrected 11□m troposphere emissivity, $\varepsilon_{stropo,\ nadir}$ (11μm) or the 11□m brightness temperature. A full list of the input values for each algorithm is listed in Table 1. The output for the LRC algorithm is as follows:

1. Array of element indices of the LRCs for the current segment
2. Array of line indices of the LRCs for the current segment

The first thing that is done for a given segment of data is the computation of the yes/no (1/0) LRC Mask. This mask simply states what pixels the LRC will be computed for. For each algorithm, the definition for the LRC mask criteria is defined in table 1.

The LRC routine loops over every line and element, calculating the LRC for each pixel individually. For all valid pixels, the LRC algorithm initially uses information from the surrounding 8 pixels (i.e a 3x3 box centered on the given pixel) to determine the direction of the gradient vector. The number of pixels used is the same for each algorithm. The validity of a given reference pixel (G_{ref}) is determined by the following criteria

1. Does the pixel have a value greater than the minimum allowed value (Min_Grad)?
2. Does the pixel have a value less than the maximum allowed input value (Max_Value)?
3. Is LRC mask is set to “Yes”?

If any of the above statements are false, the LRC algorithm will simply skip over that particular pixel. However, if all three statements are true,

then the pixel is considered valid and the algorithm will proceed to the next step.

The next step in the gradient filter is the determination of the initial direction of the gradient. Initially, the gradient test value (G_{test}), which is a local variable, set to a large number (99999) and the direction is set to missing. The gradient (G_{diff}) between the reference pixel (G_{ref}) and the neighboring pixel is calculated. This difference is only calculated if the neighboring pixel is greater than or equal to Min_Grad and less than or equal to Max_Grad. For each direction, if G_{diff} is less than G_{test} , then G_{test} is set to G_{diff}. G_{diff} is calculated for each of the 8 surrounding pixels, and the direction that has the smallest G_{test} is selected as the direction to look for the local radiative center. If the direction is set to missing, then the LRC routine moves to the next pixel in the segment. This can only occur if all the surrounding pixels are either smaller than Grad_Min or greater than Grad_Max.

The directions of the gradient are specified in the following manner:

Table 1. Definition of the directions used in the gradient filter.

Direction #	Y direction	X direction
1	Elem - 1	Line + 0
2	Elem - 1	Line + 1
3	Elem + 0	Line + 1
4	Elem + 1	Line + 1
5	Elem +1	Line + 0
6	Elem +1	Line - 1
7	Elem + 0	Line - 1
8	Elem - 1	Line - 1

One the direction of the gradient has been established, the gradient filter then looks out in the direction for one of six stopping conditions:

1. The test pixel is less than or equal to Min_Grad
2. The test pixel is greater than or equal to Max_Grad
3. The test pixel is greater than or equal to the stop value (Grad_Stop)
4. The test pixel is less than the reference pixel.
5. The gradient filter has reached the maximum number of steps to look out
6. The test pixel is at the edge of the segment

Table 2 shows how the gradient determines the test pixel. For example, for pixel 30,30 of a given segment, if the gradient direction is #3, then the gradient filter tests along (30, 30+n), where n is the current step being tested. Once one of these conditions is met, the line element number is stored as the LRC for the given reference pixel. Originally, the maximum

number of steps that could be taken was set to 150. However, a study done by Michael Pavolonis (NOAA/NESDIS) showed that the average number of steps that are needed to find the LRC is less than or equal to 30, as can be seen in figure 2.

10. CRTM

a. Data *description*

Description: Community radiative transfer model
Filename: N/A
Origin: NOAA / NESDIS
Size: N/A
Static/Dynamic: N/A

b. Interpolation *description*

A double linear interpolation is applied in the interpolation of the transmissitance and radiance profile, as well as in the surface emissivity, from four nearest neighbor NWP grid points to the satellite observation point. There is no curvature effect. The weights of the four points are defined by the Latitude / Longitude difference between neighbor NWP grid points and the satellite observation point. The weight is defined with subroutine ValueToGrid_Coord:

NWP forecast data is in a regular grid.

Suppose:
Latitude and Longitude of the four points are:
(Lat1, Lon1), (Lat1, Lon2), (Lat2, Lon1), (Lat2, Lon2)
Satellite observation point is:
(Lat, Lon)

Define
aLat = (Lat – Lat1) / (Lat2 – Lat1)
alon = (Lon – Lon1) / (Lon2 – Lon1)

Then the weights at four points are:
w11 = aLat * aLon
w12 = aLat * (1 – aLon)
w21 = (1 – aLat) * aLon
w22 = (1-aLat) * (1 – aLon)

Also define variable at the four points are:

a11, a12, a21, a22

Then the corresponding interpolated result at satellite observation point (Lat, Lon) should be:

a(Lat, Lon) = (a11*w11 + a12*w12 + a21*w21 + a22*w22) / u

Where,

u = w11 + w12 + w21 + w22

c. CRTM calling procedure in the AIT framework

The NWP GFS pressure, temperature, moisture and ozone profiles start on 101 pressure levels.
They are converted to 100 layers in subroutine Compute_Layer_Properties. The layer temperature between two levels is simply the average of the temperature on the two levels.
layer_temperature(i) = (level_temperature(i) + level_temperature(i+1))/2
While pressure, moisture and ozone are assume to be exponential with height.
hp = (log(p1)-log(p2))/(z1-z2)
p = p1* exp(z*hp)
Where p is layer pressure, moisture or ozone. p1,p2 represent level pressure, moisture or ozone. z is the height of the layer.

CRTM needs to be initialized before calling. This is done in subroutine Initialize_OPTRAN. In this call, you tell CRTM which satellite you will run the model. The sensor name is passed through function call CRTM_Init. The sensor name is used to construct the sensor specific SpcCoeff and TauCoeff filenames containing the necessary coefficient data, i.e. seviri_m08.SpcCoeff.bin and seviri_m08.TauCoeff.bin. The sensor names have to match the coefficient file names. You will allocate the output array, which is RTSolution, for the number of channels of the satellite and the number of profiles. You also allocate memory for the CRTM Options, Atmosphere and RTSoluiton structure. Here we allocate the second RTSolution array for the second CRTM call to calculate derivatives for SST algorithm.

Before you call CRTM forward model, load the 100-layer pressure, temperature, Moisture and ozone profiles and the 101 level pressure profile into the Atmosphere Structure. Set the units for the two absorbers (H2O and O3) to be MASS_MIXING_RATIO_UNITS and VOLUME_MIXING_RATIO_UNITS respectively. Set the Water_Coverage in Surface structure to be 100% in order to get surface emissivity over water. Land surface emissivity will be using SEEBOR.

Also set other variables in Surface data structure, such as wind speed/direction and surface temperature. Use NWP surface temperature for land and coastline, and OISST sea surface temperature for water. Set Sensor_Zenith_Angle and Source_Zenith_Angle in Geometry structure. Call CRTM_Forward with normal NWP profiles to fill RTSolution, then call CRTM_Forward again with moisture profile multiplied by 1.05 to fill RTSolution_SST. The subroutine for this step is Call_OPTRAN.

After calling CRTM forward model, loop through each channel to calculate transmittance from each level to Top of Atmosphere (TOA). What you get from RTSolution is layer optical depth, to get transmittance

```
 Trans_Atm_Clr(1) = 1.0

 Do Level =  2 , TotalLevels
   Layer_OD = RTSolution(ChnCounter, 1)%Layer_Optical_Depth(Level
-1)
   Layer_OD = Layer_OD /
COS(CRTM%Grid%RTM(LonIndex,LatIndex) &
                    %d(Virtual_ZenAngle_Index)%SatZenAng * DTOR)
   Trans_Atm_Clr(Level) = EXP(-1 * Layer_OD) &
                  * Trans_Atm_Clr(Level - 1)
 ENDDO
```

DTOR is degree to radius PI/180.

Radiance and cloud profiles are calculated in Clear_Radiance_Prof

```
 SUBROUTINE Clear_Radiance_Prof(ChnIndex, TempProf, TauProf,
RadProf, &
                        CloudProf)
 B1 = Planck_Rad_Fast(ChnIndex, TempProf(1))
 RadProf(1) = 0.0_SINGLE
 CloudProf(1) = B1*TauProf(1)

 DO LevelIndex=2, NumLevels
   B2 = Planck_Rad_Fast(ChnIndex, TempProf(LevelIndex))
   dtrn = -(TauProf(LevelIndex) - TauProf(LevelIndex-1))
   RadProf(LevelIndex) = RadProf(LevelIndex-1) +
(B1+B2)/2.0_SINGLE * dtrn


   CloudProf(LevelIndex) = RadProf(LevelIndex) +
B2*TauProf(LevelIndex)
   B1 = B2
 END DO
```

Transmittance, radiance and cloud profiles are calculated for both normal CRTM structure and the 2nd CRTM structure for SST.

Call Clear_Radiance_TOA to get TOA clear-sky radiance and brightness temperature.

```
SUBROUTINE Clear_Radiance_TOA(Option, ChnIndex, RadAtm, TauAtm, SfcTemp, &
                              SfcEmiss, RadClr, BrTemp_Clr, Rad_Down)
IF(Option == 1) THEN
  IF(PRESENT(Rad_Down))THEN
    RadClr = RadAtm + (SfcEmiss * Planck_Rad_Fast(ChnIndex, SfcTemp) &
          + (1. - SfcEmiss) * Rad_Down) * TauAtm
  ELSE
    RadClr = RadAtm + SfcEmiss * Planck_Rad_Fast(ChnIndex, SfcTemp) &
             * TauAtm
  ENDIF

  CALL Planck_Temp(ChnIndex, RadClr, BrTemp_Clr)

 ELSE
   RadClr = 0.0
   BrTemp_Clr = 0.0
ENDIF
```

In this subroutine, Rad_Down is optional, depending on if you want to have a reflection part from downward radiance when you calculate the clear-sky radiance. Notice that clear-sky radiance and brightness temperature on NWP grid only calculated for normal CRTM structure not the SST CRTM structure.

Also save the downward radiances from RTSolution and RTSolution_SST to CRTM_RadDown and CRTM_RadDown_SST. Save CRTM calculated surface emissivity to CRTM_SfcEmiss. The above steps are done in subroutine CRTM_OPTRAN